Ministry of Higher Education and Scientific Research

Hassiba Benbouali University of Chlef

Faculty of Technology

Department of Electrical Engineering

THESE

Submitted in fulfillment of the requirements for the degree of

DOCTORATE (LMD)

Option: Electrical engineering

By

YOUCEF BENETTAYEB

Title:

Experimental and Numerical Study of the Effect of Geometry and Climate on the Performance of a Solar Chimney Power Plantes ‘’ Étude expérimentale de l'effet de la géométrie et du climat sur les performances d’une cheminée solaire ‘’

Defended on 29/01/2025 in front of the jury composed of:

Djilali Benyoucef	Professor	University	President
Abderrahmen Benbouali	MCA	UHB-Chlef	Supervisor
Toufik Tahri	Professor	UHB-Chlef	Co- Supervisor
Hocine Tebani	MCA	University	Examiner
Mohamed Dekkiche	MCA	University	Examiner
Salah Bezzari	MCA	University	Examiner
Djahbar abdelkader	Professor	University	Invited

Acknowledgements

بسم الله الرحمن الرحيم

الحمد لله عدد ما كان وعدد ما يكون، الحمد لله الذي بنعمته تتم الصالحات، وبتوفيقه تُنال الغايات، وبنوره يُهتدى في الظلمات. ما كان لهذا الإنجاز أن يتحقق، ولا لهذا الطريق أن يُكمل، لولا فضل الله الذي أيّدني بلطفه، وثبّتني برحمته، ويسّر لي الأسباب، وسخّر لي من العون ما لا يُعد ولا يُحصى. فله الحمد أولًا وآخرًا، ظاهرًا وباطنًا. وأسأله أن يجعل ما سُطّر في هذه الصفحات علمًا نافعًا، وعملًا خالصًا لوجهه الكريم، وذخرًا لي ولوالديّ، ولكل من ساهم فيه، ولكل من مدّ يدًا أو بذل جهدًا، ظاهرًا أو خفيًّا، قريبًا أو بعيدًا، وأن يجعله خيرًا ممتدًا ونورًا لمن بعدي.

At the first I would like to express my deepest and most sincere gratitude to my supervisors, Prof. Abderrahmen Benbouali and Prof. Toufik Tahri, for their invaluable guidance, constant support, and constructive feedback throughout the course of this research. Their wisdom, patience, and encouragement have shaped not only my academic progress but also my personal development. I am truly honored to have had the opportunity to work under their supervision.

I would also like to express my profound gratitude to the distinguished members of my graduate study committee: the chairperson, Professor Djilali Benyoucef, and the esteemed jury members, Dr. Salah Bezzari, from the URAER Ghardaïa, Dr. Hocine Tebani, and Dr. Mohamed Dekkiche from the University of Chlef.

Their dedicated commitment, insightful critiques, and constructive feedback have been instrumental in refining this thesis. I sincerely appreciate their willingness to devote time and effort to this academic endeavor despite their many professional responsibilities.

In conclusion, I extend my deepest gratitude to all who have supported me throughout this journey family, friends, teachers, colleagues, and everyone who played a role in my growth and success. Your encouragement and presence, whether near or far, have been invaluable. I also humbly remember and honor those who are no longer with us, whose memories continue to inspire and guide me. Their legacy lives on in every step I take and every achievement I reach. To all, I offer my sincere thanks from the depths of my heart.

ملخص:

تمثل محطة المدخنة الشمسية تقنية واعدة لمواجهة الطلب العالمي المتزايد على الطاقة النظيفة والمستدامة. إن بساطتها الهيكلية، وانخفاض متطلبات الصيانة، وكفاءتها الاقتصادية على المدى الطويل تجعلها مناسبة بشكل خاص للتطبيق على نطاق واسع. يتكون النظام من ثلاثة مكونات رئيسية: مجمع شمسي، ومدخنة مركزية، ووحدة توربين-مولد. تقوم الإشعاعات الشمسية بتسخين الهواء تحت المجمع الشفاف، مما يحفّز حركة الحمل الحراري عبر المدخنة. وتؤدي حركة الهواء الصاعد هذه إلى تدوير التوربين الموجود في قاعدة المدخنة، مما يحوّل الطاقة الحرارية إلى طاقة ميكانيكية ثم كهربائية. ومن خلال الاستفادة من الحمل الطبيعي وتأثير الاحتباس الحراري، توفر هذه التقنية حلاً موثوقًا وصديقًا للبيئة لإنتاج الكهرباء، خصوصًا في المناطق ذات الإشعاع الشمسي المرتفع. لقد حظيت تقنية المدخنة الشمسية باهتمام بحثي متزايد كبديل محتمل للأنظمة التقليدية. وأصبح تحسين أداء وكفاءة هذه المحطات محورًا رئيسيًا في الدراسات الحديثة. وفي هذا الإطار، تعتمد هذه الدراسة نهجًا تكامليًا بين التجربة العملية والمحاكاة العددية لدراسة المعلمات الهندسية الحرجة - التي لم تحظَ باهتمام كافٍ سابقًا - بالإضافة إلى العوامل البيئية المرتبطة بالظروف المناخية المحلية. ولهذا الغرض، تم تصميم وبناء نموذج أولي مصغّر في جامعة الشلف بالجزائر، مما أتاح الحصول على بيانات فعلية عن الإشعاع الشمسي، ودرجة حرارة الهواء المحيط، وسرعة تدفق الهواء، ودرجة الحرارة الداخلية. ولتكميل الجانب التجريبي، تم تطوير نموذج ثنائي الأبعاد باستخدام تقنيات ديناميكا الموائع الحسابية لمحاكاة السلوك الحراري والانسيابي داخل النظام. وقد تم التحقق من دقة النموذج من خلال مقارنته مع بيانات مرجعية من الأدبيات. وبفضل دمج المعادلات الحاكمة ونماذج الاضطراب وآليات انتقال الحرارة، تمكنت المحاكاة من تحليل متغيرات التصميم وسيناريوهات التشغيل التي يصعب تقييمها تجريبيًا. وقد وفّر هذا النهج الهجين رؤى أعمق حول تأثير المعلمات الهندسية والبيئية على أداء النظام، وقدم توجيهات عملية لتحسين تصميم المدخنة الشمسية وفقًا للظروف المناخية المحلية. أظهرت التحاليل التجريبية والعددية المجمعة نتائج مهمة؛ حيث تبين أن قطر المدخل (20 سم) وعدد المداخل (أربعة) لهما تأثير كبير على السلوك الحراري والانسيابي للنظام، مما ينعكس بشكل مباشر على الكفاءة الكلية. ومن بين العوامل البيئية المدروسة، تبيّن أن الإشعاع الشمسي هو العامل الأكثر تأثيرًا في أداء النظام، في حين كان لتأثير درجة حرارة الهواء المحيط دور محدود. كما لعبت المكونات الهندسية الرئيسية، مثل الصفيحة الماصة، والمجمع، والمدخنة، دورًا حاسمًا في تحسين سرعة تدفق الهواء وتوزيع درجات الحرارة، مما أدى إلى زيادة في القدرة المنتجة وصلت إلى 275٪ في أفضل الحالات. وأكّدت التحاليل الموسمية موثوقية النظام طوال العام، كما أظهرت طبقة التخزين الحراري تحت المجمع فعالية في تمديد عمل النظام ليلاً. تؤكد هذه النتائج مجتمعة الإمكانات العالية وقابلية التكيف لمحطة الطاقة الشمسية المدخنة مع الخصائص المناخية المحلية لمدينة الشلف، الجزائر. كما أن شدة الإشعاع الشمسي العالية والظروف الجوية المواتية في المنطقة تُعزز من جدوى وفعالية هذه التقنية، مما يجعلها خيارًا مثاليًا لتطوير الطاقة المتجددة في المنطقة.

الكلمات المفتاحية: محطة الطاقة الشمسية المدخنة؛ دراسة تجريبية؛ محاكاة عددية؛ الظروف المناخية؛ المعلمات الهندسية؛ الأداء.

Abstract

The Solar Chimney Power Plant (SCPP) represents a promising technology for addressing the growing global demand for clean and sustainable energy. Its structural simplicity, low maintenance requirements, and long-term cost efficiency make it particularly suitable for large-scale implementation. The system consists of three primary components: a solar collector, a central chimney, and a turbine-generator unit. Solar radiation heats the air beneath the transparent collector, inducing buoyant flow through the chimney. This upward airflow drives a turbine located at the chimney's base, thereby converting thermal energy into mechanical and, ultimately, electrical energy. By harnessing natural convection and the greenhouse effect, SCPPs offer a reliable and environmentally friendly solution for renewable electricity generation, particularly in regions with high solar potential. Solar chimney technology has attracted increasing research interest as a viable alternative to conventional energy systems. Enhancing the performance and efficiency of SCPPs has become a key focus of contemporary research. Within this context, the present study adopts an integrated experimental and numerical approach to investigate critical geometric parameters—previously underexplored—as well as environmental factors influenced by local climatic conditions. To this end, a carefully designed and scaled prototype was constructed and installed at the University of Chlef, Algeria, enabling the acquisition of real-time data on solar radiation, ambient temperature, airflow velocity, and internal air temperature. This experimental configuration allows for a realistic evaluation of system behavior under the specific climatic context of the study location. Complementing the experimental work, a 2 D CFD model was developed to simulate the thermo-fluid behavior within the system. The model was rigorously validated using benchmark data from the literature to ensure accuracy and reliability. By accurately incorporating governing equations, turbulence models, and heat transfer mechanisms, the CFD simulations enabled the investigation of design variables and operational scenarios that are difficult to assess experimentally. This integrated methodology provided deeper insights into the influence of key geometric and environmental parameters on system performance and offers practical guidance for optimizing SCPPs, particularly with respect to local climate conditions. The combined experimental and numerical analysis revealed several important findings. Specifically, it was shown that both the inlet diameter (20 cm) and the number of inlets (four) significantly influence the system's thermal and aerodynamic behavior, with direct implications for overall efficiency. Among the environmental parameters studied, solar radiation emerged as the most critical driver of system performance, while ambient air temperature had a limited effect. Furthermore, key geometric components such as the absorber plate, collector, and chimney were found to play vital roles in enhancing airflow velocity and temperature distribution, resulting in a power output increase of up to 275% under optimized conditions. Seasonal analysis confirmed the system's reliability throughout the year, and the integration of a thermal storage layer beneath the collector extended operational capacity into nighttime hours. Collectively, these results underscore the strong potential and adaptability of the SCPP to the specific climatic characteristics of Chlef, Algeria. The

region’s high solar intensity and favorable atmospheric conditions further enhance the viability and efficiency of SCPP implementation, positioning it as an ideal location for the development of this renewable energy technology.

Keywords: Solar chimney power plant; Experimental Study; Numerical Simulation; Climate Conditions; geometry parameters; Performance

Résumé :

La centrale solaire à cheminée (SCPP) représente une technologie prometteuse pour répondre à la demande mondiale croissante en énergie propre et durable. Sa simplicité structurelle, ses faibles besoins en maintenance et sa rentabilité à long terme en font une solution adaptée pour des applications à grande échelle. Le système se compose de trois éléments principaux : un collecteur solaire, une cheminée centrale et une unité turbine-générateur. Le rayonnement solaire chauffe l'air sous le collecteur transparent, générant ainsi un flux d'air ascendant à travers la cheminée. Ce flux active une turbine située à la base, convertissant l'énergie thermique en énergie mécanique puis électrique. En tirant parti de la convection naturelle et de l'effet de serre, les SCPP offrent une solution fiable et écologique pour la production d'électricité renouvelable, en particulier dans les régions à fort ensoleillement. La technologie des cheminées solaires suscite un intérêt croissant en tant qu'alternative viable aux systèmes énergétiques conventionnels. L'amélioration des performances et de l'efficacité des SCPP constitue désormais un axe majeur des recherches actuelles. Dans ce cadre, la présente étude adopte une approche intégrée expérimentale et numérique pour analyser certains paramètres géométriques critiques – jusque-là peu étudiés – ainsi que les facteurs environnementaux influencés par les conditions climatiques locales. À cet effet, un prototype à échelle réduite a été conçu et installé à l'Université de Chlef, en Algérie, permettant la collecte de données en temps réel sur le rayonnement solaire, la température ambiante, la vitesse de l'air et la température interne. Parallèlement aux travaux expérimentaux, un modèle 2 D CFD a été développé afin de simuler le comportement thermo-fluidique du système. Ce modèle a été rigoureusement validé à l'aide de données de référence issues de la littérature, assurant ainsi sa fiabilité. En intégrant les équations fondamentales, les modèles de turbulence et les mécanismes de transfert thermique, les simulations CFD ont permis d'examiner des variables de conception et des scénarios opérationnels difficiles à évaluer par des moyens expérimentaux. Cette méthodologie hybride a permis une compréhension approfondie de l'effet des paramètres géométriques et climatiques sur les performances du système, et fournit des orientations pratiques pour l'optimisation des SCPP en fonction des conditions locales. L'analyse combinée expérimentale et numérique a révélé plusieurs résultats importants. En particulier, le diamètre des entrées (20 cm) et leur nombre (quatre) influencent de manière significative le comportement thermique et aérodynamique du système, avec un impact direct sur l'efficacité globale. Parmi les paramètres environnementaux, le rayonnement solaire s'est révélé être le facteur prédominant, tandis que la température ambiante avait un effet limité. Les éléments géométriques clés – tels que la

plaque absorbante, le collecteur et la cheminée – ont joué un rôle crucial dans l'amélioration de la vitesse d'écoulement de l'air et de la distribution thermique, entraînant une augmentation de la production électrique pouvant atteindre 275 % dans des conditions optimales. L'analyse saisonnière a confirmé la fiabilité du système tout au long de l'année, et l'ajout d'une couche de stockage thermique sous le collecteur a permis de prolonger le fonctionnement du système pendant les heures nocturnes. Ces résultats soulignent le fort potentiel et la capacité d'adaptation des SCPP aux caractéristiques climatiques spécifiques de la région de Chlef, en Algérie. L'intensité solaire élevée et les conditions atmosphériques favorables de la région renforcent davantage la faisabilité et l'efficacité de cette technologie, la positionnant comme une solution idéale pour le développement des énergies renouvelables dans le contexte local.

Mots-clés : Centrale solaire à cheminée ; Étude expérimentale ; Simulation numérique ; Conditions climatiques ; Paramètres géométriques ; Performance.

Liset of symbols

Liset of symbols

A	Area (m^2)
a	Ambient Temperature (k)
C_p	Specific heat capacity of air (kJ/kg.K)
D	Dimeter (m)
F	Force (N/m^3)
g	Gravitational acceleration (m/s^2)
H	Height (m)
I	Irradiation (W/m^2)
k	Turbulent kinetic energy (m^2/s)
m_a	Mass flow rate of air (kg/s).
P	Power (w)
Q	Heat transfer rate (W)
Q_v	Volumetric flow rate m^3/s
R	Radius (m)
R_a	Rayleigh number
u	Velocity magnitude (m /s)
ΔT	difference (K)

Greek Letters

α	Thermal diffusivity (m^2/s)
β	Thermal expansion coefficient (1/K)
ε	Turbulent rate of dissipation (m^2/s^3)
η	Efficiency
μ	Dynamic viscosity (kg/m.s)
v	kinematic viscosity (m^2/s)
ρ	Density (Kg/m^3)

Abbreviation

AR	Chimney outlet to inlet areas Ratio
CFD	Computational Fluid Dynamics
Ch	Chimney
Coll	Collector
out	Output
PV	photovoltaic
SCPP	Solar Chimney Power Plant

Table of Contents

List of Figures

Chapter I

Chapter II

Chapter III

Chapter IV

List of Table

Chapter I

Chapter II

Chapter III

Chapter IV

General Introduction

General Introduction

The 21st century is marked by an escalating urgency to transform global energy systems in response to the converging crises of climate change, resource depletion, and rising energy demand. As the global population expands, urbanization accelerates, and industrial activity intensifies, pressure on existing energy infrastructure grows significantly. According to recent international energy outlooks, global energy demand increased by 2.2% in the past year alone and is projected to increase by up to 18% by 2050. This upward trend, largely driven by emerging economies and expanding middle classes, underscores a critical need to transition toward clean, resilient, and sustainable energy sources [1, 2].

Despite significant advancements in renewable energy technologies, fossil fuels still dominate the global energy matrix, accounting for over 80% of total energy consumption. This persistent reliance not only perpetuates economic and geopolitical vulnerabilities but also exacerbates environmental degradation. Of particular concern is the fact that greenhouse gas emissions from energy use increased by 2.1% in the past year, exceeding the previous record set in 2022. These trends underscore the urgent need to transition from conventional, fossil-based energy systems to more sustainable, resilient and low carbon alternatives [3].

Among the portfolio of renewable technologies, solar energy emerges as a cornerstone of sustainable development. It is abundant, widely accessible and environmentally benign. Solar energy is primarily harnessed via two main approaches: photovoltaic (PV) systems, which convert sunlight directly into electricity and solar thermal systems, which concentrate solar energy to generate heat for power production or industrial processes. While PV and concentrated solar power technologies have seen broad adoption, there remains a subset of solar thermal technologies that, despite their structural simplicity and environmental promise, have received comparatively limited attention: Solar Chimney Power Plants (SCPPs).

The SCPPs represents a novel and compelling solution within the solar thermal sdomain. It operates on an elegantly simple yet highly effective principle: it converts solar radiation into mechanical energy through natural convection, subsequently generating electricity without combustion or fuel input. The system comprises three fundamental components: a collector, a central chimney and turbines positioned at the chimney base. As solar heated air rises due to buoyancy, it creates an updraft that drives the turbines, producing electricity with zero direct carbon emissions.

What distinguishes the SCPP from other solar technologies is its unique combination of simplicity, scalability and sustainability. Its minimal maintenance requirements, low operational costs and ability to function efficiently in arid and semi-arid regions make it particularly suitable for remote or underdeveloped areas. Furthermore, when integrated with thermal energy storage, SCPPs can operate beyond daylight hours, mitigating the intermittency challenges common to many renewable energy sources.

Despite these advantages, the development of SCPPs remains at an early stage. Much of the existing research is theoretical or computational in nature, with limited experimental validation. Most studies assume idealized environmental conditions, leaving open critical questions about system performance under realistic, site-specific circumstances. This research gap hinders broader implementation and limits the credibility of simulation-based design strategies.

This thesis aims to address this gap by conducting both experimental and numerical investigations of SCPP performance. The study involves carrying out an experimental study, developing a numerical model and performing simulations to analyze the effects of key geometric and environmental parameters on the system's thermal and aerodynamic behavior, and to assess its practical feasibility.

The thesis is structured as follows:

General introduction: Outlines the global energy crisis, the dependence on fossil fuels, and the urgent call for renewable alternatives. Solar energy is presented as a cornerstone of sustainable development, with the SCPP highlighted as a promising yet insufficiently explored technology

Chapter 1 introduces the SCPP from both conceptual and technical perspectives. It presents the system configuration, operating principles, and key components, followed by a review of its historical development and major international projects.

Chapter 2 presents a critical literature review, synthesizing existing numerical and experimental studies on SCPPs, with emphasis on design parameters, material selection, performance assessment, and optimization strategies.

Chapter 3 details the experimental work conducted on a custom-built SCPP prototype at Hassiba Benbouali University in Chlef. This section examines the impact of geometric

variables and climatic conditions on system performance, offering empirical insights into the system's behavior under local environmental conditions.

Chapter 4 describes a complementary numerical study using COMSOL Multiphysics, aimed at modeling airflow and heat transfer processes within the system. This approach not only supports the experimental observations but also enables the investigation of parameters that are challenging to explore through experimental methods alone, thereby enhancing the overall understanding and optimization of the SCPP design.

To conclude, this thesis concludes with a comprehensive synthesis of the experimental and numerical results, offering an integrated perspective on the study's core findings. The work reinforces the potential of SCPP technology and lays the groundwork for future research aimed at advancing sustainable energy solutions.

CHAPTER I:

GENERAL OVERVIEW OF SOLAR CHIMNEY POWER PLANT

I.1 Introduction

The growing global demand for electricity continues to challenge conventional energy generation methods, particularly fossil-fuel-based power plants, which are increasingly inadequate and environmentally harmful [3]. This situation underscores the urgent need to transition to renewable energy sources that are reliable, economically viable, and environmentally sustainable. Among these, solar energy remains a leading candidate due to its vast availability and minimal environmental footprint. However, widely used solar technologies such as PV and solar thermal systems often face persistent limitations, including high installation and maintenance costs, efficiency losses under variable climatic conditions and limited adaptability to diverse and harsh environments [4].

In this context, the SCPP represents an innovative and promising alternative, offering a structurally simple yet highly effective solution for large-scale electricity generation. By harnessing natural convection and relying on minimal mechanical complexity, SCPPs directly address the critical challenges faced by traditional solar technologies. They offer a costeffective alternative by utilizing low-cost materials and exhibit consistent efficiency and operational reliability under harsh environmental conditions. Additionally, their modular design allows for incremental expansion without significantly increasing system complexity or costs, making SCPPs a robust and adaptable solution were conventional solar technologies face limitations.

I.2 Description of Solar Chimney Power Plants

I.2.1 Key Components of Solar Chimney Power Plants

SCPP is composed of for essential components: a solar collector, a chimney, an absorber plate, and a wind turbine. Each of these elements plays a crucial role in the system's ability to convert solar energy into power.

I.2.1.1 The Collector

In SCPP, the solar air collector is a critical component for harnessing solar energy. It features a transparent surface, typically made of glass or plastic, designed to absorb solar radiation while minimizing infrared radiation losses. This surface allows sunlight to penetrate, warming the air inside the collector and increasing its temperature. The thermal energy is then converted into kinetic energy, initiating the airflow necessary for system operation.

Additionally, the collector facilitates heating of the absorber plate beneath it, which reemits long-wavelength radiation. This radiation is trapped by the transparent roof of the collector, amplifying the greenhouse effect and further raising the system's temperature (Fig I.1a). The roof, elevated several meters above the absorber plate, creates an airflow pathway that enhances the intake of ambient air from the perimeter, promoting efficient heat exchange (Fig I.1b).

The combined processes of solar radiation absorption, thermal conversion, and airflow generation make the collector indispensable for optimizing the performance of SCPPs, ensuring efficient energy conversion [5].

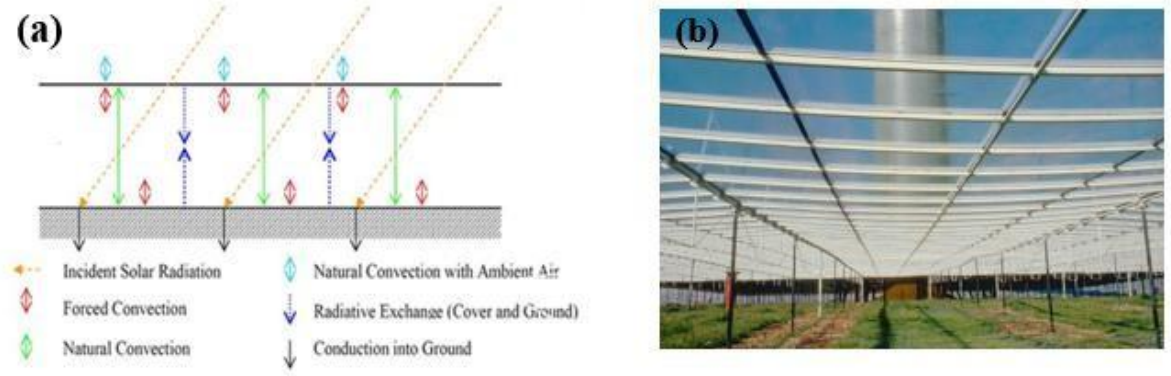

Figure I. 1: (a) Thermal balance scheme of a solar collector [6], (b) Solar collector structure of the Manzanares SCPP [7].

I.2.1.2 The absorber plate

The absorber plate constitutes a fundamental component of SCPP, functioning as the primary surface for capturing and storing solar energy transmitted through the transparent collector cover. The absorbed thermal energy is then transferred to the air beneath the collector, raising its temperature and inducing a buoyancy-driven flow toward the chimney, thereby enabling continuous power generation. To improve thermal storage, various configurations have been proposed. In certain system designs, additional heat retention strategies are incorporated, such as utilizing thermal storage materials as passive reservoirs or implementing hybrid systems that employ media such as water and stone (Fig. I.2). These configurations allow solar energy to be stored during daylight hours and gradually released at night, ensuring sustained airflow and uninterrupted system performance during periods of low or no solar radiation.

The selection of absorber materials plays a critical role in determining the overall thermal performance of the system. Materials are typically chosen for their high thermal

conductivity, durability, and capacity to retain heat over extended periods, thus supporting continuous airflow and stable turbine operation.

Beyond its thermal function, the absorber plate also contributes to the multifunctional potential of SCPPs. The area beneath the collector can be repurposed for agricultural use most notably as a greenhouse enabling concurrent energy production and food cultivation. This dual-purpose design promotes efficient land utilization and enhances both the economic viability and environmental sustainability of SCPP systems, particularly in arid and semi-arid regions [5,8,9].

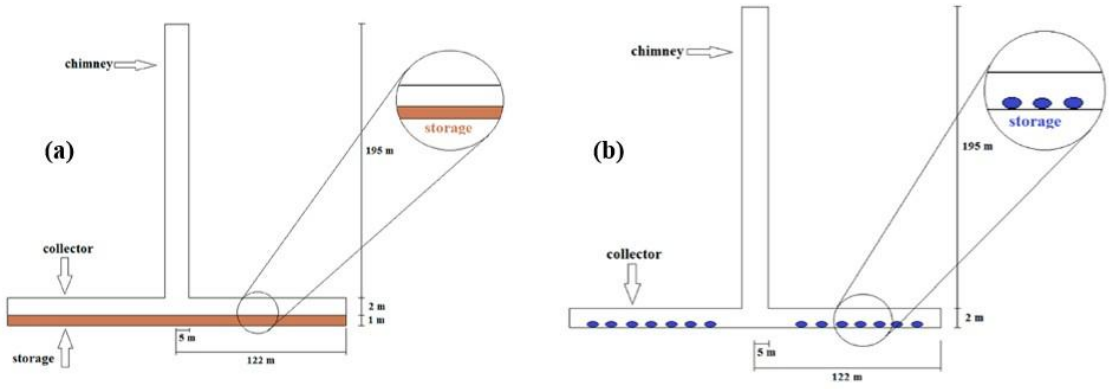

Figure I. 2: (a) General view of a SCPP with stone as the thermal energy storage, (b) a general view of a SCPP with water as the thermal energy storage [10].

I.2.1.3 The chimney

The chimney, or tower, constitutes a central element of the SCPP, functioning as the core thermal engine responsible for driving airflow throughout the system. It operates based on the buoyancy effect, whereby solar-heated air within the collector becomes less dense and rises through the chimney. This temperature-induced density gradient, established between the hot air at the base and the cooler air at the top, creates a pressure differential that generates a continuous upward airflow. The magnitude of this pressure difference and consequently, the airflow velocity is directly influenced by the height of the chimney, making it a critical parameter in the system's overall performance.

To withstand the mechanical and environmental demands imposed by tall structures, chimneys are typically constructed using robust materials such as reinforced concrete and structural steel. Advanced engineering practices, including modular assembly and aerodynamic optimization, are applied to address challenges associated with structural stability, wind loads, and thermal expansion. Despite the large-scale nature of these components, their design is often informed by the well-established principles of natural draft cooling towers, enabling effective

integration within the broader SCPP framework. In addition to its structural role, the chimney plays a vital aerodynamic function by sustaining and amplifying the upward motion of heated air, thus enabling continuous energy conversion without reliance on external mechanical systems. It also facilitates a low-pressure zone at the collector's center, reinforcing the convective airflow pattern essential for efficient system operation.

Overall, the chimney embodies a multifunctional component that seamlessly integrates thermal, aerodynamic, and structural roles. Its design governed by parameters such as height, diameter, construction method, and material selection are pivotal to optimizing the efficiency, scalability, and long-term viability of SCPP systems. Common construction approaches include free standing reinforced concrete towers, guyed steel tubes, and cable net structures clad with flexible membranes or sheet metal, each tailored to meet specific performance, cost, and environmental criteria [5,8,9]. A photograph of a typical SCPP chimney is shown in Figure I.3.

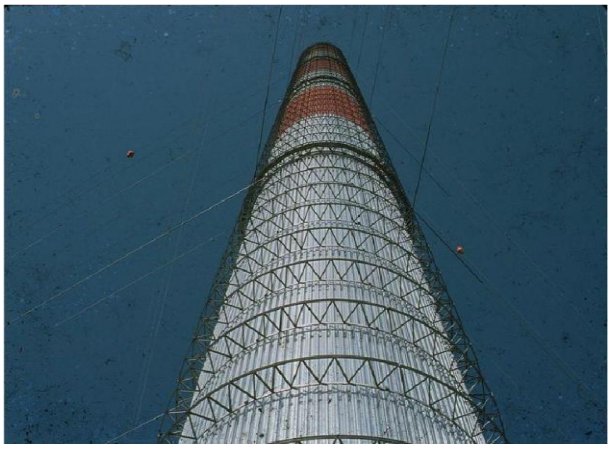

Figure I. 3: The chimney structure of SCPP [11].

I.2.1.4 The turbine

The turbine is a vital component of the SCPP (Fig. I. 4), responsible for converting the kinetic energy of the upward-moving heated air into mechanical power, which is subsequently used to generate electricity. It is typically installed at the base of the chimney between the collector outlet and the chimney inlet where the airflow is most concentrated and stable, allowing for maximum energy extraction. The turbine is usually equipped with four blades, although the number may vary depending on the design and power requirements. These blades are designed to efficiently harness the rising airflow and drive the generator.

Unlike conventional wind turbines, which operate under fluctuating atmospheric conditions, SCPP turbines benefit from a steady and directed airflow confined within the chimney. This

stability reduces dynamic loads on the blades, increases mechanical reliability, and contributes to a longer operational lifespan. Additionally, the ducted turbine setup enhances flow control and allows for higher theoretical efficiency. Owing to the predictable and unidirectional airflow, SCPP turbines can, under ideal conditions, achieve efficiencies approaching 100%, surpassing the Betz limit [5,8,9].

Figure I. 4: Schematic view of SCPP turbine configurations [7].

I.2.2 Working Principle of Solar Chimney Power Plants

A SCPP operates by converting solar radiation into electrical energy through a series of energy transformations governed by established physical principles. An illustration of the operational mechanism of SCPP is provided in Figure I. 5.

The process begins as solar radiation passes through the transparent cover of the solar collector, which is designed to allow both direct and diffuse solar radiation to penetrate and reach the ground or the absorber plate located beneath. The absorber plate effectively captures the solar energy and transfers it to the surrounding air through the greenhouse effect. This heating process increases the air temperature beneath the collector, creating a density and pressure gradient between the heated air inside the system and the cooler ambient air outside.

As the air heats up, it becomes less dense and begins to flow towards the center of the collector, where it enters the base of the vertical chimney. The chimney, positioned centrally within the collector, acts as a conduit for the rising warm air. The density difference between the heated air and the cooler surrounding air generates buoyancy, driving the warm air upward through the chimney. Additionally, the pressure difference between the base and the exit of the chimney enhances the upward airflow, further accelerating the movement of air through the system.

At the base of the chimney, a turbine is strategically placed. The kinetic energy of the fast-moving air drives the turbine blades, which are connected to a generator. The generator then converts the mechanical energy of the rotating turbine into electrical energy, completing the process of transforming solar thermal energy into electricity. This sequence of energy conversions solar to thermal, thermal to kinetic, and kinetic to electrical underpins the operation of the SCPP.

During periods of intense solar radiation, excess heat is stored in the absorber plate or in the ground beneath the collector. This stored thermal energy allows the system to maintain its operation even during nighttime or cloudy days, ensuring a continuous and stable power output.

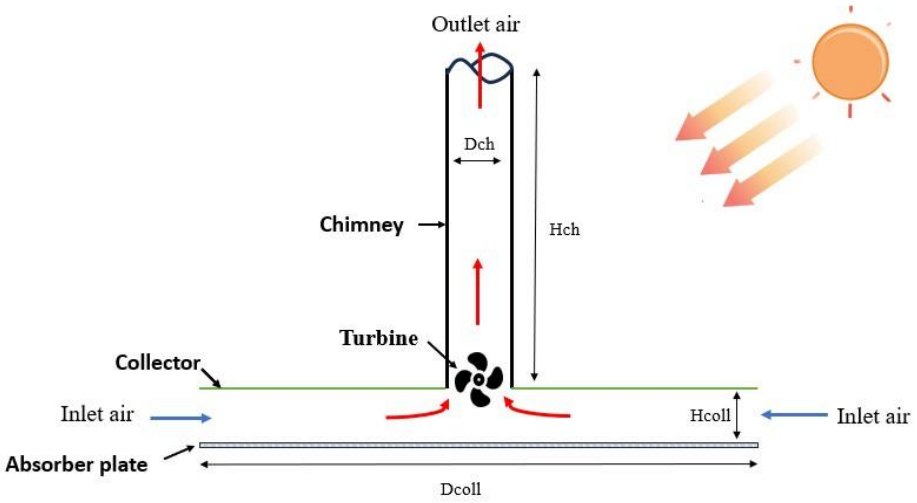

Figure I. 5: Operational Mechanism of SCPP.

I.3 Evolution of Solar Chimney Power Plants: A Historical Perspective

The concept of utilizing heated air to generate mechanical power dates back to the Renaissance. The renowned Italian polymath Leonardo da Vinci (1452–1519) proposed an ingenious system, later termed the 'smoke jack,' which harnessed the movement of hot air rising in a chimney to drive a windmill. This windmill, in turn, powered a roasting spit above a fireplace.

Da Vinci's pioneering sketches, created around 1500, represent one of the earliest documented examples of updraft principles, which form the basis of modern SCPP (see Figure I.6) [6,12].

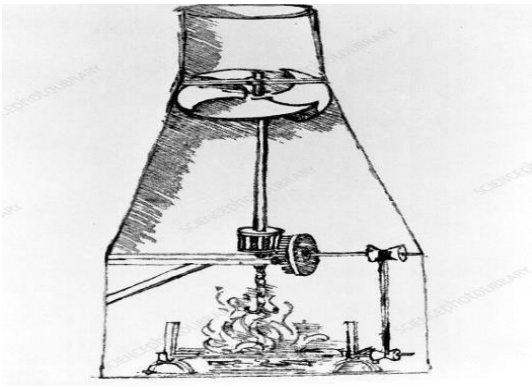

Figure I. 6: Leonardo da Vinci's smoke jack with its chimney [6].

Building on these early principles of updraft and solar energy utilization, the idea of generating electricity from solar chimneys was first formally proposed in 1903 by Spanish artillery colonel Isodoro Cabanyes. His concept, known as the 'Proyecto de motor solar' (solar engine project), described an apparatus consisting of an air heater attached to a building with a chimney. Inside the house, a wind propeller was placed, driven by the buoyant hot air rising from the chimney. This movement powered the propeller to generate electricity, as illustrated in Figure I. 7 [6,12,13].

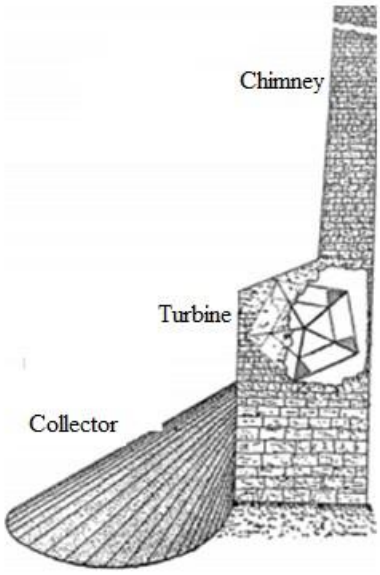

Figure I. 7: Solar engine project proposed by Isodoro Cabanyes [6].

Building on earlier concepts, Professor Bernard Dubos further advanced the solar chimney idea in 1926 by proposing the construction of a SCPP on the slopes of a high mountain in North Africa. Observing the natural sand whirls in the southern Sahara, Dubos envisioned utilizing the slant of the mountain to enhance the efficiency of the solar chimney system. He presented this design to the French Academy of Sciences, proposing the creation of a Solar Aero-Electric Power Plant. Dubos' study outlined the system's working principles and key components, forming an early theoretical foundation for the SCPP concept as shown in Figure I.8 [6,12,13].

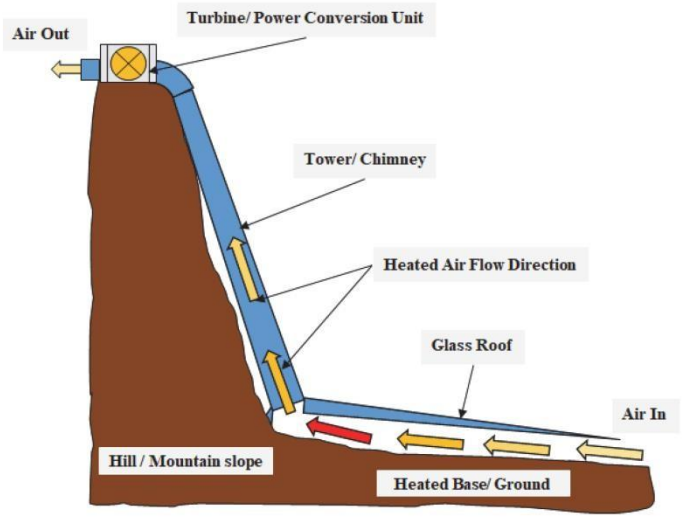

Figure I. 8: Solar aero-electric power plant proposed by Prof Bernard Dubos [6].

The concept of SCPP advanced significantly during the 20th century. In 1931, Hanns Günther described a chimney design achieving air velocities of 50 m/s (Fig I.9), marking an early use of updraft for energy generation. In 1956, Ridley patented a design featuring two chimneys one heated, the other using cold air to drive a turbine [6,10-12].

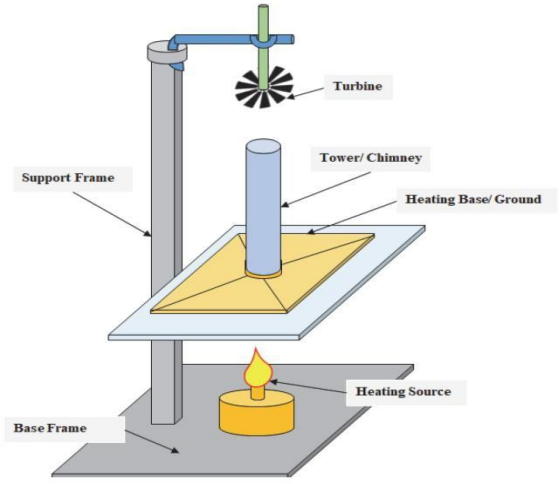

Figure I. 9: Solar chimney proposal of Prof Dubos presented by Günther, 1931 [6].

In 1964, French scientist Nazare patented a diffuser-shaped tower for SCPPs, utilizing desert heat to power turbines. Nazare also proposed building a solar chimney in Algeria (Fig I.10), inspired by the desert's natural sand vortexes [6,12,13].

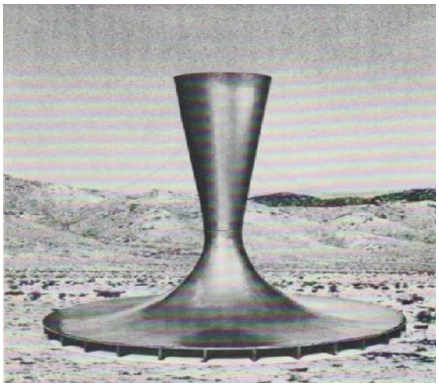

Figure I. 10: The solar tower proposed by Prof Nazare [6].

The energy crisis of the 1970s further spurred interest in renewable energy sources, prompting renewed research into solar chimneys. Building on these developments, the first functional SCPP prototype was constructed in 1982 in Manzanares, Spain, under the leadership of German civil engineer Jörg Schlaich (Fig I.11). This project, funded by the German Ministry of Research and Technology, featured a chimney with a height of 195 m and a diameter of 10 m, coupled with a solar collector spanning 46,000 m², with a mean radius of 122 m and an average roof height of 1.85 m. The plant achieved a maximum power output of 50 kW and demonstrated upwind velocities of approximately 9m/s under load conditions and 15m/s during release. This pioneering project, which operated from 1982 to 1989, provided a practical demonstration of the SCPP concept and marked a significant milestone in the development of renewable energy technologies [7,9].

Figure I. 11: SCPP of Manzanares, Spain [7].

I.4 Worldwide Solar Chimney Power Plant Projects: A Comparative Overview

I.4.1 Prototype of Manzanares

The Manzanares SCCP, constructed in 1982 in Manzanares, Spain, was the first largescale prototype to demonstrate the viability of SCPP technology. Designed by German engineer Jörg Schlaich, the plant served as a proof of concept for generating electricity using solar-induced convection. The plant operated from 1982 to 1989, successfully generating a peak power output of 50 kW. As the first experimental model of its kind, the Manzanares prototype remains a crucial source of large-scale data, providing valuable insights into the performance and optimization of SCPP systems [7,9].

The key technical specifications and performance data of the Manzanares plant are summarized in the following Table I.1 [7,9]:

Table I. 1: Characteristics of the Manzanares Prototype

Parameter	Value
Chimney Height	195 m
Chimney Diameter	10 m
Collector Radius	122 m
Collector Height	1.85 m
Typical collector air temp. increase	20 k
Design irradiation	1000 W/ m^2
Air Velocity	9 m/s load conditions 15 m/s no-load conditions
Power Output	50kW

I.4.2 Buronga Solar Chimney Power Plant: A Visionary Australian Project

The Buronga SCPP, located near Mildura, Australia, represents one of the most ambitious SCPP projects to date. Developed by Enviro Mission in collaboration with the German engineering firm Schlaich, Bergemannund Partner, the project aims to construct a towering 1000 m high concrete chimney, with a collector diameter of 7000 m, designed to generate 200 MW of electricity. Though the project has faced challenges, including financial difficulties and

delays, its large-scale design and potential to deliver renewable energy make it a significant model for future SCPP plants.

The Buronga plant will operate with 32 turbines, generating a nominal output of 200 MW. The estimated construction cost is 400 million Euros, with an expected electricity production price four times higher than that of coal-fired plants. However, the project developers plan to enhance its economic viability by leveraging additional revenue streams such as tourism [13-16].

The key technical specifications and the performance data for the Buronga project are summarized in the following Table I.2:

Table I. 2: Characteristics of the Buronga Power Plant

Parameter	Value
Chimney Height	1000 m
Chimney Diameter	120 m
Collector Diameter	7000 m
Collector Height	1.85 m
Typical collector air temp. increase	343.15 K
Design irradiation	1000 W/ m^2
Power Output	200 MW

Despite its recognized potential, the Buronga project has not yet entered the construction phase, and its long-term prospects remain uncertain. Nevertheless, it continues to serve as a key reference in the ongoing development of large-scale solar chimney technology.

I.4.3 Solar chimney Project, Ciudad Real

The Ciudad Real SCCP, located in Fuente el Fresno, Ciudad Real, Spain, is set to become the largest solar chimney installation in Europe. The project consists of a 750-meterhigh chimney located at the center of a solar collector with a diameter of 3 km, covering an area of 350 hectares. This facility is designed to generate 40 MW of electricity, which will be enough to meet the energy demands of approximately 120,000 people.

The project is a collaborative effort between the Spanish companies IMASA and CAMPO3, and the German firm Schlaich Bergermann. The plant is expected to produce the equivalent of 140,000 barrels of oil annually and reduce CO_2 emissions by 78,000 tons per year. It will also enable vegetable cultivation under glass, utilizing 250 hectares for agricultural production.

Along with electricity generation, the project aims to incorporate telecommunications equipment, fire surveillance systems, and offer a tourist attraction for public visits. The estimated cost of the project is 240 million Euros [13-16].

The key technical specifications and the performance data for the Ciudad Real project are summarized in the following Table I.3:

Table I. 3: Characteristics of the Ciudad Real SCPP.

Parameter	Value
Chimney Height	750 m
Collector Diameter	3km
Covered Area	350 hectares
Design irradiation	1000 W/ m^2
Air Velocity	12 m/s (43 km/h)
Power Output	40 MW

I.4.4 Project Namibian - Green tower

The Namibian SCPP, known as green tower, is an ambitious project planned by the South African intellectual property company Hahn & Hahn. The project aims to address Namibia's electricity supply deficit. It will consist of a chimney structure with a height of 1.5 km and a diameter of 280 m. With an estimated cost of 1 billion US dollars, the plant is expected to generate 400 MW of electricity by creating an upward air current that will drive turbines. The base of the chimney will be surrounded by a greenhouse spanning 38.5 km^2 (7 km in diameter), offering the possibility of agricultural use. The Namibian government has approved the project, and the national electricity distribution company has committed to partially financing a feasibility study [6,13].

The key technical specifications and the performance data for the Namibian project are summarized in the following Table I.4:

Table I. 4: Characteristics of the Namibian Project.

Parameter	Value
Chimney Height	1.5 Km
Chimney Diameter	280 m
Collector Diameter	7 km
Power Output	400 MW

I.4.5 China's Solar Chimney Power Plant: A Landmark in Renewable Energy

The Jinshawan SCCP in Wuhai, located in the Inner Mongolia Autonomous Region of northern China, represents the first combined solar and wind energy system in the country. This 200-kW prototype, which began construction in May 2009, produces 400MWh of electricity annually, saving 100 tons of carbon emissions and 900 tons of water compared to thermal power plants.

Co-developed by the Inner Mongolia University of Science and Technology and the Polytechnic University of Madrid, the plant consists of three key components: a solar collector, a chimney, and a wind generator. The solar energy captured beneath a glass cover heats the sand, which then releases the stored heat during the night, driving the turbine inside the chimney.

This project, supported by the Ministry of Science and Technology of the regional government, is planned to expand in three phases:

Phase 1: A 200-kW prototype occupying 40,000 m^2 of desert.

Phase 2: A 2.2 MW power plant occupying 220,000 m^2 of desert.

Phase 3: A 25.1 MW solar chimney plant occupying 2.5 million m^2 of desert [9,10].

I.5 Advantages and Disadvantages of Solar Chimney Power Plants

I.5.1 Advantages

SCPP represent a sustainable and technologically advanced solution to renewable energy generation, offering a range of distinct advantages over conventional power generation systems:

- Sustainability: SCPPs utilize abundant solar energy, ensuring a renewable, continuous, and eco-friendly power supply. This reduces reliance on fossil fuels, contributing to global efforts to mitigate climate change.
- Operational Simplicity and Clean Technology: The technology behind SCPPs is straightforward, eliminating the need for fossil fuels and cooling towers, which reduces capital and operational costs. This simplicity lowers the risk of technical failures and enhances environmental safety.
- Cost-effectiveness and Feasibility: Construction materials such as concrete, steel, and glass are widely available and cost-efficient, making SCPPs financially viable, particularly in regions with limited industrial infrastructure. These lower construction costs promote broader feasibility and adoption.
- Independence in Remote Areas: SCPPs are suitable for remote locations, where connection to power grids is challenging. Their ability to operate autonomously reduces the need for extensive infrastructure, making them ideal for low-density and geographically isolated regions.
- Resource Efficiency: SCPPs can repurpose existing infrastructure, such as former thermal power plant chimneys, minimizing new construction requirements and reducing associated costs.
- Long Lifespan and Low Maintenance: With minimal moving parts, SCPPs have an extended operational life (80–100 years) and require low maintenance, enhancing their long-term economic viability.
- Zero Fuel Requirement: By operating without fossil fuels, SCPPs reduce operational expenses, offering a more cost-effective alternative to conventional power plants while also eliminating greenhouse gas emissions.
- Environmental Impact: SCPPs generate electricity without producing pollutants or greenhouse gases, making them an environmentally friendly solution for sustainable energy production.

- Reliable Power Generation: The integration of thermal energy storage systems allows SCPPs to generate electricity consistently, ensuring dependable 24-hour energy generation, even during periods of low sunlight.
- Economic and Social Benefits: SCPP projects stimulate local economies utilizing regional resources and labor, particularly in areas with limited industrial capacity. The long operational lifespan and minimal maintenance contribute to sustainable economic development.

I.5.2 Disadvantages

A significant limitation of SCPPs lies in the intermittent nature of their power generation, as energy output is directly affected by variations in solar radiation throughout the day and across different seasons. This dependence on solar availability can compromise the system's reliability, particularly during periods of low sunlight. Nonetheless, ongoing advancements in thermal energy storage technologies have effectively mitigated this issue, allowing for extended and more consistent operation. As a result, SCPPs are increasingly capable of delivering stable energy output, even under less favorable solar conditions.

I.6 Conclusion

This chapter provided a comprehensive introduction to SCPP, offering a detailed exploration of their design, working principles, historical development, and real-world applications. The discussion emphasized the significance of key physical phenomena such as air density variations and pressure differentials that underpin their operation.

Furthermore, the comparative overview of global SCPP projects highlighted the potential of this technology in diverse climates and regions, underscoring its adaptability and scalability. The evaluation of advantages and limitations reinforced the need for continued research to address efficiency challenges and enhance system performance.

This foundational chapter sets the stage for the subsequent investigation into the optimization of SCPP configurations, focusing on the interplay between geometric design and environmental factors to maximize energy output.

CHAPTER II: ADVANCEMENTS IN SOLAR CHIMNEY POWER PLANTS: A REVIEW OF GEOMETRY, MATERIALS, AND EFFICIENCY INNOVATIONS

II.1 Introduction

The Solar Chimney Power Plant represent a promising technology in the field of renewable energy, utilizing solar energy to generate electricity through the integration of greenhouse heating principles, natural convection, and wind energy conversion. This technology was first envisioned in the early 20th century, but SCPP gained global recognition following the successful operation of the Manzanares project in Spain during the 1980s, which achieved a power generation capacity of 50 kW. The success of this model not only demonstrated the feasibility of SCPP as a sustainable energy source but also contributed to stimulating global research and development efforts.

Over time, academic and industrial interest in SCPP has increased significantly, with researchers continuously working to improve their efficiency and scalability. Through the application of theoretical, numerical, analytical, and experimental methods, significant advancements have been made in understanding and developing this technology. As a result, SCPP have become an important area of research in renewable energy, offering a pathway toward sustainable electricity generation with minimal environmental impact. This chapter aims to provide a comprehensive review of the existing literature on SCPPs, with a particular focus on both numerical and experimental investigations. Special emphasis is placed on studies related to geometry optimization, material selection, and performance evaluation, as well as innovative design configurations that have contributed to the advancement of SCPP technology.

II.2 Optimization in Solar Chimney Power Plants

Extensive research has been conducted to enhance the efficiency of energy production and improve overall performance. These efforts have concentrated on optimizing geometric parameters, such as height, diameter, radius, structural shape, and overall design, while also identifying suitable materials to achieve improved thermal and structural performance. By refining these parameters, researchers aim to maximize heat absorption efficiency, improve airflow dynamics, enhance adaptability to varying environmental conditions, and sustainably increase the effectiveness of the energy conversion process.

II.2.1 Research review on collector

The collector is one of the fundamental components of the SCPP. Variations in the geometry and design of the collector have a direct impact on the key performance parameters of, including velocity, temperature, airflow rate, efficiency, and power output. Karimi-Pour-Fard and Beheshti [17] provides valuable insights into the impact of geometric parameters on system performance. Their Computational Fluid Dynamics (CFD) study, conducted on the Manzanares prototype, specifically examined the effects of optimal sizing and energy storage under the climatic conditions of Isfahan, Iran. Their findings revealed that doubling the collector radius from 122 m to 244 m resulted in a substantial increase in power output, from 42 kW to 126 kW. However, this expansion led to a 35% reduction in efficiency, from 0.68% to 0.44%, indicating that beyond an optimal size, larger collector radii could detrimentally affect performance. Furthermore, the study showed that at a collector height of 2 m, the system achieved a power output of 44 kW with an efficiency of 0.68%. In contrast, raising the height to 3 m caused an 11.4% decrease in power output (dropping to 35.96 kW) and a 17.64% reduction in efficiency (falling to 0.56%), implying that higher collector heights negatively impact the system's overall performance. Additionally, adjusting the collector slope to 2° resulted in a significant 55% increase in power output, from 44 kW to 70 kW. This adjustment also improved the airflow and the amount of air passing through the system (mass flow rate), leading to a corresponding increase in overall system efficiency.

Esfidani et al. [18] further explored the influence of design parameters on SCPP performance, utilizing a mathematical model based on the Manzanares pilot plant. Their study corroborated the findings of Karimi-Pour-Fard and Beheshti, demonstrating that increasing the collector radius, while maintaining an ambient temperature of 300 K, increased power output but led to a reduction in efficiency. Specifically, at a radius of 122 m, the system efficiency was 0.53%, which decreased by 40% to 0.31% when the radius was expanded to 240 m. In addition, the authors observed that increasing the collector height in a non-inclined configuration resulted in decreased power output and efficiency. At the reference height, the system achieved an efficiency of 0.79% with a power output of 298kW. However, when the height increased to 4 m, efficiency dropped by 26.6% to 0.55%, and power output decreased by 29.1% to 211.29 kW, further emphasizing the detrimental impact of height increases.

Nouar et al. [19] conducted an analysis of SCPP systems using a theoretical model they developed. They applied the model to simulate the climatic conditions of Algeria, using

the geometric parameters of the Manzanares prototype, to estimate the power output. Their results indicated that during June, a SCPP system with a 100 m collector radius would produce approximately 71 kW of power, while a 122 m prototype radius would increase the output to 106 kW. For a 200 m collector radius, the power output would surpass 260 kW.

In a similar vein, Koonsrisuk et al. [20] analysed the Manzanares prototype using both mathematical and CFD models. They investigated the effect of the chimney height-to-collector radius squared ratio and found that increasing the radius from 122 m to 244 m resulted in a 30% increase in mass flow rate, leading to a power output of 165 kW. This reinforces the notion that collector radius expansion plays a critical role in enhancing mass flow rate and power output. Ikhlef and Larbi [21] extended these findings by utilizing a numerical model of the Manzanares prototype to simulate the effects of energy storage on SCPP performance under Algerian climatic conditions. Their results showed that increasing the collector radius from 120 m to 240 m quadrupled the power output, from 50 kW to 200 kW, reinforcing the positive correlation between collector radius and power generation (Fig II.1). Additional studies also support this trend, confirming that larger collector radii consistently yield higher power outputs, further strengthening this observation [22, 23].

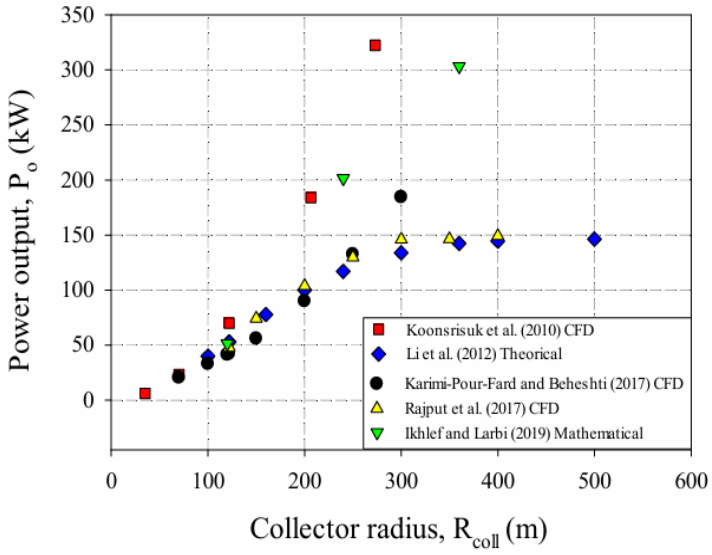

Figure II. 1: Evaluation of the effect of collector radius variation on the power output of the Manzanares prototype, as reported in the literature by Koonsrisuk et al. [20], Li et al. [23], Karimi-Pour-Fard and Beheshti [17], Rajput et al. [22], and Ikhlef and Larbi.

Ming et al. [24] conducted a 3D numerical analysis of the Manzanares prototype, showing that increasing the collector radius to 200 m raised the pressure difference from 167 Pa to 272 Pa. This increase led to an improvement in system efficiency from 0.71% to 0.75%.

Bhoraniye et al. [25] employed a CFD model to analyse how geometric parameters affect the performance of SCPP systems. Their analysis, based on the Manzanares prototype geometric parameters, indicated that increasing the collector radius to 320 m, under conditions of 1000 W/m² radiation intensity and 302 K ambient temperature, led to higher airflow and power output. However, they observed that a radius of 395 m was the optimal point for power generation, with no further performance gain observed with larger radii.

Dhahri et al. [26] used CFD analysis to study how geometric parameters affect the Manzanares pilot plant. With an ambient temperature of 293 K and 800 W/m² radiation, a 1 m collector height increased the temperature by 22.3°C with a mass flow rate of 949 kg/s. At 3 m height, the temperature rise dropped to 5.5°C, while the mass flow reached 1087 kg/s.

Gitan et al. [27] examined the influence of collector slope on SCPP performance in Malaysian climatic conditions, based on the geometric measurements of the Manzanares pilot facility. Their results indicated that a 10° collector slope produced the highest power output, which was 3.5 kW higher than that of the horizontal collector. They also found that the collector efficiency reached 51% of its maximum, while the system's overall efficiency was 0.16% of its maximum

Semai et al. [28] performed a numerical study using the geometric configuration of the Manzanares pilot plant to examine the effects of the collector structure and the integration of a thermal energy storage layer on the performance of a SCPP. The model was validated using experimental data from the Manzanares plant, while the simulations were conducted under the climatic conditions of Adrar, Algeria. The analysis includes two configurations: a converging collector with a lower inlet 2 m and higher outlet 4 m, and a diverging collector with a higher inlet 4 m and lower outlet 2 m. Results indicated that the convergent type collector achieved a 5% higher maximum power output than the non-inclined collector, with an efficiency peak of 0.45% at 17:00, and 18% higher than the non-inclined version.

Gholamalizadeh and Kim [29] investigated the effect of collector slope on SCPPs using a CFD model based on the geometric configuration of Manzanares pilot plant. With constant ambient conditions 300K, and 850 W/m² radiation, a 1.85 m inlet height resulted in a mass flow rate of 727.31 kg/s, an efficiency of 32.1%, and power output of 50.94 kW. Increasing the outlet height to 3 m improved mass flow to 759.63 kg/s, efficiency by 34.8%, and power output to 55.05 kW. However, increasing the outlet height further from 3 m to 5 m had minimal effect.

Hassan et al. [30] conducted a CFD study based on the Manzanares pilot plant's data to investigate the impact of the collector slope on the SCPP system. They claimed that increasing the collector slope would result in a higher airflow rate and improved mass flow in the system, assuming an ambient temperature of 303K on June 1st, 2016 at 13:00.

Ahirwar and Sharma [31] developed a CFD model based on the geometric dimensions of the Manzanares pilot plant. Their simulations indicated that the maximum power output occurred at a chimney height of 190 m when a ground heat flux of 500 W/m² was applied, with the chimney height varied between 180 and 205 m. They further investigated the effect of collector slope, considering discrete values of 10, 20°, 40°, 60°, and 80°. The results showed that, at a baseline performance of 37.084 kW output and 9.31 m/s chimney inlet velocity, increasing the slope to 40° would raise the inlet velocity by 13.69% to 10.38 m/s and the power output by 34.72% to 49.96 kW. Nevertheless, they claimed that further increases in slope would have a detrimental effect, ultimately reducing both chimney inlet velocity and power output.

Gholamalizadeh and Kim [32] performed a geometric optimization of SCPPs with a particular focus on the collector design. Using a multi-objective genetic algorithm, they evaluated the impact of key collector parameters namely, radius, inlet height, and outlet height on system performance. Their study demonstrated that incorporating an inclined collector roof significantly improves output, with an increase of up to 27.73% in the Manzanares prototype. The results showed that optimizing the collector geometry alone, such as adjusting inlet and outlet heights, plays a crucial role in enhancing the thermo-economic performance of SCPPs.

Choi et al. [33] studied the effect of collector radius and outlet height on the performance of large-scale SCPP using an analytical model. For a fixed chimney height of 1000 m, increasing the collector radius from 1500 m to 3000 m significantly enhanced the power output, from 51 MW to 109.5 MW. However, beyond this radius, the increase in power output became less significant, and further expansion led to decreased system performance. Additionally, when the collector entrance height was held constant at 5 m, a non-inclined collector produced 27.81 MW. By inclining the collector at a slope of 0.38 and raising the outlet height to 25 m, the power output increased to approximately 109.73 MW.

Ghalamchi et al. [34] investigated the effect of collector geometry and inlet height on the performance of SCPP. Their study revealed that increasing the collector diameter led to a

significant enhancement in power output. Specifically, they found that a 500-m high chimney, when paired with a 420 m diameter collector, generated 468 kW. In their small-scale experimental setup (Fig II.2), the authors also observed the influence of the inlet height, noting that an increase from 6 cm to 12 cm resulted in a reduction in air temperature, airflow rate, and power output, with the outlet height maintained at 6 cm.

Figure II. 2: The experimental work by Ghalamchi et al. [34].

Cottam et al. [35] designed a large-scale SCPP system featuring a 1000 m high chimney with a 55 m radius, and a 2150 m radius collector with a 4 m height entrance. Using a steady-state analytical model, they found that increasing the collector height from 4 m to 8 m led to a 30% increase in power output, rising from 48.92 MW to 63.59 MW. Additionally, they examined the impact of collector profiles on performance and demonstrated that exponential and sloped collectors outperformed non-inclined collectors in terms of power output. However, their study also revealed that, beyond a certain optimal point, increasing the collector outlet height caused performance to decline.

Toghraie et al. [36] conducted an investigation to assess the impact of geometric parameters on the performance of SCPP using a 3D CFD model under controlled environmental conditions (800 W/m² solar radiation and 308 K ambient temperature). Their results showed that a solar chimney with a 100 m chimney height with 8 m diameter, and a 25 m horizontal collector radius with a 2 m collector hight generated 14.25kW of power. Expanding the collector radius to 500 m increased power output by 1415 kW, However, the

efficiency decreased significantly, dropping from 0.003 at a height of 25 m to 0.00195 at 500 m, primarily due to the influence of the collector radius on the system's temperature distribution. Moreover, increasing the collector height reduced power output, efficiency and temperature. At a 1 m height, the system produced 82.5 kW, but at 10 m, power output decreased to 52.5 kW, accompanied by a drop in efficiency, highlighting the inverse relationship between height and performance.

Zhou et al. [37] conducted experiments on a small-scale SCPP model featuring an 8 m tall chimney with a 0.7 m diameter. Their findings revealed that increasing the collector radius at a constant radiation intensity of 850 W/m² significantly enhanced power output, rising from 2.087 W at a 2 m collector radius to 5.01 W at a 5 m radius an increase of approximately 140%.

Similarly, in another experimental study, Al-Azawiey et al. [38] analysed a prototype SCPP with a 6.3 m tall and 0.32 m diameter chimney, paired with collectors of 3 m and 6 m diameters. They observed that at similar radiation intensities (806–808 W/m²), the air velocity in the chimney increased from 1.56 m/s to 2.25 m/s when the collector diameter doubled, resulting in a 44.23% enhancement in airflow rate.

Larbi et al. [39], employing a mathematical model, assessed the potential of an SCPP system in Algeria's Adrar region, known for its high solar radiation levels. They projected that a system with a 200 m tall and 10 m diameter chimney, coupled with a 500 m diameter collector, could generate between 140 and 200 kW annually. At a constant irradiance of 800 W/m² and an ambient temperature of 30°C, increasing the collector diameter from 444 m to 690 m could boost power output by 140%, from 142 kW to 342 kW.

Zhou et al. [40] developed a mathematical model to evaluate an SCPP located on the Qinghai–Tibet plateau. Their analysis indicated that a system with a 1000 m tall and 80 m diameter chimney, coupled with a 5650 m diameter collector, could produce 100 MW of power under an 800 W/m² radiation intensity and a 20°C atmospheric temperature. Moreover, at the same conditions, a smaller collector with a 1750 m diameter yielded 10 MW, while a 3935 m diameter collector increased the output to 50 MW, demonstrating a fourfold improvement.

Hamdan [41] assessed the performance of SCPP systems, comparing a constant density model with a more realistic numerical discrete model that accounts for density

variations in the chimney. Their analysis indicated that an SCPP system with a 1000 m tall chimney and a 100 m diameter would yield a 35 MW power output when paired with a 1412 m diameter collector, under conditions of 263 W/m² radiation and an ambient temperature of 303 K. If the collector diameter were increased to 1778 m, the power output would rise to 50 MW.

Gholamalizadeh and Mansouri [42] conducted an in-depth numerical analysis of SCPP systems. Their results demonstrated that increasing the collector diameter from 40 m to 80 m, while maintaining a 60 m tall and 3 m diameter chimney at 800 W/m² radiation, would increase the mass flow rate by approximately 43%, and boost power output by 233%. They also highlighted that enlarging the collector diameter could reduce the energy unit cost.

Guo et al. [43] explored the performance of a large-scale SCPP system proposed for Hami, China, utilizing a comprehensive theoretical model. Their analysis reveals that an SCPP system with a 1000-m tall chimney and a 120 m diameter could generate 100 MW of power with a 5500 m diameter collector, under 1000 W/m² radiation and a 300 K ambient temperature. Furthermore, increasing the collector diameter to 8000 m would enhance power output by 51%, reaching approximately 151 MW under identical conditions.

Ngala et al. [44] developed a mathematical model to evaluate the performance of an SCPP system in semi-arid regions of Nigeria, considering the effects of geometric and environmental factors. They concluded that an SCPP with a 700 m high, 10 m diameter chimney could produce 3900 MW of power with a 300 m collector diameter under 800 W/m² radiation and 35°C temperature. Additionally, they projected that increasing the collector diameter to 600 m would increase the power output to 15600 MW. The system was also predicted to generate an average of 3000 MW per month year-round with a 700 m collector diameter.

Khelifi et al. [45] created a mathematical model based on one-dimensional heat and mass transfer to optimize and evaluate SCPP systems. They claimed that an SCPP model with a 100 m high chimney could produce 0.25 MW of power with a 150 m radius collector under 1000 W/m² radiation and an ambient temperature of 298 K. Increasing the collector radius to 300 m would raise the power output to 1 MW under the same conditions.

Kalantar and Zare [46] estimated the potential power output of an SCPP system in Yazd, Iran, using a 3D, five-degree CFD model based on the Manzanares prototype geometric

parameters. Their analysis revealed that with a 60 m collector radius, the power output would be 28 kW. With a 240 m collector radius, the power output would exceed 110 kW, representing a fourfold increase compared to the reference geometry.

Najmi et al. [47] evaluated the performance of SCPP systems using a MATLAB code they developed. Their analysis, based on measurements from the Kerman prototype, indicated that a collector height of 1.5 m resulted in a temperature difference in the system that was 1°C higher than when the collector height was 2 m.

Ayadi et al. [48] developed a CFD model to study the impact of collector height on the temperature, pressure, and velocity distributions. They investigated collector heights of 0.05, 0.10, 0.15, and 0.20 m. Their results showed that increasing the collector height at an ambient temperature of 306 K and under constant radiation of 800 W/m² led to a reduction in the chimney inlet velocity from 2.4 m/s to 1.85 m/s, which in turn caused a 33% decrease in the power output.

Kasaeian et al. [49] developed a small-scale experimental SCPP system (Fig II.3) with a fixed collector outlet height of 1 m to investigate the influence of varying the collector inlet height on system performance. They observed that when the collector inlet height was 5 cm and the ambient temperature was 25°C, the chimney entrance velocity was 2.78 m/s. However, when the inlet height was raised to 15 cm, the entrance velocity decreased by 16%, and the chimney temperature decreased from 47.16°C to 38.57°C.

Figure II. 3: The experimental SCCP of Kasaeian et al. [49].

Ayadi et al. [50] conducted a CFD analysis to explore the impact of different collector slopes 1°, 1.5°, and 2° on SCPP performance, using a collector with a diameter of 2.75 m and a height of 0.05 m, alongside a chimney with a 0.16 m diameter and a height of 2.75 m. They highlighted that a divergent collector had a negative effect on the system at a constant radiation of 800 W/m², as compared to a non-inclined collector. They reported that the maximum air velocity in the horizontal collector was 2.13 m/s, which decreased to 1.89 m/s with a 1° divergent slope. In contrast, the convergent collector design increased the air velocity, reaching 2.31 m/s at 1° and 2.36 m/s at 1.5°, both higher than the non-inclined configuration. Similar trends were observed in the temperature and pressure distributions.

Al-Kayiem and Al-Nakeeb [51] assessed the effect of the collector slope on collector efficiency over four different seasons using the finite difference method. They found that a 1° convergent collector was 124% more efficient in winter and 57.4% more efficient in summer compared to a horizontal collector.

II.2.2 Research review on chimney

The chimney, analogous to the collector, represents a critical structural element within the SCPP, with parameters such as height, radius, and geometric configuration playing a pivotal role in determining the system's performance.

Karimi-Pour-Fard and Beheshti [17] analysed the performance of the Manzanares SCPP under Iranian climatic conditions using Ansys Fluent software, focusing on the effects of chimney height and diameter. Their results showed that increasing chimney height up to 685 m improved both power output and efficiency, but further height increases led to a decline in performance. At 200 m, the system produced 40.35 kW and 0.66% efficiency, while at 400 m, power output increased to 60.85 kW and efficiency to 0.98%. Additionally, the study found that a chimney radius of 6.17 m yielded the highest power output of 45.48 kW, a 3.7% increase compared to the reference radius value, and improved system efficiency by 4.5%, reaching 0.69%.

Ikhlef and Larbi [21] examined an SCPP system comparable to the Manzanares prototype in Algeria climatic conditions and concluded that raising the chimney height significantly enhances performance. For instance, at a chimney height of 200 m, the system could generate 52.5 kW, while at 300 m chimney height, the power output would increase to 111.66 kW.

Similarly, Dhahri et al. [26] investigated the mass flow rate of the Manzanares pilot plant under stable conditions, including an ambient temperature of 293 K and solar radiation of 800 W/m². They observed that the mass flow rate, initially 1075.56 kg/s at 200 m, would rise by 13.4%, reaching 1220 kg/s at 300 m.

Shahi et al. [52] developed a CFD model based on the Manzanares SCPP project geometry and highlighted the benefits of increased chimney height. At 1000 W/m² irradiance and 291.65 K ambient temperature, they calculated a power output of 48.04 kW. With a chimney height of 400 m, the power output surged by 138%, reaching 114.35 kW, while the mass flow rate rose by 30%, attaining 1038.59 kg/s.

Cuce et al. [53] analysed the influence of chimney height on the performance of the Manzanares SCPP. Their results demonstrated that increasing the height enhanced power output, efficiency, mass flow rate, and pressure difference while reducing temperature gains in the collector. This effect was observed for chimney heights ranging from 100 to 500 m under radiation intensity of 1000 W/m² and ambient temperature of 293.15 K. Based on numerical models,

Similar results were observed, as several studies that also utilized the dimensions of the Manzanares prototype confirmed that increasing the chimney height leads to a marked improvement in the power output [19, 20, 23, 54].

Xu and Zhou [55] conducted CFD simulations of SCPP based on the Manzanares pilot plant's geometry. They investigated the system's performance by varying the chimney outlet to the inlet area ratio (AR), which represents the degree of divergence, over a wide range of values. Their study involved calculating the total pressure potential, which combines buoyancy forces and static pressure recovery, using an effective pressure potential recovery coefficient. The results showed that maximum performance was achieved at AR of 8.7, where the power output increased by a factor of 10.9, reaching 231.7 kW compared to the reference case. However, when the AR exceeded 8.7, reverse flow occurred within the chimney, leading to reductions in both airflow velocity and power output, thereby degrading overall system performance.

Hu et al. [56] developed a CFD model to study the impact of varying the ratio between the chimney's exit and entrance areas on the performance of solar chimneys. Using the dimensions of the Manzanares pilot plant as a reference, they explored the varying of AR

from 1 to 32. They concluded that an AR of approximately 10 was optimal for the pilot plant, yielding the highest system performance. They also noted that exceeding this AR led to a decline in performance. For chimney heights of 100 m, 200 m, and 300 m, they provided normalized results correlating AR with divergent chimney angles, emphasizing that increasing AR beyond the peak value negatively impacted performance.

Hassan et al. [30] numerically investigated the effect of divergent chimney angles on the Manzanares pilot plant. The cylindrical reference case yielded 34 kW, whereas a 1° divergence produced the highest output of 70 kW. Increasing the angle to 2° and 3° resulted in 65 kW and 59 kW, respectively, with larger angles causing further efficiency losses.

Ahirwar and Sharma [31] identified that for a chimney height of 190 m, based on the Manzanares pilot plant's dimensions, increasing the chimney's inclination angle improved power output. Specifically, they reported that setting the angle to 6° could increase power output by 95%, from 37.08 kW in a non-inclined setup to 72.33 kW.

Similar investigations have been conducted on variations in the chimney's geometric configuration and their effects on system performance, with the primary distinction being the use of a different geometry compared to Manzanares.

Choi et al. [33] performed an analytical study of a large-scale SCPP system, which featured a 100 m radius chimney and a 3000 m radius collector, operating under constant conditions of 1000 W/m² radiation intensity and 20°C ambient temperature. Their results indicated that increasing the chimney height resulted in a significant rise in power output. Specifically, with a chimney height of 500 m, the power output was 42.25 MW, and at 1000 m, the power output increased by 160%, reaching 110 MW. Additionally, they demonstrated that while enlarging the chimney diameter initially led to an exponential increase in power output, this effect began to diminish after a certain point.

Toghraie et al. [36] developed a 3D CFD model for a SCPP with a 100 m collector radius and an 8 m chimney diameter. Their findings indicated that increasing the chimney height, while keeping the radiation intensity constant at 800 W/m² and the ambient temperature at 308 K, resulted in enhanced power output, efficiency, pressure difference, and mass flow. Specifically, the power output increased from 24 kW at a 25 m chimney height to 313.5 kW at a 500 m chimney height. Moreover, their investigation of the chimney diameter revealed that both power output and efficiency peaked at a specific diameter, with further

increases leading to diminishing returns and negatively affecting system performance, including mass flow and pressure.

Zhou et al. [37] examined the impact of varying chimney heights in a small-scale SCPP featuring a chimney with a diameter of 0.7 m and a collector radius of 5 m. Using a mathematical model based on experimental data under a constant solar radiation intensity of 850 W/m², they found that a 4 m chimney height produced 2.26 W of power. Doubling the chimney height to 8 m increased the power output by 118%, reaching 4.94 W.

In an experimental study, Kasaeian et al. [57] validated their numerical model against experimental data from a SCPP constructed with a 2 m chimney height. Their analysis indicated that increasing the chimney height to 3 m enhanced the system's performance, with airflow velocity improvements ranging from 4% to 25% under different conditions.

Bernardes et al. [27] introduced a combined analytical and numerical approach to assess solar chimney performance. The model predicted that a system with a 3.5 m entrance height and a 4100 m collector diameter, coupled with a chimney 1000 m tall and 120 m in diameter, could achieve a 50% performance improvement, producing 0.929 GWh daily. An increase of 100% in chimney height was predicted to elevate the daily generation to 2016 GWh.

Nizetic et al. [59] proposed a simplified model to calculate the power output of SCPP systems in the Mediterranean region. They showed that a chimney height of 200 m, coupled with a collector diameter of 1250 m at an ambient temperature of 288 K, resulted in a chimney efficiency of 0.69%. When the chimney height was increased to 1000 m, the efficiency rose to 3.41%.

Larbi et al. [39] evaluated the effects of varying chimney height and collector diameter on system performance. They designed a model with a 10 m diameter chimney and a 2.5 m collector height, which produced 342 kW under a constant radiation intensity of 800 W/m², a collector diameter of 600 m, a chimney height of 250 m, and an ambient temperature of 300 K. Increasing the chimney height to 483 m under the same conditions resulted in a 116.95% rise in power output, reaching 742 kW.

Sangi [60] evaluated the performance of an SCPP system proposed for various cities in Iran using a simplified numerical model that incorporated environmental and geometric factors. the results indicated a direct correlation between power output and both chimney

height and collector diameter, with significant power increases achieved when both parameters were scaled up.

Al Alawin et al. [61] simulated the impact of chimney height on an SCPP system under the geographic and climatic conditions of Jordan. They observed that increasing the chimney height led to improvements in airflow rate, pressure difference, efficiency, and volumetric flow rate for a system with a collector diameter of 40 m and a chimney diameter of 3.5 m. They also reported a corresponding rise in power output, with a maximum output of 85 kW achieved at a chimney height of 210 m. However, beyond this height, further increases in chimney height caused a decline in power output.

Hamdan [41] concluded that an SCPP system featuring a 100 m diameter chimney and a 2000 m collector diameter could generate 5.81 MW of power with a chimney height of 400 m under a radiation intensity of 263 W/m² and an ambient temperature of 303 K. Increasing the chimney height to 800 m would boost the power output by 179.8%, reaching 16.26 MW.

Ngala et al. [44] reported that an SCPP system with a collector diameter of 700 m and a fixed chimney diameter of 10 m could achieve a power output of 1500 MW with a chimney height of 300 m under ambient conditions of 350 K and a consistent solar irradiance of 800 W/m². Doubling the chimney height to 600 m would result in a 100% increase in power output, reaching approximately 3020 MW.

Khelifi et al. [45] showed that for a system with a 200 m chimney height, the power output would be 1852.57 kW, which would double to 3696.44 kW with a 400 m chimney height, indicating a linear relationship between height and power output.

Motoyama et al. [62] conducted laboratory-based experimental research and concluded that the air velocity in a divergent chimney (Fig II.4) design could be 50% higher than that of a cylindrical chimney under identical conditions. Furthermore, they observed that the rotational speed increased by 44.4% in the divergent chimney. Similarly, Ohya et al. [63] experimentally demonstrated that a divergent chimney structure (Fig II.5) could achieve a power output 4–5 times greater than that of a cylindrical chimney under comparable conditions.

By examining chimney angles of 2°, 4°, and 6°, they highlighted that the optimal airflow velocity and power output were achieved with a 4° design.

Figure II. 4: The divergent chimney realized by Motoyama et al. [62].

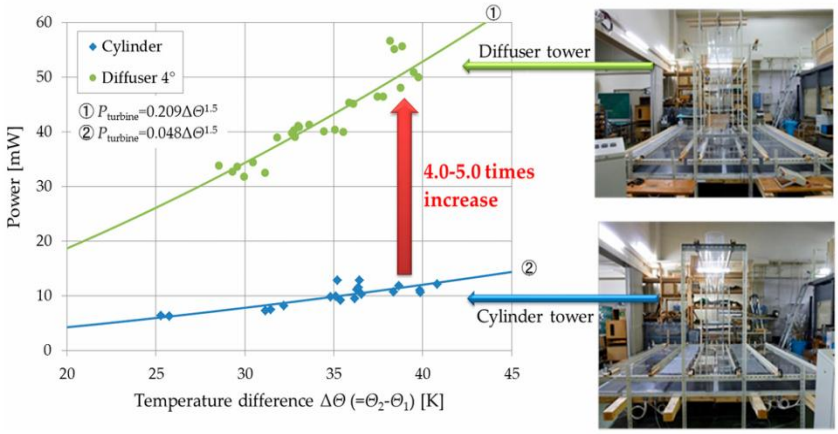

Figure II. 5: Experimental step by Ohya et al. [63].

Nasroui et al. [64] employed CFD to evaluate the performance of hyperbolic chimney models against cylindrical designs, using a scaled-down solar chimney model. Their findings revealed that the divergent design outperformed the cylindrical model in terms of temperature, pressure, and velocity distributions, leading to superior overall performance.

Al-Kayiem and Al-Nakeeb [51] compared divergent and convergent chimney designs with cylindrical ones using the Finite Difference Technique. They reported that the hydrothermal efficiency of a convergent chimney was double that of the other configurations across all seasons.

Pattanashetti and Madhukeshwara [65] analysed the performance of a solar chimney with a chimney height of 100 m and a collector radius of 100 m using a 1° isometric CFD

model. With a fixed inlet diameter of 4 m, they varied the AR by changing the exit diameter between 2.83 m and 16 m. Their results indicated that an AR of 9 yielded maximum performance, while higher AR values adversely affected the system. They also noted that designs could produce up to 100 times more kinetic energy under a radiation intensity of 800 W/m².

Ghorbani et al. [66] proposed a hybrid dry cooling tower with a chimney height of 200 m and a collector radius of 100 m. They found that incorporating a 1.5° divergent chimney angle increased airflow velocity over the radiators from 5.65 m/s to 6 m/s, marking a 6.2% improvement compared to a non-inclined design. Das and Candramohan [67] developed small-scale solar chimney models with heights of 7 m and 3.5 m using a 3D computational model. They assessed the performance of various chimney structures and determined that the optimal power output and airflow velocity were achieved with a 2° divergent chimney design. They noted that larger angles negatively impacted the system's efficiency.

Koonsrisuk and Chitsomboon [68] designed a solar chimney model with a 100 m high chimney, a 100 m radius, and a 2 m high collector, using computational fluid dynamics. They fixed the chimney inlet diameter at 4 m and performed simulations in various configurations by adjusting the AR, varying the exit radius between 2.83 m and 16 m. From their simulations using a 5° axial symmetric CFD model, they found that when the AR value was 16, the system's power output increased 94.29 times compared to the reference situation.

II.2.4 Research review on absorber surface

The absorber surface also plays a crucial role in the system's performance by efficiently absorbing solar radiation and storing the energy in the ground. The stored energy is then transferred to the system when sunlight is unavailable, which enhance the collector's power output. Researchers have investigated various surface modifications of the absorber and the utilization of different materials to enhance its performance.

Mandal et al [69] investigates the impact of a modified absorber surface featuring multiple triangular wavy peaks on the performance of a SCPP (Fig II.6). Using a 3D simulation with ANSYS Fluent, RNG k-ε turbulence modelling, and the discrete ordinates solar ray-tracing model, the research focuses on key performance indicators such as velocity, temperature, pressure, efficiency, power output, and exergy. The findings show that the wavy ground absorber surface outperforms the traditional flat ground absorber, with an increase in

wavy wall amplitude leading to a notable improvement in power generation. The maximum power generation increased by 58.61%, reaching 82.5 kW, and the efficiency improved by 61.83% are observed with higher amplitude single triangular wavy walls. The study also demonstrates that exergy utilization efficiency improves with wall undulations but decreases with increased amplitude. Mathematical correlations for key performance parameters are developed, and the proposed design could offer practical applications for SCPPs in hilly or uneven terrain, providing power to remote areas.

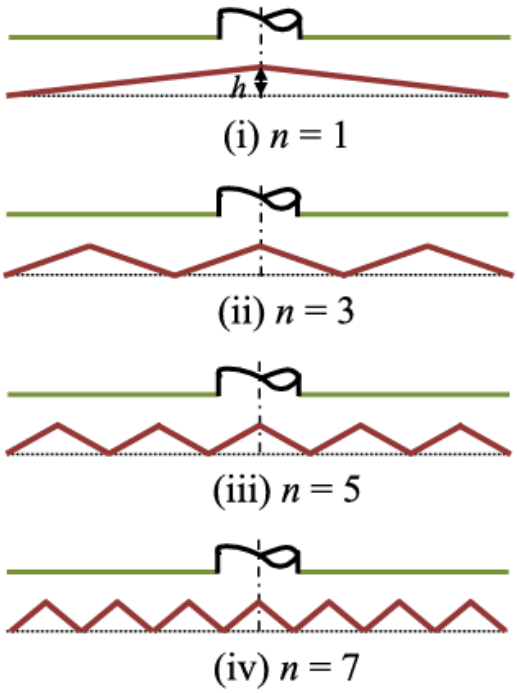

Figure II. 6: wavy triangular absorber configurations by Mandal et al [69].

Biswas et al. [70] investigates the use of a stair-shaped ground surface (Fig II.7) in a SCPP to improve efficiency. Using a finite volume method-based solver, the study analyses the plant's performance for varying dimensions of the stair-shaped absorber. The results show that the stair-shaped absorber can increase power generation by up to 80%, with power output improving from 51 kW to 92 kW, compared to a flat ground surface. The sloped ground absorber generates 82 kW, approximately 19% less than the stair-shaped absorber. Although the chimney's exergy efficiency increases with stair height, this enhancement has a negligible effect on the system's overall exergy efficiency.

Cuce et al [71] investigates the impact of ground slope on the performance of SCPPs (Fig II.8). Using ANSYS FLUENT, a 3D model based on the Manzanares pilot plant's geometry is developed with the discrete ordinates solar ray tracing algorithm and RNG k-ε

turbulence model. The analysis reveals that with a solar intensity of 1000 W/m², the maximum velocity inside the system is 14.2 m/s, which aligns closely with experimental data 15.0 m/s. The study examines performance with varying ground slopes 0.1° to 0.5°, showing that a 0.5° slope increases the maximum air velocity by 37%, reaching 19.51 m/s, and boosts power output by 17.7%, from 54.3 kW to 63.95 kW. This highlights the importance of sloping ground in enhancing turbulent effects and improving electrical power output in SCPPs.

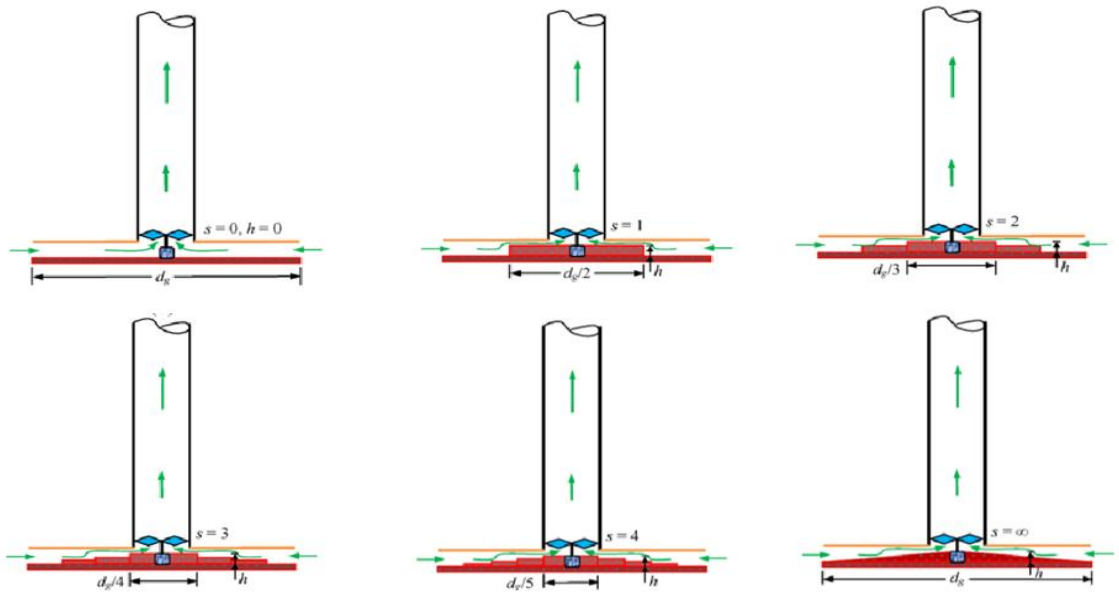

Figure II. 7: Different configurations absorber with stair-shaped by Biswas et al. [70].

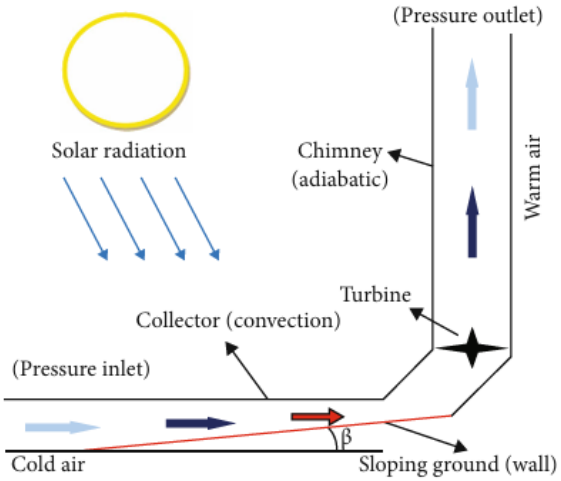

Figure II. 8: sloping ground configurations absorber by Cuce et al. [71].

Atia et al [72] investigates the effect of different absorber surface shapes on the performance of SCPPs. The research explores several absorber configurations; including right

triangle, equilateral triangle, rectangle, and semi-circle (Fig II.9), while also examining the impact of absorber surface height. The modelling of heat transfer and fluid flow within the chimney is based on conservation equations, with the finite volume method applied to solve the equations using ANSYS Fluent software. The model is validated through comparison with experimental data, demonstrating good agreement. The results indicate that the rectangular-shaped absorber with height of 7.5 cm produces the highest power generation, with a significant increase of up to 67.4% compared to the baseline flat-chimney absorber. The study highlights that increasing the absorber surface height improves both velocity and temperature within the system.

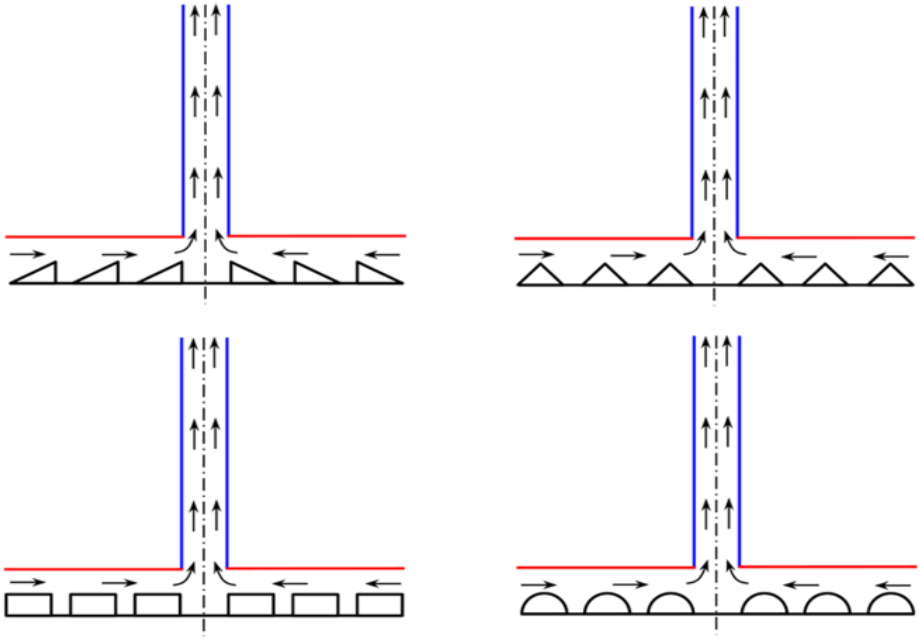

Figure II. 9: Modified absorber surface cases by Atia et al. [72].

Cuce et al. [73] proposes a novel ground design for SCPPs to enhance energy storage and improve airflow from the collector to the chimney. By inclining the ground at a distance of 21 m from the chimney inlet (Fig II.10 a), the design boosts air movement. CFD analyses using ANSYS Workbench, based on the Manzanares pilot plant dimensions, is performed with RNG k-ε turbulence and DO solar ray tracing models. The results, verified with experimental data, show a 34.1% increase in air velocity from 14.202 m/s to 19.046 m/s and a 23.04% increase in power output from 54.333 kW to 66.855 kW.

Mandal et al [74] examines the influence of ground absorber slope and various chimney shapes on the performance of a SCPP (Fig II.10 b).

The findings reveal that the combination of a ground absorber slope angle of 0.6 degrees and a divergent chimney leads to substantial improvements in power generation, with a significant increase of up to 80%, reaching 92 kW, compared to the traditional Manzanares SCPP.

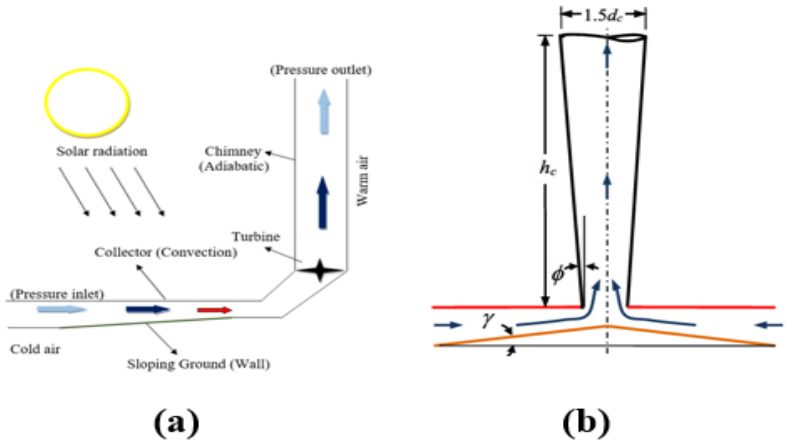

Figure II. 10: Différent absorber plate configuration for SCPP system (a) Cuce et al [73] (b) Mandal et al [74].

II.2.4 Research review on the SCCP turbine

In addition to the collector, chimney, and absorber surface, the turbine constitutes a key element of a SCPP and serves as the only moving part within the system. Its efficiency is directly influenced by key design parameters, including its configuration, placement, and the number of turbines used, factors that are essential for optimizing the plant's overall performance.

In the first experimental SCPP, the Manzanares Solar Chimney was equipped with a four-bladed horizontal-axis turbine, installed approximately 9 meters above ground level at the base of the chimney. This position was deliberately selected to align with the region of maximum air velocity, produced by the pressure differential induced by the upward movement of heated air. During operation, the turbine experienced airflow velocities of approximately 9 m/s under load, reflecting conditions where the turbine actively generated power and encountered mechanical resistance. In contrast, during startup (no-load condition), airflow velocities reached up to 15 m/s due to the absence of load, resulting in reduced mechanical resistance. The turbine had a nominal power output of 50 kW.

Subsequent research by T.P. Fluri and T.W. von Backström [75] examined various turbine configurations for large-scale SCPPs to evaluate their energy performance and

efficiency. Their study compared three designs: a single vertical-axis turbine, multiple vertical-axis turbines, and multiple horizontal-axis turbines (Fig. II.11). The findings demonstrated that high efficiency could be maintained across operational ranges with a well-optimized turbine, particularly when equipped with a variable-speed drivetrain. Among the configurations, the single vertical-axis turbine exhibited slightly superior efficiency and energy yield, primarily due to reduced aerodynamic losses. However, this design also produced high torque, raising concerns regarding the cost and complexity of the required drivetrain. Furthermore, the study confirmed the widely accepted turbine efficiency of approximately 80% and emphasized that further performance improvements could be achieved through careful aerodynamic optimization of flow passages.

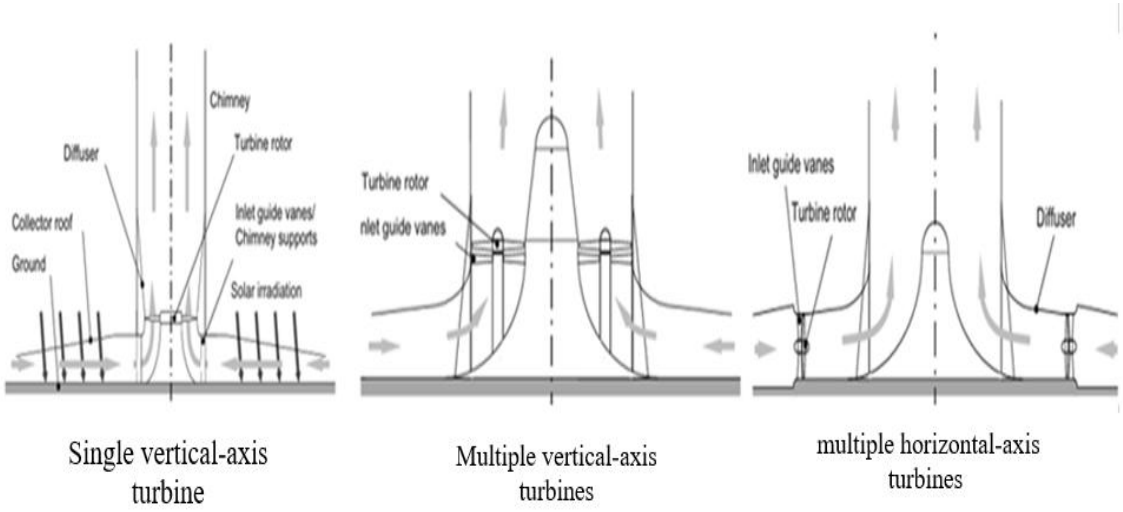

Figure II.11: Schematic illustration of the different turbine configurations used in a SCPP [75].

Tingzhen et al. [76] conducted numerical simulations on SCPPs integrated with turbines, dividing the system into three regions: the collector, chimney, and turbine. Using the Spanish prototype as a case study, they analysed a 3-blade turbine configuration, demonstrating a peak power output slightly above 50 kW. Their study also investigated the impact of turbine rotational speed on chimney outlet parameters, confirming the validity of their numerical approach.

Additionally, they designed and simulated a large-scale MW-class SCPP with a 5-blade turbine (Fig II.12), revealing a maximum power output of 10 MW and a turbine efficiency of 50%. These findings provide valuable insights for optimizing turbine design in large-scale SCPP applications.

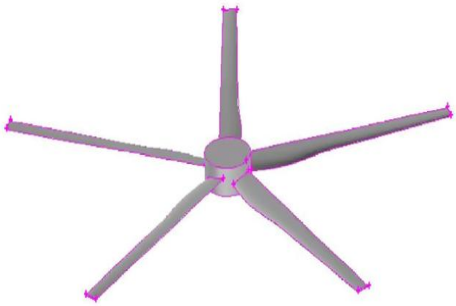

Figure II. 11: Schematic view of turbine configurations proposed by Tingzhen et al [76].

Zuo et al [77] introduced an air turbine design approach for SCPP, drawing inspiration from axial flow hydraulic turbines and axial-flow pump impellers. The proposed method optimizes the turbine pressure drop ratio to enhance performance. To validate its effectiveness, three-dimensional numerical simulations were conducted for the Spanish prototype system, incorporating the newly designed turbine impeller as illustrate in Figure II.13. The findings demonstrated that this method significantly improves turbine performance, with a maximum power output of 53.49 kW, representing a 30.46% increase over the original Spanish prototype. The study further highlighted that the pressure drop and pressure drop ratio reached 178.63 Pa and 0.95, respectively, which contributed to a substantial improvement in available power. Moreover, solar radiation levels influence turbine efficiency, with higher radiation increasing the range of rotational speeds at which the turbine operates efficiently.

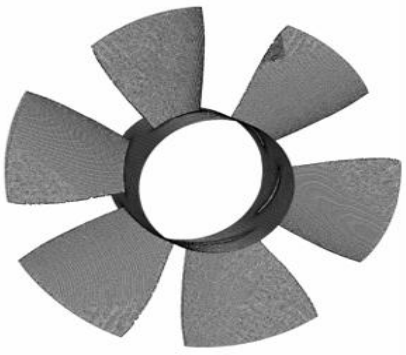

Figure II. 12: Turbine designed by Zuo et al [77].

Caicedo et al [78] investigated the feasibility of using a radial inflow (RIF) turbine in SCPP to address the challenge of manufacturing cost-effective turbines. Unlike conventional axial turbines, the proposed design features straight blades to minimize flow restrictions and improve efficiency. The study utilized 3D CFD simulations incorporating the RNG k-ε turbulence model and a discrete ordinates radiation model to evaluate the turbine's performance within the Manzanares prototype. Three turbine designs were analysed (Fig II.14). The third design was identified as the optimal configuration, delivering a peak power output of 77.7 kW at 15 rpm under a solar radiation intensity of 850 W/m², thereby exceeding the power output of the original axial turbine by more than 40 kW.

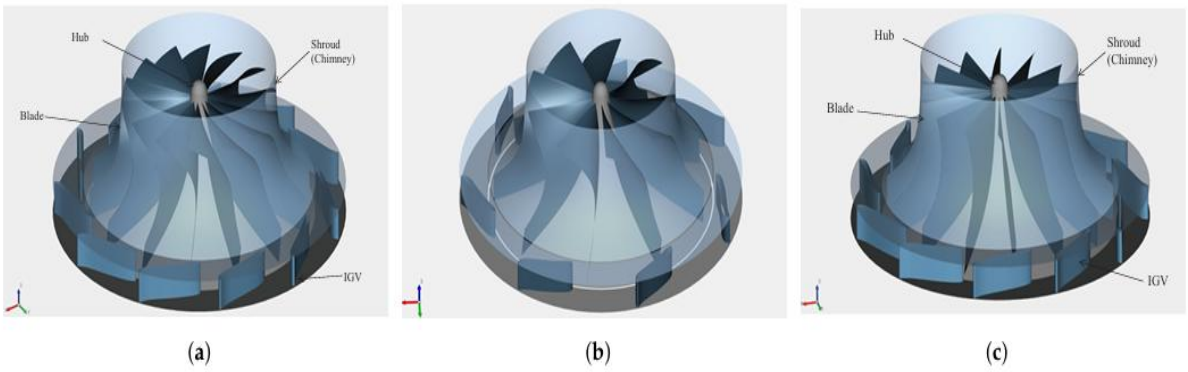

Figure II. 13: Schematic of the proposed radial turbine (a) First design; (b) second design; (c) third design [78].

Kasaeian et al. [79] developed a mathematical model to describe airflow through the turbine of an SCPP and conducted a 3D CFD simulation of the Manzanares prototype, incorporating turbine blades. The numerical results were validated against experimental data, ensuring accuracy. A series of 12 simulations examined the effects of turbine rotational speed, blade count (Fig II.15), chimney height, and collector diameter on system performance. Findings indicated that increasing the rotational speed reduced air mass flow but enhanced torque and power. A higher blade counts also led to increased torque and power but reduced mass flow. Additionally, increasing chimney height and collector diameter improved air mass flow and power output.

The five-blade turbine achieved the highest power output of approximately 91 kW. These results provide key insights into optimizing turbine design for enhanced SCPP efficiency.

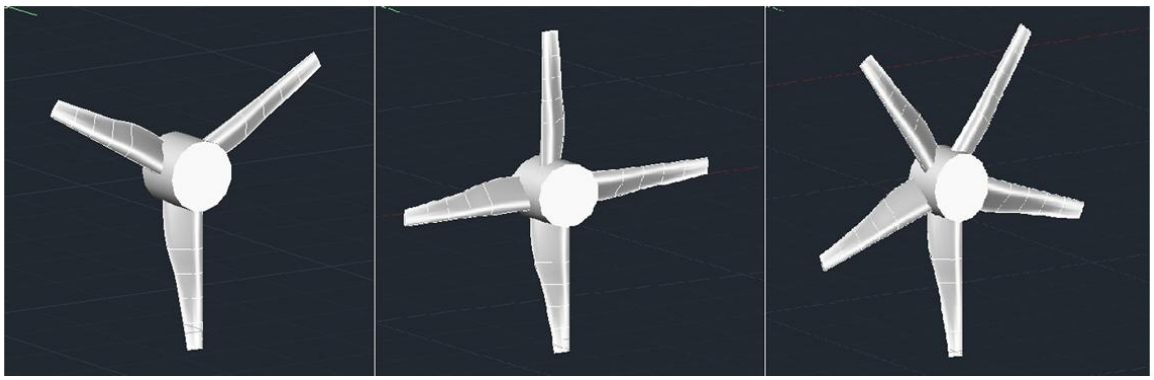

Figure II. 14: Design Models of Turbines with 3, 4, and 5 Blades [79].

II.3 Overview of Material Selection for SCPP Components

Material selection plays a critical role in the design and operational performance of SCPPs. The thermal behaviour, structural durability, and cost effectiveness of key components such as the collector cover, chimney, and absorber plate are significantly influenced by the materials used in their construction. Based on a comprehensive review of both experimental and numerical investigations, the most commonly utilized materials for each component have been identified and are summarized in the following tables.

II.3.1 Collector Cover Materials

Table II.1 shows the most commonly used materials for the collector cover in SCPP studies. These materials are mainly divided into two groups: plastics and glass. Plastic materials such as general plastic, polyethylene, Perspex, and acrylic glass are widely used, especially in small-scale or experimental systems, because they are lightweight, cheap, and easy to install. On the other hand, glass materials are also frequently used due to their better thermal and optical properties. Among all the glass types, acrylic glass appears to be the most commonly selected.

This pattern shows that researchers often choose materials based on a balance between performance and practical considerations like cost and availability.

Table II. 1: The most common collector materials used.

Studies	Materials
Haaf et al. [7] Hassan et al. [30] Kasaeian et al. [49] Mekhail et al. [92] Mandal et al [93] Azizi et al. [95]	Plastic
Das et al. [80] Zaho et al. [94] Ikhlef et al [96] Shabahang et al [97] Esmail et al [98]	glass
Al-Azawiey et al. [38]	Perspex
Ghalamchi et al. [34] Ghalamchi et al. [84]	soda lime glass
Al-Kayiem et al. [86] P. N. Belkhode et al.[88] Khadersab et al [89]	acrylic glass
Lal et al. [87]	Transparent polyethylene
Balijepalli, et al. [90]	glazed glass
Naceur et al. [91]	polyethylene

II.3.2 Chimney Materials

Table II.2 lists the most commonly used materials for chimneys in SCPP research. Concrete is the most frequently reported material, particularly in large-scale or pilot systems, due to its high structural strength, low cost, and favourable thermal properties. In contrast, lightweight materials such as PVC and polycarbonate are commonly selected for small-scale or laboratory models because they provide acceptable thermal and mechanical performance at a very low cost, making them ideal for low-budget experimental setups.

Steel is also employed in some cases for its mechanical robustness and resistance to high temperatures. Overall, the choice of chimney material reflects a balance between thermal performance, mechanical stability, and practical construction considerations.

Table II. 2: The most common chimney materials used.

Studies	Material
Haaf et al. [7] Ikhlef et al [96]	Concrete
Ayadi et al. [48] Shabahang et al [97] Naceur et al. [91] Hassan et al. [30] Mekhail et al. [92] Azizi et al. [95]	PVC
Ghalamchi et al. [34] Rabehi et al. [83]	Polycarbonate
Esmail et al [98]	steel

II.3.3 Absorb plate Materials

Table II.3 outlines the various materials used for absorber plates in SCPP systems, reflecting a wide range of thermal and practical considerations. Traditional ground surfaces remain a common choice in early or simplified models due to their accessibility and passive heat storage capabilities. Metal plates such as steel, aluminium, copper, and iron are frequently employed in experimental setups for their high thermal conductivity, which enhances heat transfer to the airflow within the system. In contrast, non-metallic materials such as gravel, sand, chipboard wood, granite, and concrete have also been investigated for their thermal mass, availability, and suitability for passive solar heating.

The diversity of materials reported highlights the experimental interest in balancing conductivity, thermal inertia, cost, and local availability in absorber plate design.

Table II. 3: The most common absorber plate materials used.

Studies	**Material**
Haaf et al. [7]	Ground surface
Mandal et al [93]	Steel
Ghalamchi et al. [34] Naceur et al. [91]	Aluminium plate
Das et al. [85] Balijepalli, et al. [90]	Copper plate
Khadersab et al [89]	iron sheets
P. N. Belkhode et al.[88] Ikhlef et al [96] Zaho et al. [94]	Gravel and sand
Ayadi et al. [48]	Chipboard wood
Cao et al. [81]	Granite
Nasirivatanetal. [82]	Concrete

Figure II.16 compiles several of the most referenced small-scale experimental SCPP prototypes. This visual comparison highlights the diversity in design choices, particularly in terms of chimney height, collector slope, overall structural configuration, and the materials used, as explored across different studies.

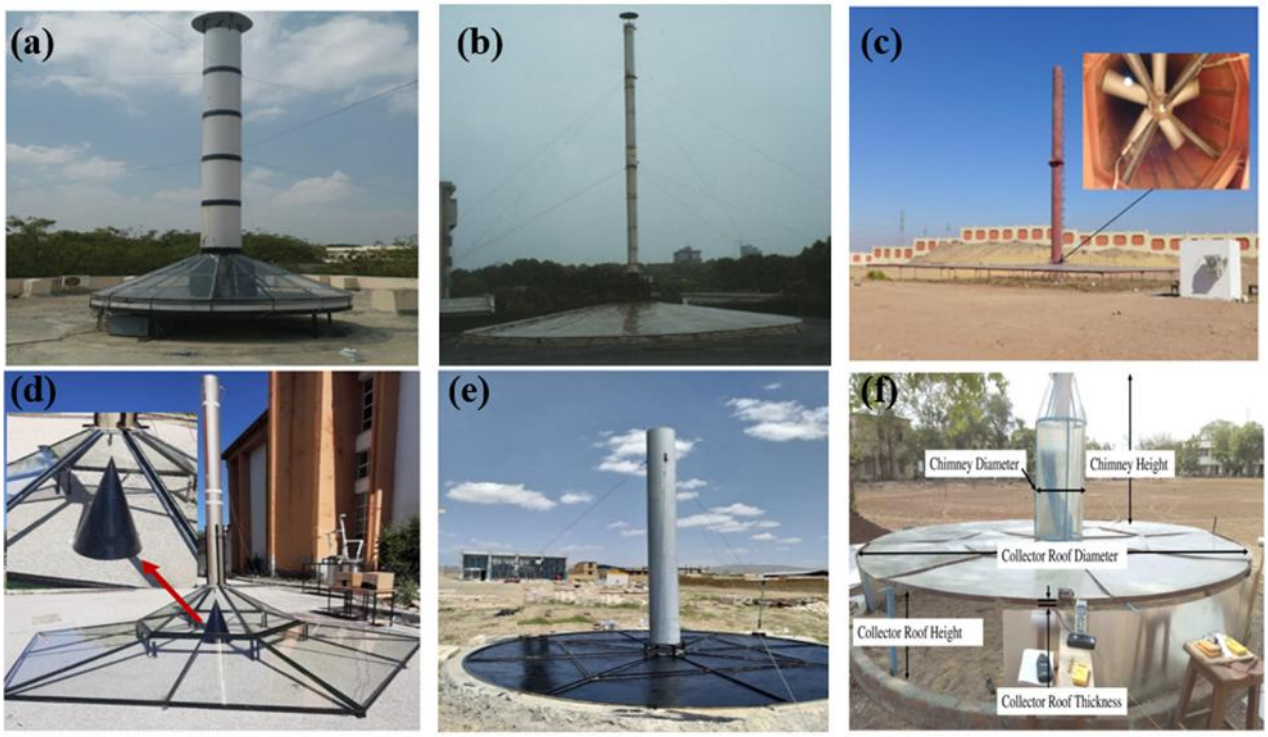

Figure II. 15: Experimental works on Solar Chimney Power Plants:(a) Balijepalli, et al. [90]) (b) Zaho et al. [94] (c) Esmail et al [98] (d) Ikhlef et al [96] (e) Shabahang et al [97] (f) P. N. Belkhode et al. [88].

II.4 Advanced Strategies for Solar Chimney Power Plants

Researchers have investigated various strategies to enhance the efficiency of SCPPs. Among these, integrating SCPPs with other renewable energy systems has proven effective in forming hybrid configurations that not only maximize energy output but also improve system reliability. Furthermore, the application of SCPPs in alternative domains extends their functional scope beyond traditional power generation, contributing to improved efficiency and long-term sustainability.

In this context, Eryener and Kuscu [99] conducted an experimental study on a hybrid solar updraft tower system that integrated a transpired solar collector with PV panels, covering 42% of the collector surface. The system, installed at Trakya University in Turkey, enabled

ambient air to enter through perforations in the transpired collector, where it was preheated before rising through the tower to generate electricity. The experimental setup consisted of 28 PV panels, each with a rating of 265 W, mounted on a polycarbonate sheet that allowed sunlight to reach the ground surface. The system layout is shown in Figure II.17. To evaluate the system's thermal and aerodynamic performance, measurements of temperature, humidity, velocity, and pressure were conducted at critical points, including beneath the collector, at the tower inlet, and near the turbine. Data acquisition was performed continuously using an automated monitoring system, and thermal imaging was utilized to assess the surface temperature distribution. The experimental results indicated a 2% increase in efficiency compared to standalone PV modules, along with a 16–18% enhancement in hybrid power generation efficiency over conventional solar updraft tower configurations.

Figure II. 16: Hybrid SCPP Configuration with PV Collector Integration by Eryener and Kuscu [99].

Huang et al. [100] investigated a hybrid SCPP with photovoltaic cells to enhance air purification (Fig II.18). The system included a 205.5 cm chimney height and a 260 cm collector diameter, tested in a room with rock wool panels and a glass wall. A solar simulator and various sensors monitored environmental conditions and airflow. Covering 50.60% of the acrylic glass with PV panels reduced airflow by 14% but significantly increased electric power generation. This hybrid setup improved solar power efficiency by 16–18% compared to conventional designs.

Ouahrani et al. [101] examined the performance of a hybrid SCPP at Ouargla University by integrating a geothermal hot water pipe spirally within the collector, as illustrated in Figure II.19. The system, featuring an 8 m chimney height and a 12 m collector diameter, aimed to sustain power generation at night. Hot water at 80 °C with a flow rate of 3

L/s was supplied through a 0.016 m tube diameter. During the day, solar heating alone raised temperatures to 68.3 °C with air velocities of 5.8 m/s, while combining solar and geothermal heating increased temperatures to 80 °C and air velocities to 7.1 m/s. This approach enhanced power generation, demonstrating geothermal heating's potential in hybrid SCPPs.

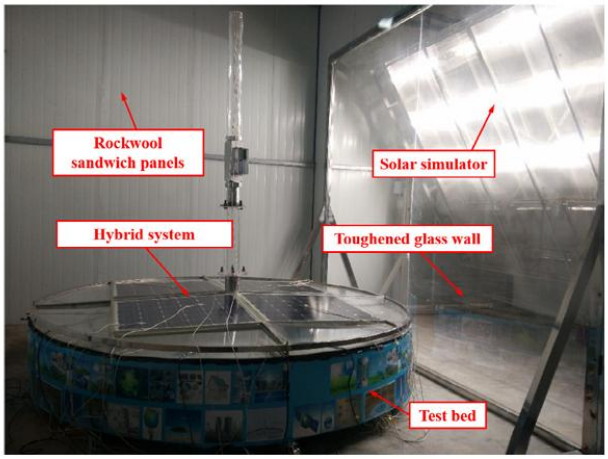

Figure II. 17: Configuration of the Hybrid SCPP-PV System by Huang et al. [100].

Figure II. 18: Configuration of the Hybrid SCPP with Geothermal Integration by Ouahrani et al [101].

Aliaga et al. [102] introduced a novel SCCP system incorporating a heat exchanger, which included a chimney, solar mirrors, and the heat exchanger itself. In this setup, the solar mirrors concentrated solar energy, which was then transferred via the heat exchanger to warm the air, generating additional driving force for the turbine. When scaled to a plant in Spain, the system was projected to produce 53 kW of power. The heat exchanger demonstrated an efficiency of 73%, representing a 59% improvement over traditional systems, with a power density of 1.7 W/m². The overall thermal efficiency of the modified system was found to be 0.17%.

Shahdost et al. [103] explored a hybrid SCPP model that uses exhaust gases from a fossil-fuel power plant as the heat source, eliminating the need for a traditional collector. The system, featuring a 3 m high chimney with a 10 cm diameter (Fig II.20), achieved enhanced fluid flow due to the buoyancy effect created by the hot exhaust gases. Temperature and velocity measurements were conducted using thermal sensors and hot wire devices. This approach not only improved power generation and efficiency but also reduced capital costs and enabled nighttime electricity production.

Figure II. 19: Pilot Hybrid SCPP Using Exhaust Gases by Shahdost et al. [103].

Zuo et al. [104] investigated a hybrid SCPP integrated with a distillation unit to produce both freshwater and electrical power. The system used six solar stills and seawater as the working fluid. A 4 m high grey PVC chimney with a 315 mm outer diameter housed a wind turbine-generator set. The study found that positioning solar stills at one-third of the collector radius optimized freshwater production, particularly between sunset and early morning. The chimney's air temperature rose by up to 17°C during the day and above 5°C at night, driving power generation, which peaked at 0.71 MW during daylight. The system achieved a solar energy efficiency of up to 21.8%, demonstrating its potential for commercial hybrid SCPP applications.

Akbarzadeh et al. [105] presented a comprehensive numerical and experimental study on the development of a hybrid Solar Chimney Power Plant (SCPP) integrated with a desalination unit, implemented in northern Victoria, Australia. The system combined a 6-hectare solar pond with a depth of 3 m and a chimney 200 m in height and 10 m in diameter. This configuration achieved a 0.4% improvement in energy conversion efficiency and

provided round-the-clock electricity generation. The research was motivated by earlier experimental validation at the RMIT Campus in Bundoora (Figure II.21), where a small-scale prototype had been built. The prototype featured a flexible chimney 8 m tall and 0.35 m in diameter, placed beside a solar pond of 4.2 m in diameter and 1.85 m depth. The successful performance of this model guided the transition to the large-scale system. To optimize its operation, two modes were introduced: indirect heating through a water-to-air exchanger and direct thermal contact. In both cases, heated brine from the lower pond layers was circulated through the chimney, transferring thermal energy to the air before returning to the pond, thus generating the buoyant airflow required to drive the turbine.

Figure II. 20: Hybrid SCPP and Solar Pond Configuration by Akbarzadeh et al [105].

II.5 Conclusion

This chapter provided a comprehensive review of recent developments in SCPPs, with particular emphasis on geometric configurations, material innovations, and strategies for enhancing system efficiency. Special consideration was given to numerical investigations, especially those employing geometries similar to the well-established Manzanares prototype, as well as studies both numerical and experimental that utilized alternative geometrical configurations.

These investigations offered a broad perspective on the design and performance of key SCPP components, including the collector, chimney, absorber plate, turbine, and their integration. Emphasis was placed on the influence of geometric parameters such as collector radius and slope, chimney height and diameter, absorber plate inclination, and turbine

placement and design. By analyzing a range of structural configurations and material selections, the reviewed literature contributes to a deeper understanding of how these design features impact overall system efficiency. Furthermore, several advanced strategies identified in the literature were highlighted, including the integration of SCPPs with other renewable energy systems, aim to optimize component design and improve the performance and reliability of the overall system. Collectively, the findings presented in this chapter establish a solid foundation for the subsequent chapters, which seek to address previously unexamined limitations through a combined experimental and numerical investigation.

CHAPTER III:
EXPERIMENTAL STUDY ON THE SOLAR CHIMNEY POWER PLANT

III.1 Introduction

Although numerous numerical and analytical studies have explored the performance of SCPPs, experimental investigations remain limited particularly those examining the direct impact of geometric design features under real operating conditions. To address this gap, a novel experimental prototype was developed at our home institution, the University of Chlef, Algeria. As the first system of its kind in the region, it was specifically designed to investigate geometric parameters whose effects have not been subjected to rigorous experimental evaluation until now, while also capturing the influence of local climatic conditions on overall system performance. This chapter presents a detailed experimental investigation into the influence of air inlet geometry specifically the diameter and number of air inlets on the performance of a SCPP. Three air inlet diameters (10 cm, 20 cm, and 30 cm) were examined to evaluate their impact on airflow velocity, temperature distribution, and overall thermal performance. In a second phase, the number of air inlets was varied to identify configurations that could further enhance performance. The objective of this investigation is to discover geometric configurations that optimize energy conversion, particularly under the specific climatic conditions of Chlef, where solar radiation and ambient temperature vary significantly. The combination of novel geometric testing and region-specific environmental data offers new insights into the practical operation and optimization of SCPPs.

III.2 Experimental Set-Up

III.2.1 Location, Geometry, and Material Selection for the Prototype

Selecting the optimal location is a crucial step in developing a solar energy control system, as environmental and geographical factors play a decisive role in its performance. A site within the University of Chlef, Algeria (1.34275°E, 36.15101°N), was strategically chosen due to its favorable conditions, including steady wind currents and continuous solar radiation throughout the day. These factors create an ideal environment for maximizing the operational efficiency of the prototype and ensuring reliable performance. Once the location is determined, optimizing the geometric dimensions of critical components becomes essential, as these parameters directly influence the system's efficiency and operational performance. Based on previous studies and models of SCPPs, the selection of chimney height and diameter, as well as the collector's diameter and inclination, is carefully considered.

Additionally, market availability and cost are taken into account as key factors in the design process.

The slenderness ratio of a chimney, defined as the ratio of its height (H_{ch}) to its diameter (D_{ch}), is a key design parameter influencing both structural stability and airflow characteristics. Previous studies have suggested an optimal slenderness ratio in the range of 6 to 8 [106]. However, various experimental and numerical investigations have employed a wider range of values; for example, the Spanish prototype implemented a ratio of 19 [6], while other works have utilized ratios of 15.63 [107] and 16.67 [108], and a wide range of H_{ch} to D_{ch} is available in literature. In this study, a chimney height of 6 m and a diameter of 0.40 m were selected, corresponding to a slenderness ratio of 15. This configuration was chosen to ensure compatibility with previous research while maintaining practical feasibility for the experimental setup. Regarding the collector, the ratio of chimney height to collector diameter (D_{coll}) is a key parameter in determining the optimal collector size. Studies indicate that the acceptable range for this ratio falls between 0.8 and 5 [85, 109]. To ensure compliance with this criterion, a collector diameter of 6 m was selected, resulting in a calculated ratio of 1.

The geometry of the collector cover has also been investigated in the literature. In general, the majority of studies and laboratory-scale experimental setups have employed a horizontal or flat collector configuration, corresponding to an inclination angle of 0° [7, 88, 97, 98]. However, one investigation examined a range of collector inclination angles between 20° and 35°, and found that optimal performance was achieved at an inclination angle of 30° [80]. This suggests that a moderate inclination can enhance thermal and aerodynamic behavior under certain conditions. In contrast, other research has shown that inclination angles exceeding 6° may lead to adverse airflow phenomena beneath the collector, including the formation of recirculation zones and vortices driven by density gradients, which can significantly reduce system efficiency [30]. Based on these insights, the present study adopts a collector inclination angle of 5°, aiming to avoid the onset of flow instabilities observed at higher angles. The specific geometrical parameters of the experimental setup are summarized in Table 1.

Table III. 1: The specific geometrical dimensions.

Parameter	Dimension (m)
Chimney height	6
Chimney diameter	0.40
Collector diameter	6
Collector height	0.40
Collector slope	5°

Once the geometric dimensions of the SCPP components are established, the next critical phase in the system's development involves selecting appropriate materials for each component. This selection is primarily guided by technical and functional requirements, such as thermal and mechanical efficiency, along with the need to ensure structural integrity and long-term operational stability. Additionally, practical considerations including cost-effectiveness and the availability of suitable materials play a crucial role in shaping these choices. A comprehensive overview of the selected materials is presented in Table 2.

Table III. 2: Selected Materials for SCPP Components.

Parameter	Materials
Chimney	PVC
Collector	Plastic
Ground	sand and gravel

III.2.2 Detailed Procedure of Construction Processes

The structure is installed at the center of the ground to avoid potential shading from surrounding trees. A reinforced structural frame is then constructed to ensure stability and support both the chimney and the collector cover. This frame consists of 15 steel columns, four of which have increased thickness to withstand the chimney’s load. The columns are securely anchored using concrete, while interlocking aluminum bars are mounted on the steel columns to provide stability for the collector cover.

Subsequently, multiple layers of crushed rock and sand are laid on the ground as thermal storage materials. The chimney is then installed at the center of setup. In the final stage, the collector cover is positioned, completing the setup. The fully assembled experimental setup is shown in Figure III.1.

Figure III. 1: Structural frame of the SCPP.

III.2.3 Measuring Instruments

The selection of suitable equipment for the SCPP experiment is essential to ensure accurate and reliable measurements. This enables effective monitoring of key parameters, including velocity, temperature, and solar radiation.

III.2.3.1 Measuring the Temperature within the system

To measure the temperature within the system, DHT11 temperature sensors were utilized (Fig III.2) and installed at various locations inside the solar chimney. Their technical specifications are summarized in Table 3.

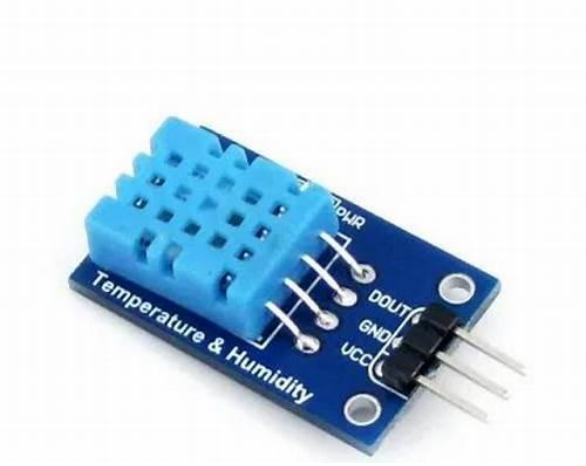

Figure III. 2: DHT11 sensor.

Table III. 3: DHT11 Specifications [110].

Operating Voltage	3.5V to 5.5V
Operating current	0. 3mA
Output	Serial data
Temperature Range	0°C to 50°C
Humidity Range	20% to 90%
Resolution	Temperature and Humidity both are 16-bit
Accuracy	±1°C and ±1%

III.2.3.2 Measuring air velocity within the system

For measuring airflow velocity at the chimney opening, an HP86A anemometer was employed (Fig III. 3). A detailed overview of its specifications is provided in Table 4.

Figure III. 3: HP86A anemometer.

Table III. 4: Anemometer Specification [111].

Brand Name	Hold Peak
Model Number	HP-866A
Wind Speed Range	0.3-40m/s
Temperature range	-10-60°C
Wind flow range	0-999900m3/min
Wind Speed sensitivity	+-0.1dgts(m/s)
Connect to PC with USB	YES
Real Time Measure	YES

III.2.3.3 Measuring Ambient Temperature and Global Solar Radiation

The measurement of local climatic conditions such as solar radiation, ambient temperature, humidity, and wind parameters was carried out using the Vantage Pro2 weather station installed at the experimental site (Fig. III.4). The Vantage Pro2 Plus is a professional-grade meteorological station designed for high-precision environmental monitoring. It provides accurate and reliable data with real-time updates. The system records key atmospheric variables including temperature, humidity, wind speed and direction, barometric pressure, and solar radiation, making it particularly suitable for environmental research and renewable energy

applications. Equipped with either wireless or wired data transmission and a robust sensor suite, the station ensures stable long-term performance under varying climatic conditions.

Figure III. 4: Vantage Pro2 weather station

III.2.3.4 Measurement Support Systems and Data Processing

In addition to the primary measurement instruments, auxiliary electronic components such as an Arduino microcontroller and a laptop computer were employed to support data acquisition and processing tasks. The Arduino system was interfaced with DHT11 sensors for monitoring ambient temperature and humidity, an SD card module for onboard data storage, and a Real-Time Clock (RTC) module to ensure accurate time-stamped data logging (Fig. III.5.a). The Arduino was programmed and managed using the Arduino IDE software, with data transferred to the laptop via USB. For air velocity measurement, the HP86A anemometer is directly connected to the laptop (Fig. III.5.b) and operate using the manufacturer's proprietary data logging software, allowing continuous velocity recording for subsequent analysis.

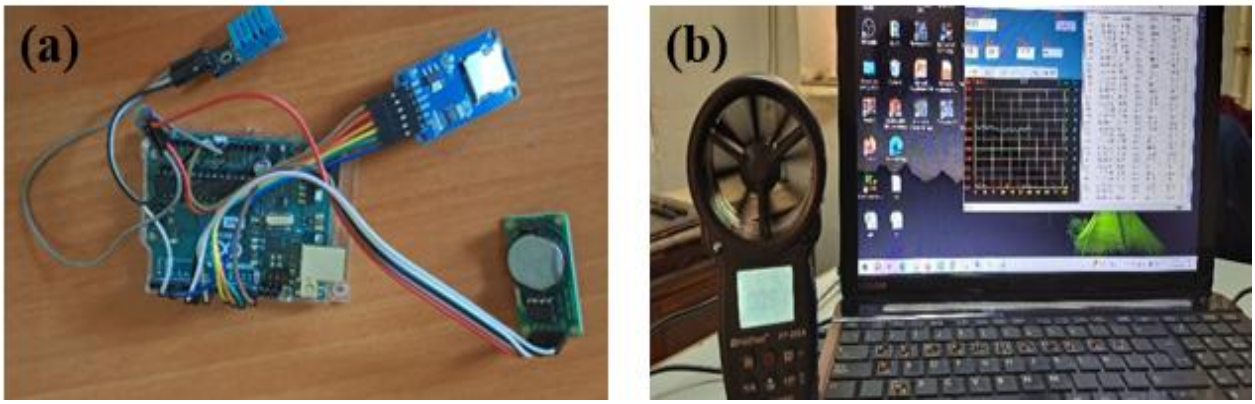

Figure III. 5: a) Arduino connected to DHT11 sensors, b) HP86A anemometer connected to a laptop.

To ensure accurate monitoring of the thermal and airflow characteristics within the SCPP system, a schematic representation was developed to illustrate the placement of the sensors and measurement devices. This schematic provides a clear overview of the distribution of thermal sensors along the absorber plate and at the chimney base, as well as the positioning of the anemometer at the chimney outlet. Figure III.6 presents the schematic diagram of the sensor configuration. Figure III.7 shows a photographic view of the constructed SCPP prototype.

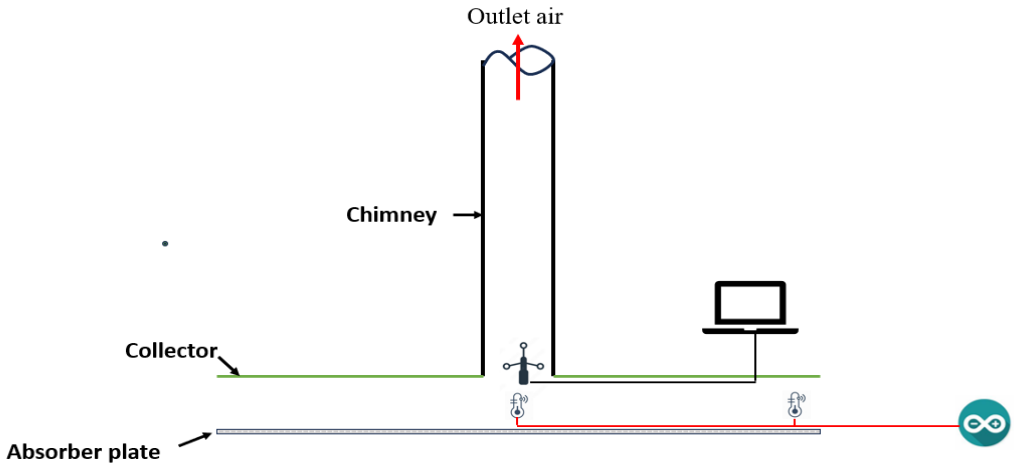

Figure III. 6: Schematic diagram of the experimental SCPP showing the placement of installed sensors and instrumentation.

Figure III. 7: Photographic view of the constructed SCPP prototype.

while Figure III.8 highlights the actual installation of sensors and instrumentation on the experimental setup.

Figure III. 8: Photographic view of the experimental SCPP setup with the installed sensors and instrumentation.

III.3 Results and Discussion

III.3.1 Measurement of Environmental Parameters

Meteorological parameters, specifically solar irradiance and ambient temperature, were continuously monitored throughout the experimental period in Juin 2024. Data collection was conducted daily from 08:00 to 19:00 to capture the full range of diurnal variations in solar exposure and temperature. The recorded values exhibited a consistent trend across all test days, with only minor fluctuations, indicating stable weather conditions during the study period. Due to this stability, a single representative day was selected for detailed analysis. The solar irradiance and ambient temperature on this chosen day closely aligned with the overall average values recorded during the entire monitoring period.

This approach ensures that the analyzed data accurately reflects the typical meteorological conditions of the experimental site (Fig. III.9)

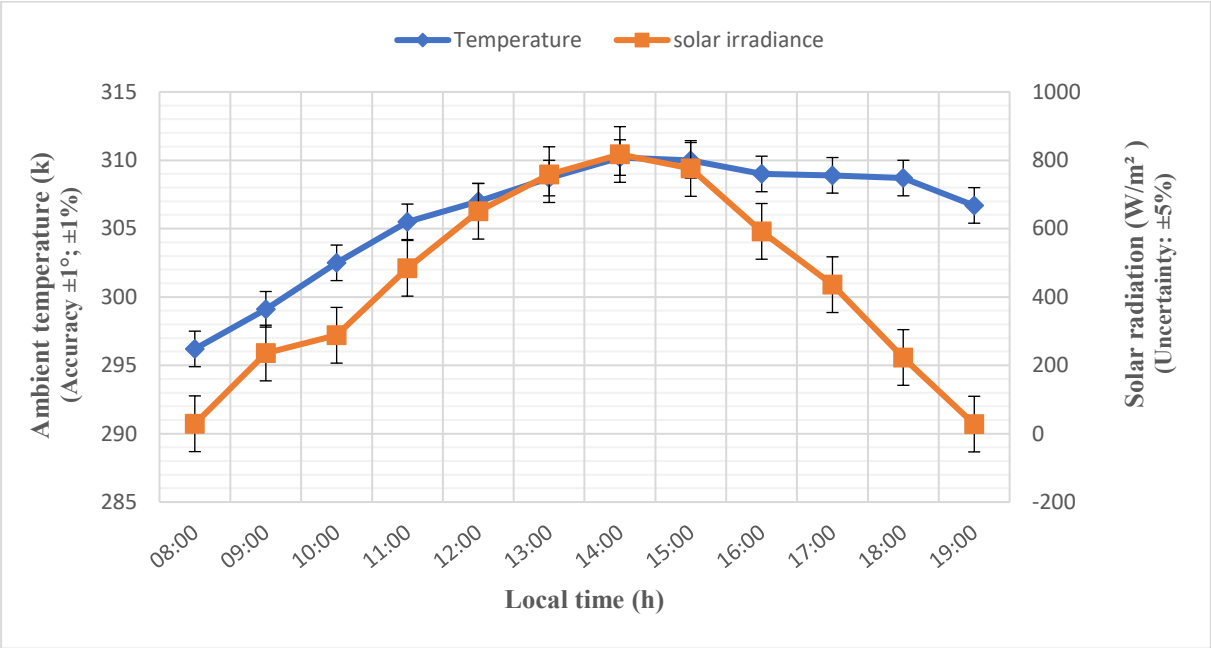

Figure III. 9: Solar irradiance and ambient temperature measured in Chlef during the experimental Period.

Figure III.9 presents the hourly evolution of solar irradiance and ambient temperature throughout the selected day. Solar irradiance began at a low level of 29 W/m² at 08:00, progressively increased during the morning hours, and reached a peak value of 817 W/m² at 14:00. After this maximum, solar irradiance gradually decreased, returning to 28 W/m² by 19:00. Ambient temperature followed a similar trend, starting at 295.1 K in the early morning and rising steadily to a maximum of 310 K between 14:00 and 15:00. A slight decline was observed in the late afternoon and evening, with the temperature decreasing to 302.3 K by 19:00. The data highlights the region's significant solar energy potential and confirms its suitability for renewable energy applications. In particular, the consistently high levels of solar irradiance observed throughout the day indicate that this site is especially well-suited for the deployment of SCPPs, which rely heavily on sustained and intense solar input to operate efficiently.

III.3.2 Influence of the Geometric Parameters on the performances of the SCPP

The air inlet configuration plays a crucial role in determining the airflow behavior and thermal performances of a SCPP. It directly influences air velocity, temperature distribution, and overall system efficiency. Despite its significance, air inlet geometry has been largely

overlooked in the existing literature. To date, no study has comprehensively investigated these parameters through either experimental or numerical methods. This section aims to address this gap by analyzing the effect of air inlet design on SCPP performance.

III.3.2.1 Effect of Air Inlet Diameter

III.3.2.1.1 Impact on Maximum Air Velocity

Figure III.10 illustrates the variation in maximum air velocity at the chimney base, where the system was consistently configured with four air inlets to ensure uniform air entry conditions. The analysis covers three distinct air inlet sizes: 10 cm, 20 cm, and 30 cm as illustrated in Figure III.11. Each configuration exhibited a parabolic velocity profile that closely followed the diurnal variation in solar irradiance, indicating a strong correlation between solar radiation intensity and airflow velocity within the system. As solar irradiance increases throughout the morning, it heats the collector surface, creating a stronger thermal gradient between the collector and the chimney. This intensified gradient enhances the buoyancy effect, driving greater airflow through the system. The airflow velocity reaches its maximum between 14:00 and 15:00, aligning with the peak in solar irradiance, thus confirming the strong dependence of air velocity on solar energy input.

Among the tested configurations, the 10 cm inlet produced the lowest airflow velocity, with a maximum of approximately 2.5 m/s. This outcome is attributed to the limited cross-sectional area of the air inlet, which constrains the mass flow rate despite the presence of a strong thermal gradient. The 20 cm inlet exhibited the most favorable performance, achieving the highest velocity of approximately 2.9–3.0 m/s. This configuration offers an optimal balance between cross-sectional area and driving pressure, ensuring both a sufficient mass flow rate and a strong pressure gradient. Conversely, the 30 cm inlet, owing to its larger area and consequently higher mass flow rate, resulted in a slightly lower velocity range of 2.6–2.7 m/s. This modest increase is due to the distribution of buoyancy-driven pressure over a wider section, which reduces the pressure gradient per unit area. Consequently, the 20 cm air inlet

diameter can be considered the most effective in enhancing airflow at the chimney base, thereby improving the overall performance of the solar chimney system.

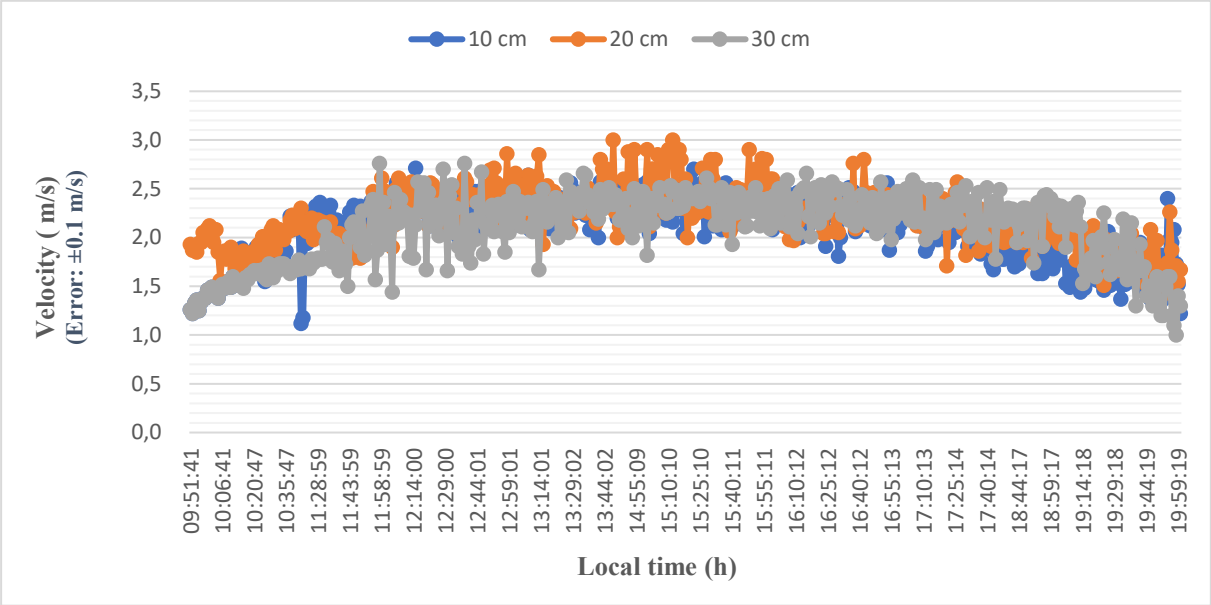

Figure III. 10: Maximum air velocity for different air inlet diameters: 10 cm, 20 cm, and 30 cm.

Figure III. 11: Inlet size configurations used in the experimental setup.

III.3.2.1.2 Impact on Air temperature within the System

Figure III.12 presents the diurnal variation in the temperature difference ΔT between the inlet and the central region of the solar collector for three distinct air inlet diameters: 10 cm, 20 cm, and 30 cm, implemented within a four air inlets configuration. Across all cases, ΔT exhibits a steady increase from the morning hours until early afternoon, driven by the progressive rise in air temperature within the collector as a direct response to the intensification of incident solar radiation. The temperature differential reaches its maximum between 13:00 and 15:00, coinciding with the period of peak solar irradiance. This peak signifies substantial thermal

energy accumulation within the collector, particularly at the chimney base, where the air experiences the greatest heating. Among the examined configurations, the 20 cm inlet diameter consistently produces the highest ΔT, with values reaching approximately 20 K between 13:00 and 15:00. This performance suggests an optimal trade-off between airflow rate and heat absorption, promoting efficient thermal storage and enhancing the buoyancy-driven airflow through the chimney. Conversely, the 10 cm air inlet diameter exhibits a slightly reduced temperature differential, which may be attributed to restricted airflow that limits the mass flow rate of air through the system. This reduction in mass flow consequently diminishes the convective heat transfer within the collector domain, resulting in lower overall air temperatures. In the case of the 30 cm air inlet diameter, the system demonstrates a comparatively lower ΔT during the early hours of operation, likely due to excessive airflow rates that induce premature cooling of the collector before sufficient thermal energy is accumulated. Nonetheless, the thermal performance of this configuration improves during the later part of the day. In summary, the 20 cm air inlet diameter offers the most favorable thermal performance among the tested geometries, indicating its superior ability to enhance internal air temperature which is critical to improving the overall efficiency of the solar chimney system.

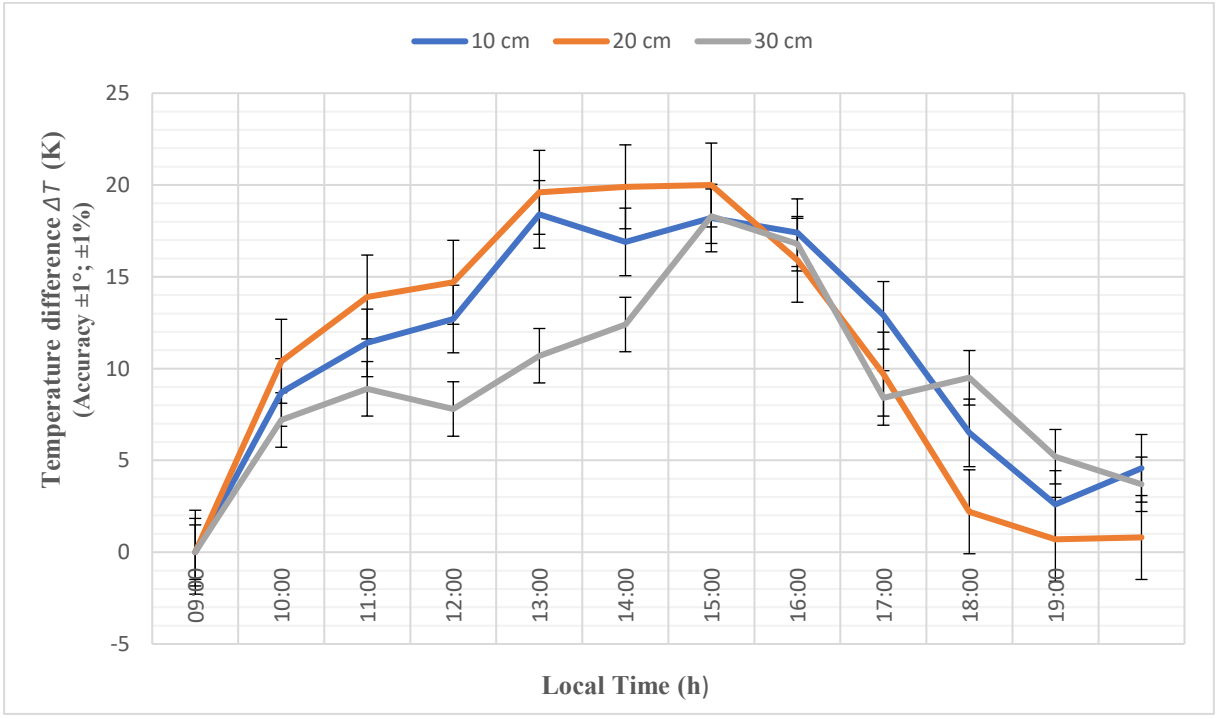

Figure III. 12: Temperature difference for different air inlet diameters.

III.3.1.2.1 Effect of Air Inlet Number

III.3.1.2.1 Influence on Maximum Air velocity

After determining the optimal air inlet diameter, the next phase of the investigation focused on evaluating the effect of the number of air inlets on airflow characteristics within the system. To this end, three experimental configurations were tested, incorporating 2, 4, and 6 air inlets, respectively. For each configuration, measurements of the maximum air velocity at the base of the chimney were recorded from 09:00 to 19:00, covering the full range of daily solar irradiance and thermal variation.

The results presented in Figure III.13 illustrate the temporal evolution of maximum air velocity for each air inlet configuration. During the morning period (before 12:00), all configurations exhibit a gradual increase in velocity, corresponding to the rising solar irradiance and the progressive heating of air within the collector. Between approximately 12:00 and 15:00, when solar intensity peaks, the airflow velocity attains its maximum across all cases. Among the configurations tested, the 4 air inlets setup consistently achieves higher velocity values compared to the 2 air inlets system. This demonstrates that increasing the number of inlets enhances the intake of ambient air, which is subsequently heated more effectively within the collector due to the greenhouse effect. The augmented volume of incoming air amplifies the buoyancy-driven flow through the chimney by increasing the pressure difference across the system. In contrast, although the 6 air inlets configuration potentially facilitates greater air entry, it does not yield superior performance. The excess air flow may reduce the average residence time within the collector, thereby limiting the heating effect. Moreover, the increased number of inlets can lead to uneven airflow distribution, generating turbulence and flow disturbances that disrupt the steady movement of air toward the chimney. This turbulence diminishes the buoyancy-driven draft, consequently reducing air velocity at the chimney base. As a result, the 6 air inlets configuration exhibits a less favorable velocity profile compared to the 4 air inlets case.

After 15:00, as solar irradiance declines, all configurations show a gradual reduction in airflow velocity, reflecting the decrease in thermal input and buoyancy-driven forces. In conclusion, the study confirms that while increasing the number of air inlets can enhance system performance.

This improvement is limited to an optimal point. The 4 air inlets configuration achieves the best compromise between enhanced air intake and flow stability, thereby optimizing overall system efficiency.

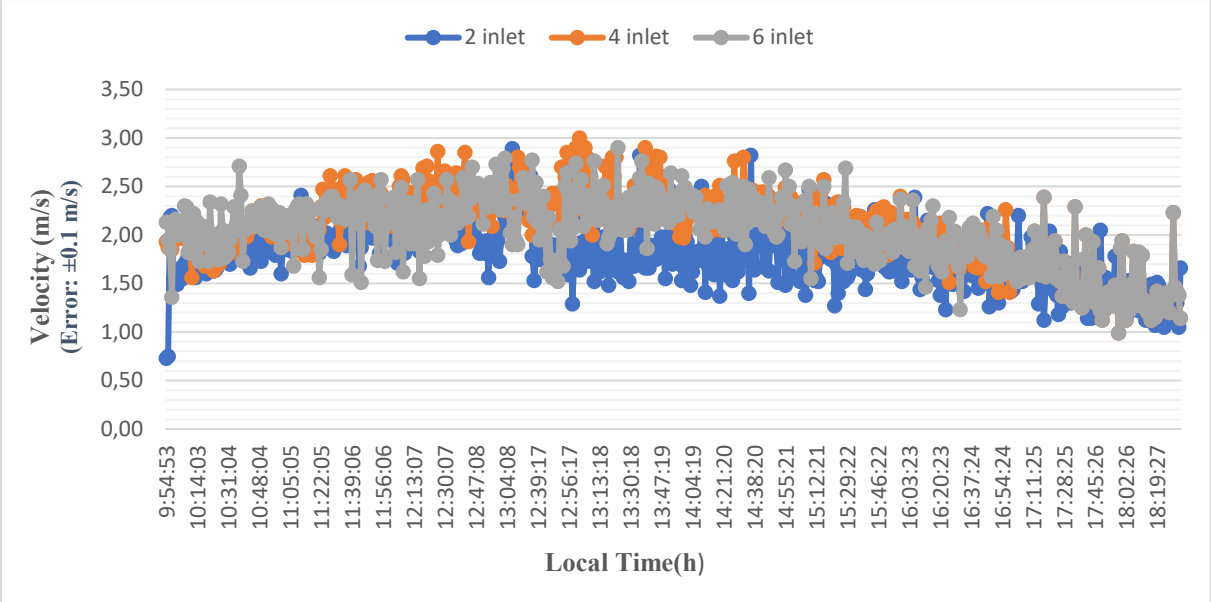

Figure III. 13: Effect of inlet number on maximum air velocity.

III.3.1.2.2 Influence on Maximum Air temperature within the System

In line with the investigation into air velocity, the impact of air inlet number on the maximum air temperature within the system, specifically at the center of the collector, was also analyzed. Temperature measurements were recorded hourly from 09:00 to 19:00 for three different air inlets configurations (2, 4, and 6), enabling a comparative analysis of thermal behavior under varying air inlet conditions. The results, presented in Figure III.14, reveal several key trends. At 09:00, air temperatures were relatively low across all configurations, reflecting the limited solar irradiance in the early morning. Among the three setups, the 4 air inlets system exhibited the highest air temperature 308 K, compared to 305 K and 305 K for the 2 air inlets and 6 air inlets configurations, respectively. This early thermal advantage persisted and became more pronounced as the day progressed. Between 10:00 and 14:00, air temperatures steadily increased in all configurations, correlating with the rise in solar irradiance. During this period, the 4 air inlets configuration consistently recorded the highest temperatures, peaking at 324 K at 14:00. This suggests that the 4 air inlets configuration achieves an optimal balance between air intake and heat retention, allowing for more efficient heating of the air due to enhanced interaction with the collector surface and the improved greenhouse effect. The 2 air inlets system consistently lagged behind, while the 6 air inlets

configuration showed moderate gains but failed to match the thermal performance of the 4 air inlets system. Despite its increased air intake capacity, the 6 air inlets configuration yielded lower peak air temperatures throughout the day. This result indicates that excessive airflow may reduce the air residence time within the collector, reducing the residence time of air within the collector, which prevents the collector from effectively transferring heat to the airflow. From 15:00 to 19:00, a gradual decrease in air temperature was observed across all configurations, corresponding to the reduction in solar intensity during the late afternoon.

In conclusion, the temperature analysis supports the findings from the air velocity measurements. While increasing the number of air inlets improves air intake, optimal thermal performance depends on a balance between air flow and thermal exposure. The 4 air inlets configuration consistently provides the highest temperatures, demonstrating superior energy conversion efficiency. In contrast, the 2 air inlets configuration limits the airflow rate, while the 6 air inlets configuration reduces the time available for effective heat transfer. These results underscore the importance of selecting the optimal number of air inlets to maximize system efficiency.

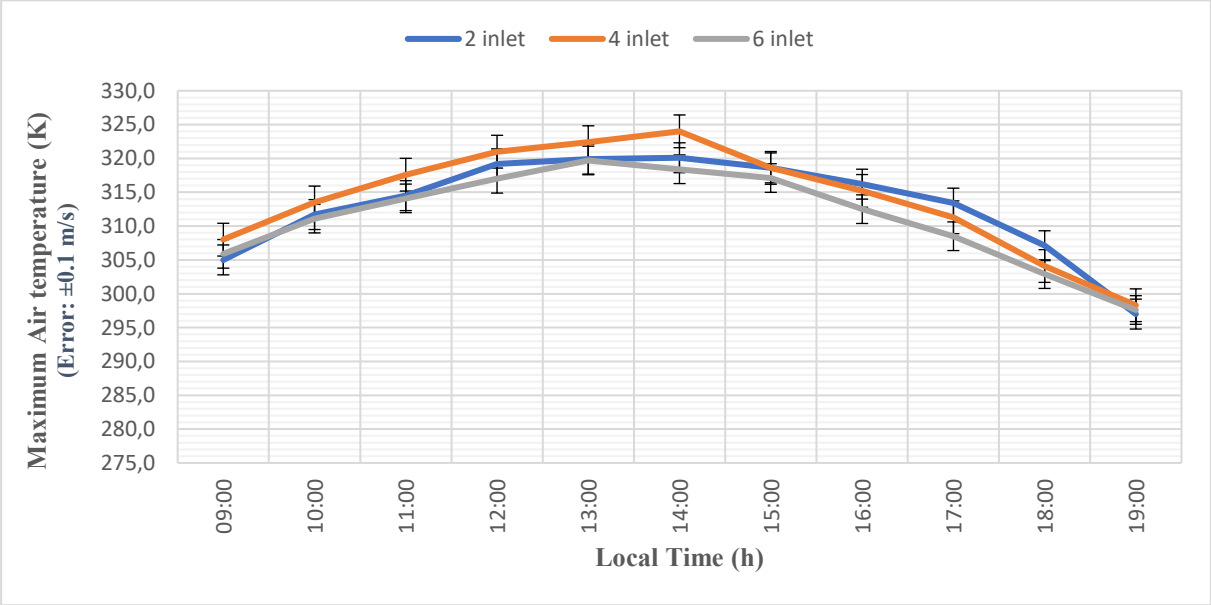

Figure III. 14: Effect of air inlet number on maximum air temperature within the system.

III.3.3 Influence of Environmental Conditions on SCPP Performance

A comprehensive 24-hour experimental investigation was conducted in June 2024 to assess the influence of ambient temperature and solar irradiance on the operational performance of the SCPP. Hourly measurements of solar irradiance and ambient air temperature were systematically recorded using a Vantage Pro weather station installed at the site. These real

environmental data ensure the analysis accurately reflects authentic operating conditions and captures the dynamic interactions between external climatic variables and the system's thermal-aerodynamic behavior. As illustrated in Figure III.15, solar irradiance and ambient temperature were monitored continuously throughout the study period. Solar irradiance exhibited a pronounced diurnal cycle, rising from 236 W/m² at 09:00 to a peak of 817 W/m² at 14:00, before declining to zero after 20:00. This pattern delineates the window of maximum solar availability critical for initiating and sustaining the thermal processes that generate airflow within the SCPP. Concurrently, ambient temperature followed a typical daily variation, increasing from 299.1 K in the morning to a maximum of 310.1 K at 16:00, and then gradually decreasing to 292.1 K by 06:00 the next day. These environmental fluctuations provide essential context for evaluating the system's thermal response.

Figure III.16 depicts the temporal profiles of internal air temperature and air velocity at the chimney base. Internal air temperature increased from 311 K at 09:00 to a maximum of 332.5 K at 14:00, while air velocity concurrently rose from 2.12 m/s to a peak value of 3.00 m/s at 13:00. These results underscore a strong correlation between solar radiation intensity and thermal buoyancy enhancement; elevated solar input leads directly to increased internal air temperature and amplified convective flow. Following sunset, as solar irradiance diminishes to zero, both internal air temperature and air velocity exhibit a marked decline. During nighttime, air velocity stabilizes within a range of 0.5 m/s to 2.01 m/s, and internal air temperature remains near 293 K. The analysis clearly demonstrates that solar irradiance is the predominant driver of SCPP performance. The diurnal variations in maximum air velocity and temperature inside the chimney closely track solar irradiance fluctuations, with peak values coinciding with peak solar irradiance around midday. In contrast, although ambient temperature gradually decreases during nighttime particularly after midnight it exerts a negligible influence on internal air velocity and temperature. This disparity highlights the secondary role of ambient temperature relative to solar irradiance, emphasizing that the latter constitutes the principal energy source governing the temperature gradient, buoyancy forces, and resulting airflow within the system.

Furthermore, despite the absence of solar input at night, the SCPP sustains a residual airflow and elevated internal temperature, attributable to the inclusion of sand and gravel beneath the absorber plate. These materials function as passive thermal energy storage media, absorbing heat during daylight and releasing it gradually throughout the night. This thermal inertia supports a sustained temperature gradient between the collector and ambient air, thereby

prolonging buoyant airflow beyond sunset. Such an approach effectively extends the operational period of the SCPP, enhancing its overall energy yield.

The strategic integration of sand and gravel as thermal storage layers beneath the collector surface significantly increases the system's thermal inertia, enabling extended performance and improving reliability and efficiency under realistic environmental conditions. Moreover, the local climatic characteristics marked by high solar irradiance and stable diurnal temperature variations are particularly conducive to the application of solar chimney technology, reinforcing the SCPP's potential as a sustainable and efficient renewable energy solution.

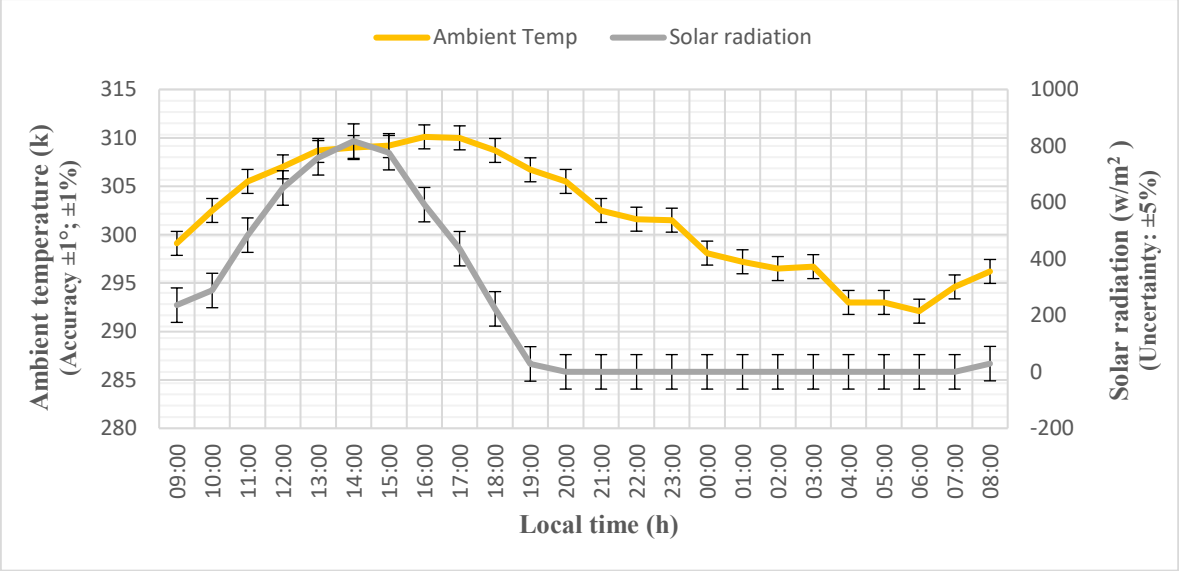

Figure III. 15: 24-Hour Variation of Solar Radiation and Ambient Temperature in Chlef.

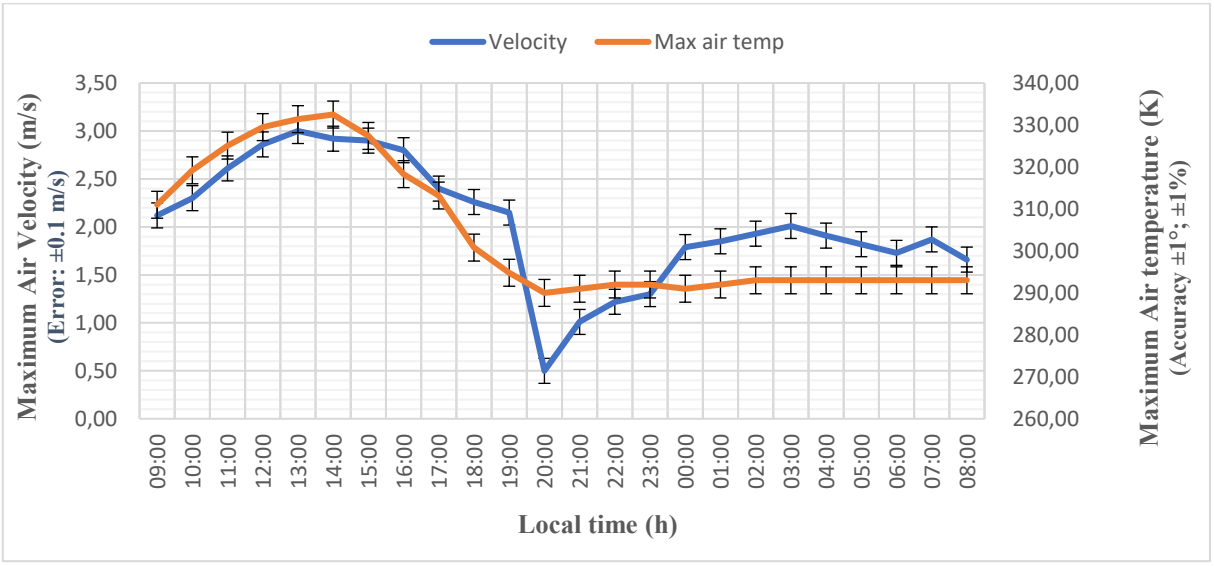

Figure III. 16: 24-Hour Profiles of air temperature and air velocity within the system.

III.3.4 Comparison of the influence of local climatic on SCPP Performance

To assess the impact of the local climate on the performance of the SCPP, experimental measurements of air velocity and maximum air temperature within the system were recorded over the course of a clear day in Mars and again in June. These two months were deliberately selected to represent the transition between the two predominant climatic seasons in Chlef, Algeria, a region characterized by a mild-to-cool winter and a hot, dry summer. Mars was chosen as it represents a typical winter month, while June corresponds to the onset of peak summer conditions, which are typically associated with the highest levels of solar irradiance. This selection allows for a representative comparison of the SCPP's performance under the most contrasting seasonal conditions that define the local semi-arid climate.

As shown in figure III.17, the air velocity within the chimney follows a diurnal profile consistent with the pattern of solar irradiance. In Mars, the air velocity increased from 2.05 m/s at 09:00 to a peak of 2.90 m/s at 14:00, and then gradually declined to 2.10 m/s by 19:00. In contrast, the June measurements exhibit slightly improved performance, starting at 2.12 m/s, peaking at 3.00 m/s at 13:00, and decreasing to 2.15 m/s at 19:00. The higher peak observed in June can be attributed to increased solar irradiance, which enhances buoyancy-driven airflow within the system. Overall, these results confirm that the SCPP performs reliably throughout the year, with improved airflow during summer conditions. This indicates that the system is well-adapted to the solar and thermal characteristics of the local climate in Chlef.

The analysis of maximum air temperature further supports the system's responsiveness to seasonal changes. In Mars, the temperature increased from 308.0 K at 09:00 to a maximum of 324.0 K at 14:00, before dropping to 298.3 K at 19:00. In June, the thermal profile showed consistently higher values throughout the day, reaching a peak of 332.5 K at 14:00 8.5 K higher than in Mars. These elevated temperatures correspond to higher solar irradiance and ambient air temperature during summer. The regular increase in temperature, particularly around midday, highlights the chimney's effective thermal performance under strong solar irradiance. This trend confirms the system's capacity to operate efficiently across seasonal variations, reinforcing its suitability for the climatic conditions typical of Chlef.

The experimental results demonstrate that the SCPP operates effectively under both winter and summer conditions. However, performance indicators particularly maximum air velocity and temperature are significantly enhanced in June. These findings validate that the SCPP design is well-suited to the local climate, benefiting from the region's high solar irradiance. The system consistently generates meaningful airflow and thermal gradients across

seasons, confirming its feasibility and reliability as a renewable energy solution for semi-arid regions like Chlef.

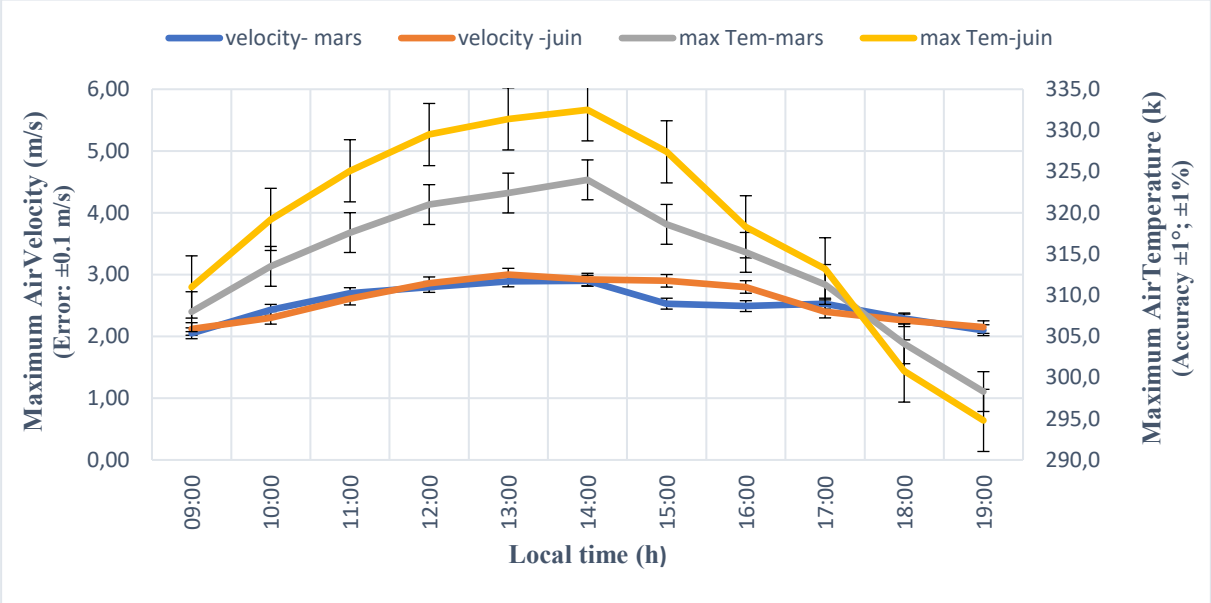

Figure III. 17: Air velocity and temperature variation inside the chimney: Mars vs. June.

III.4 Conclusion

In this study, we sought to develop a comprehensive and realistic understanding of the impact of geometric configurations and climatic conditions on the performance of a SCPP. To achieve this, the current chapter presented a structured experimental analysis examining the influence of specific geometrical and environmental parameters on the operational efficiency of the system.

A prototype was constructed and tested under real environmental conditions to assess the effects of specific geometrical parameters, such as the air inlet diameter and the number of air inlets. Additionally, the study analyzed the impact of solar irradiance and ambient temperature using actual meteorological data recorded over different seasons.

The main findings are summarized as follows:

– The 20 cm air inlet diameter yielded the best performance, with a maximum air velocity of 3.0 m/s and a temperature difference (ΔT) of 20 K, offering an optimal trade-off between intake area and pressure gradient.

– The 4 air inlets configuration consistently demonstrated superior aerodynamic and thermal performance compared to the 2 and 6 air inlet designs, achieving a maximum air velocity of 3.0 m/s and a peak internal temperature of 324.0 K.

– Solar irradiance was identified as the primary driver of system performance, strongly correlating with both internal temperature and airflow rate, while the effect of ambient air temperature was found to be negligible.

– Seasonal measurements showed that the SCPP operates reliably across different climatic conditions.

– The use of sand and gravel as thermal storage beneath the collector enabled sustained airflow during nighttime, supporting extended daily operation and improving the overall efficiency of the system.

While experimental investigations provide valuable and realistic insights into system performance, they also enable the investigation of specific geometrical and environmental parameters under real world conditions, offering empirical validation that strengthens the reliability of observed phenomena. However, some configurations such as complex changes in the geometry of the absorber surface may be impractical to test experimentally due to high costs or technical limitations. To overcome these constraints, numerical simulations offer a flexible and cost-effective alternative, allowing for the detailed investigation and exploration of a broader range of design scenarios. The next chapter is therefore dedicated to the numerical modeling of the SCPP, providing deeper insights into configurations that are difficult or impossible to realize experimentally.

CHAPTER IV: MODELING, SIMULATION, AND NUMERICAL ANALYSIS OF SOLAR CHIMENY POWER PLANTS

IV.1 Introduction

Following the experimental investigation presented in the previous chapter, which provided valuable insights into the influence of environmental conditions and specific geometric configurations on the performance of the SCPP, this chapter presents a complementary numerical study aimed at expanding and deepening the analysis. Certain configurations could not be examined experimentally due to the physical and practical limitations of the testing environment. To address these constraints, a detailed two-dimensional (2D) numerical model is developed using COMSOL Multiphysics to simulate the coupled thermal and fluid dynamic behavior of the SCPP. The model is designed to closely replicate the real system's behavior by precisely defining the geometry, applying the governing equations, and implementing appropriate turbulence and heat transfer models, along with suitable boundary conditions.

This investigation focuses on the influence of specific geometric parameters, namely the absorber plate surface, collector inclination, and chimney configuration. A thorough assessment of these features requires a controlled numerical framework capable of isolating and evaluating their effects. Using CFD techniques, the study analyzes airflow patterns, heat transfer mechanisms, and energy conversion processes within the system. The outcomes not only reinforce the experimental findings but also provide deeper insight into how geometric optimization can enhance the overall efficiency and performance of the solar chimney system.

IV.2 Modelling Numerical and Simulation

IV.2.1 Geometry of SCPP

The study begins with the development of a 2D axisymmetric geometric model of the SCPP using COMSOL Multiphysics. Each component of the SCPP is represented as a 2D geometric shape, ensuring an accurate yet simplified representation of the system (Fig. IV.1). The dimensions adopted for this model are based on those of the Spanish prototype, as it serves as the primary experimental reference and the most reliable source of large-scale operational data for SCPPs. Over its years of operation, the Spanish prototype has provided extensive experimental results, making it an ideal benchmark for validating the numerical approach employed in this study. Consequently, the geometric dimensions used in this study, is detailed

in Table IV.1, correspond directly to those of the Spanish prototype, ensuring consistency and enabling robust model validation.

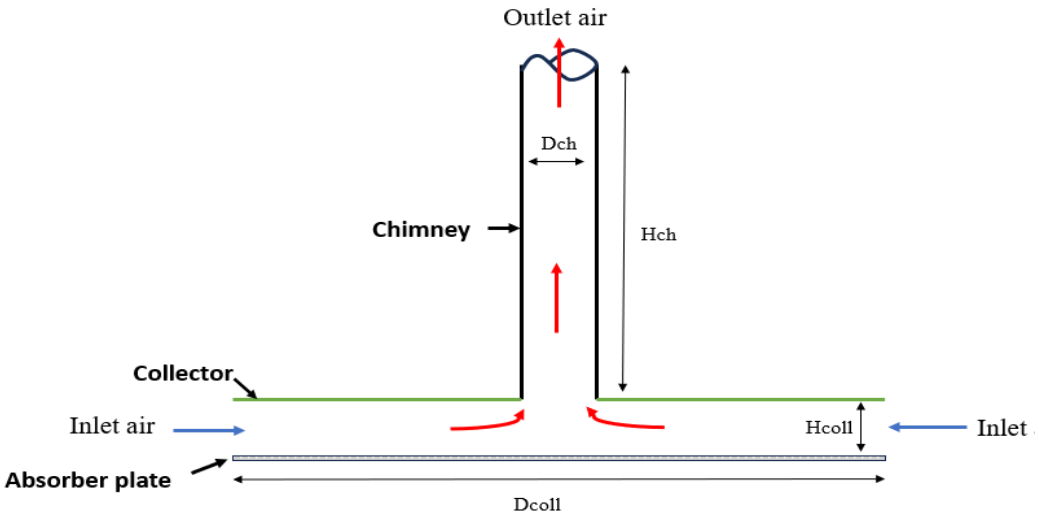

Figure IV. 1: SCPP model design.

Table IV. 1: Geometrical parameter of the SCCP.

Parameters	Dimension (m)
Chimney height (H_{ch})	194
Chimney radius (R_{ch})	5
Collector radius (R_{coll})	122
Collector height (H_{coll})	1.85

IV.2.2 Assumptions of numerical model

Airflow within the SCPP is simulated under the following simplifying assumptions:

- The model is a 2D axisymmetric representation of the SCPP.
- The airflow is treated as a time-dependent, compressible fluid.
- The environmental conditions are assumed to remain constant.
- The boundary conditions, including inlet, outlet, and wall conditions, are carefully defined to replicate real operating scenarios.
- Solar radiation is assumed to remain constant throughout each process.

IV.2.3 Characterization of fluid flow dynamics in Solar chimney power plants

Before conducting simulations, it is crucial to characterize the fluid flow regime, whether laminar or turbulent. Given the absence of an external forced flow mechanism within the SCPP, air movement is predominantly driven by greenhouse and buoyancy effects, resulting in natural convection. Therefore, the flow behavior is assessed using the Rayleigh number (Ra), which is determined by the following equation:

$$Ra = \frac{g\ \beta\ \Delta T H_{coll}^3}{\alpha v} \tag{IV.1}$$

where ΔT,H_{coll}, g , β, α and v represent the temperature difference (K), the collector height (m), the gravitational acceleration (m/s²), the thermal expansion coefficient (1/K), the thermal diffusivity (m²/s), and the kinematic viscosity (m²/s), respectively.

The calculated Rayleigh number exceeds 10^9, indicating that the fluid flow is within the turbulent regime.

IV.2.4 The turbulence model.

It has been established that the airflow within the solar chimney operates in a turbulent regime, which requires the use of appropriate turbulence models for accurate flow characterization. Various turbulence models have been applied in the literature to analyze SCPP performance, including the Realizable k-ε model [55,56,117-119], the Standard k-ε model [64,115,116], the RNG k-ε model [71,73,112-114], the *k-ε* turbulence model [120–123].

The k-ε turbulence model was employed in this study due to its proven reliability in capturing buoyancy-driven and natural convection flows, which are predominant in SCPP operation. Its widespread adoption stems from its optimal balance between computational efficiency and accuracy in turbulence modelling

The governing equations solved by COMSOL, are expressed as follows:

Continuity equation

$$\frac{\partial \rho}{\partial t} + \nabla \cdot (\rho u) = 0 \tag{IV.2}$$

Momentum equation

$$\frac{\partial \rho u}{\partial t} + \rho(\nabla \cdot u)u = \nabla \cdot [-pI + k] + F\ \rho g \tag{IV.3}$$

$$k = (\mu+\mu_T)(\nabla_u + (\nabla_u)^T) - \frac{2}{3}(\mu+\mu_T)(\nabla \cdot u)I - \frac{2}{3}\rho kI \quad \text{(IV.4)}$$

Energy equation

$$\rho C_p \frac{\partial T}{\partial t} + \rho C_p u \cdot \nabla T + \nabla \cdot q = Q+Q_p + Q_{vd} \quad \text{(IV.5)}$$

where u is velocity magnitude (m/s) F is volume force (N/m^3), ρ density (Kg/m^3), μ is dynamic viscosity (kg/m s) and μ_T is the turbulent dynamic viscosity coefficient.

The equations for the turbulence model are also expressed as follows:

Turbulent kinetic energy (k) equation:

$$\rho \frac{\partial k}{\partial t} + \rho(u \cdot \nabla)k = \nabla \cdot \left[\left(\mu + \frac{\mu_T}{\sigma_k}\right)\nabla k\right] + P_K - \rho\varepsilon \quad \text{(IV.6)}$$

Turbulent rate of dissipation (ε) equation:

$$\rho \frac{\partial \varepsilon}{\partial t} + \rho(u \cdot \nabla)\varepsilon = \nabla \cdot \left[\left(\mu + \frac{\mu_T}{\sigma_\varepsilon}\right)\nabla \varepsilon\right] + C_{\varepsilon 1}\frac{\varepsilon}{K}P_K - C_{\varepsilon 2}\rho\frac{\varepsilon^2}{K} \quad \text{(IV.7)}$$

where $\mu_T = \rho C_\mu \frac{k^2}{\varepsilon}$ the turbulent viscosity and $\varepsilon = \rho C_\mu^3 \frac{k^{3/2}}{L_T}$ is the energy dissipation.

$$P_K = \mu_T \left[\nabla u : \left(\nabla u + (\nabla u)^T - \frac{2}{3}\right)(\nabla . u)^2\right] - \frac{2}{3}\rho K \nabla - C_{\varepsilon 2}\rho\frac{\varepsilon^2}{K} \cdot u \quad \text{(IV.8)}$$

The turbulence constants $C_{\varepsilon 1}$, $C_{\varepsilon 2}$, σ_ε and σ_K used in K-ε turbulence model, are summarized in Table IV.2.

Table IV. 2: The turbulence constants.

$C_{\varepsilon 1}$	$C_{\varepsilon 2}$	σ_ε	σ_K	C_μ
1.44	1.92	1.33	1	0.99

IV.2.5 Performance Assessment of SCPP

The accurate estimation of power output and efficiency is fundamental for the evaluation and optimization of SCPP. Among the various methods proposed in the literature, the most widely accepted approach estimates the power output based on the pressure drop across the turbine, which is expressed as follows:

$$P_{out} = \eta_{tur} \cdot \Delta p \cdot Q_v \quad \text{(IV.9)}$$

where η_{tur} denotes the turbine efficiency, commonly assumed to be 0.8 based on previous studies [6, 21, 40], Δp represents the pressure drop across the turbine which is typically determined as the product of the of the average pressure at the chimney's base and pressure drop , typically taken as 2/3 according to references [26, 27, 29, 34].), and Q_v is the volumetric flow rate of air passing through the turbine.

Collector efficiency:

$$\eta_{coll} = \frac{Q}{A_{coll}\, I} = \frac{m_a C_p (T_0 - T_a)}{A_{coll}\, I} \tag{IV.10}$$

Chimney efficiency:

$$\eta_{ch} = \frac{g H_{coll}}{C_p (T_0 - T_a)} \tag{IV.11}$$

Overall efficiency:

$$\eta_O = \frac{P_{out}}{A_{coll}\, I} \tag{IV.12}$$

were, Q is Heat transfer rate (W), C_p is Specific heat capacity of air (kJ/kg), A_{coll} is collector area. I is Irradiation (W/m²) and m_a is mass flow rate of air at Chimney base in (kg/s).

IV.2.6 The Boundary conditions for SCPP

Boundary conditions are crucial in numerical simulations, as they ensure an accurate representation of the physical model and contribute to obtaining reliable results. In this study, the boundary conditions, summarized in Table IV.3, are established based on previous research [74, 7, 70]. including the application of a constant solar radiation of 1000 W/m² to the collector, which is modelled as a semi-transparent surface with a heat transfer coefficient of 10 W/m² to ensure realistic thermal interactions. Meanwhile, the absorber plate is treated as an opaque surface with a zero-heat flux condition (q = 0 W/m²) to accurately capture its thermal behavior. The system operates under standard ambient conditions, with an atmospheric pressure of 101 kPa and a temperature of 302 K, which are imposed at the collector inlet to replicate real-world environmental conditions. To maintain continuity in airflow dynamics, the chimney outlet is set at the same pressure and temperature. Additionally, the chimney walls are assumed to be adiabatic (q = 0 W/m²), preventing heat loss to the surroundings.

The thermophysical properties of air used in this analysis are presented in detail in Table IV.4.

Table IV. 3: Applied boundary conditions.

Surface	Type	Value
Collector inlet	pressure temperature,	$P = 101\ kPa, T_a$ =302 K,
Chimney outlet	Pressure, temperature	$P = 101\ kPa, T_a$ =302 K,
Collector	semi-transparent	h =10 W/m^2
Chimney wall	Adiabatic wall	q = 0/m^2
Absorber	Opaque wall	q=0 W/m^2

Table IV. 4: the thermophysical properties of the air used in this analysis [71].

Thermophysical properties	Thermal conductivity (W/mK)	Specific heat (J/kgK)	Thermal expansion coefficient (1/K)
Air	0.0242	1006.43	0.00331

IV.2.7 Mesh generation

The accuracy and reliability of a CFD model are significantly influenced by the quality of the mesh used in the analysis. A well-refined mesh enhances numerical stability, improves solution convergence, and ensures precise results. To evaluate the impact of mesh refinement on simulation accuracy, a sensitivity analysis was conducted by testing different mesh densities and assessing their effect on the maximum air velocity at the chimney base and the highest temperature within the computational domain. Four mesh configurations: Fine, Plus Fine, Extra Fine, and Extremely Fine were examined, with the number of elements ranging from 6,775 to 8,457. As summarized in Table IV.5, increasing the mesh density beyond a specific threshold had minimal influence on the computed values. The maximum air velocity at the chimney base varied slightly between 15.3 m/s and 15.4 m/s, while the peak temperature remained constant at 322 K across all cases. This stability indicates that the solution has reached mesh independence, meaning further refinement would not significantly alter the results. Consequently, the Extra Fine mesh was selected for the final simulations (Fig IV.2)

as it provides an optimal balance between computational efficiency and accuracy. Employing an Extremely Fine mesh would only increase computational demands without yielding any meaningful improvement in precision.

Table IV. 5: Mesh Sensitivity Analysis: Number of Elements and Their Impact on Velocity and Temperature

Size	Number of elements	Max air velocity (m/s)	Max temperature (K)
Fine	6775	15.3	322
Plus Fine	7049	15.4	322
Extra Fine	7192	15.3	322
Extremely Fine	8457	15.3	322

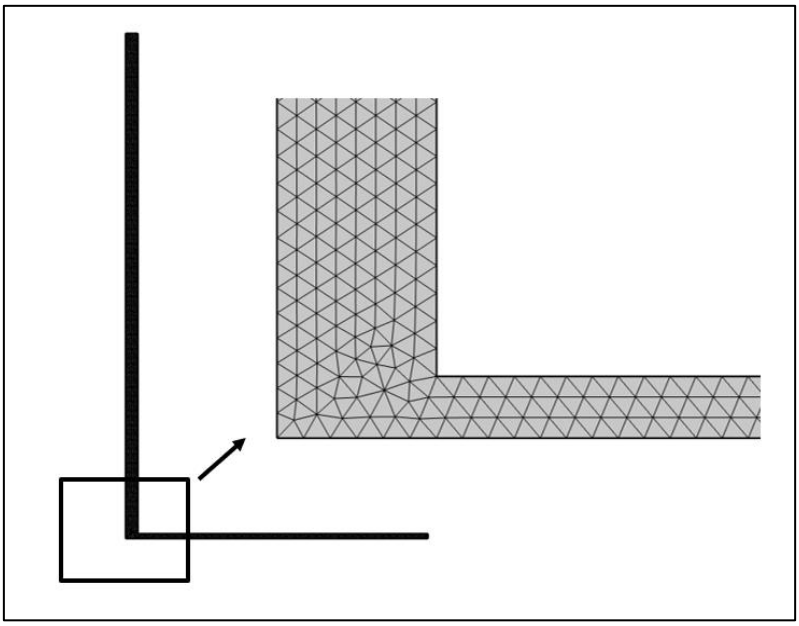

Figure IV. 2: Meshing view of the SCPP system.

IV.2.8 Validation of Simulation Results

To ensure the reliability of the numerical model before conducting extensive simulations, a validation study is performed by comparing the obtained results with both experimental and numerical data available in the literature [7, 117, 74, 70], particularly referencing the Manzanares prototype. This validation primarily focuses on key performance parameters, namely the chimney base velocity and the temperature rise within the system.

The airflow characteristics within the SCPP are depicted in Figure IV.3, illustrating the velocity distribution between the system's inlet and outlet. The simulation results reveal that the highest air velocity is recorded at the chimney base, reaching 15.3 m/s. A comparative analysis with previously published studies (Table IV.6) confirms a strong correlation, reinforcing the credibility of the model.

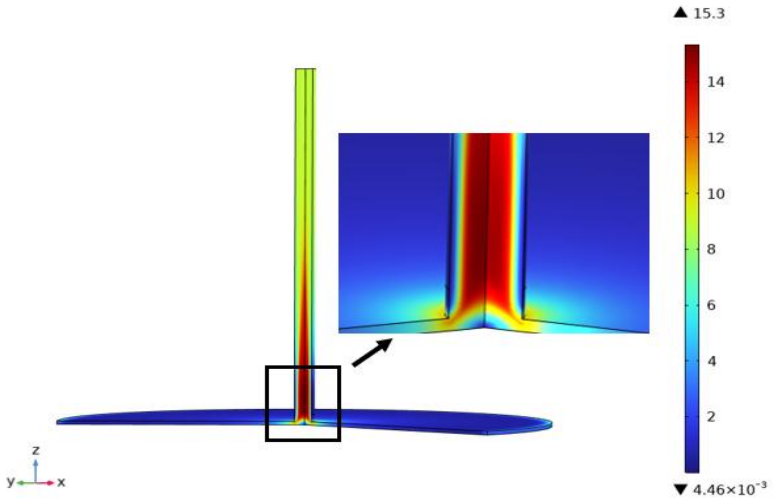

Figure IV. 3: Velocity distributions in the Solar Chimney Power Plant.

Table IV. 6: Comparison of maximum air velocity in Present and Published Studies.

Studies	Type of study	air velocity (m/s)
Present study	Numerical	*15.3*
HAAF et al. [7]	Experimental	*15*
Saad et al. [115]	Numerical	*14*
Cuce et al. [69]	Numerical	*14.20*
Biswas et al. [68]	Numerical	*10.47*
Mandel et al. [72]	Numerical	*11*

Additionally, Figure IV.4, presents the temperature profile inside the SCPP. The air temperature at the collector inlet starts at 302 K, progressively increasing to 322 K at the chimney inlet, resulting in a net temperature rise of 20 K. Further comparison with numerical and experimental data from existing studies (Table IV.7) demonstrates a high degree of consistency with the present results, substantiating the accuracy of the proposed model.

A comprehensive comparison confirms the reliability of the model. Therefore, the validated numerical model can be confidently employed to proceed with further investigations in this study.

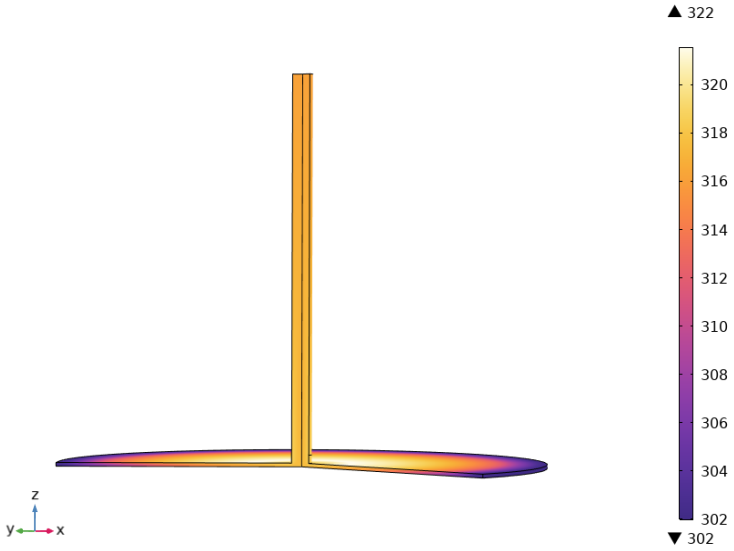

Figure IV. 4: Temperature distribution in the Solar Chimney Power Plant.

Table IV. 7: Comparison of Temperature Rise in Present and Published Studies.

Studies	Type of study	Temperature rise (K)
Present study	Numerical	*20*
HAAF et al. [7]	Experimental	*20*
Saad et al. [115]	Numerical	21.77
Cuce et al. [69]	Numerical	20
Biswas et al. [68]	Numerical	*17*
Mandel et al. [72]	Numerical	19

IV.3 Geometric parameter investigation

This study presents a detailed numerical investigation aimed at optimizing the key geometric parameters of a SCPP, particularly those configurations that could not be examined through experimental methods. The investigation focuses on three main geometric factors: the absorber plate defined by its slope (α) radius (R); the collector inclination (β); and the chimney angle (θ). The optimization process is carried out in three sequential phases.

the first phase, the geometry of the absorber plate is investigated by varying its slope and radius, with the aim of identifying their influence on the performance of the SCPP. Once the most effective absorber plate configuration is established, the second phase concentrates on optimizing the collector inclination. This is achieved by adjusting the collector angle and analyzing its impact to ensure efficient integration with the absorber, thereby enhancing solar energy capture and overall system efficiency. The third phase is dedicated to optimizing the chimney configuration, focusing on its interaction with the previously optimized absorber and collector to maximize the performance of the SCPP. The schematic representation of the SCPP, including the parameters under investigation absorber slope angle α, absorber radius R, collector inclination β, and chimney inclination θ is illustrated in Figure IV.5.

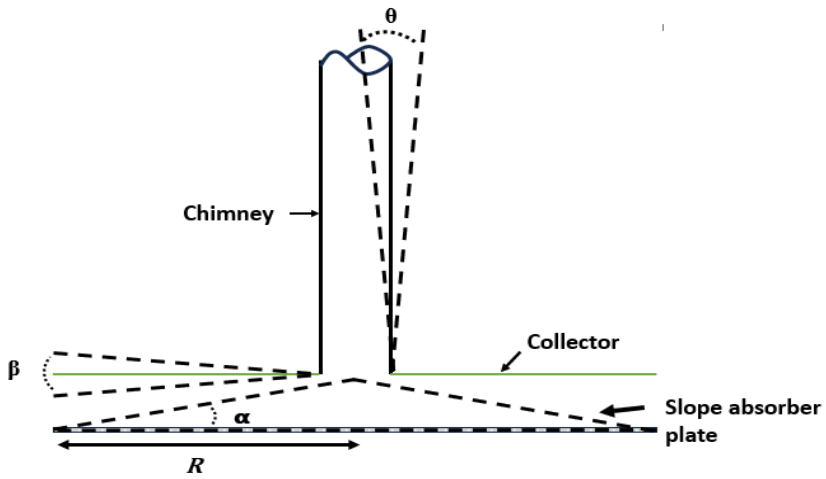

Figure IV. 5: Schematic Diagram of the Geometric Optimization Process for SCPP.

IV.3.1 Optimization of absorber plate inclination

Researchers have investigated a variety of absorber plate geometries to enhance the efficiency of SCPPs. These include sloped triangular, semi-circular, rectangular, right-angled triangular, equilateral triangular, and sinusoidal triangular (wavy) configurations [69–74]. Among the investigated geometries, the sloped absorber (singular triangular-shaped) has demonstrated notable potential in enhancing thermal efficiency, airflow behavior, and power generation. Despite this recognized superiority, previous studies have addressed the configuration only from limited perspectives, without examining its dimensional variations or identifying optimal parameters of the slope absorber. This study, therefore, aims to determine the most effective dimensions of the singular triangular absorber for the Manzanares plant, with the objective of improving overall power output.

Building on this research gap, the present section investigates the influence of absorber slope angle α and absorber radius R on system performance, as showing in figure IV.5. The analysis begins with a transition from a flat (horizontal) absorber plate to an initial sloped configuration, followed by a detailed evaluation of inclination angles ranging from 0° to 0.60°. In addition, the effect of varying the absorber radius between 5 and 122 m is examined. The objective is to determine the optimal sloped absorber design capable of enhancing overall power generation efficiency.

IV.3.1.1 Influence of absorber slope

As outlined in the preceding section, the analysis proceeds by transitioning from a flat (horizontal) absorber plate to a sloped configuration. In this stage, the absorber radius is fixed at 122 m, while the slopped angle α is systematically varied from 0° to 0.60° to assess its influence on system performance. The corresponding numerical results are presented in Figure IV.6, which illustrates the variation of maximum air velocity and maximum air temperature as a function of absorber inclination.

The influence of α on maximum air velocity was first examined under the baseline configuration, corresponding to a horizontal plate ($\alpha = 0°$), where the velocity was 15.3 m/s. As the slope increased, the velocity rose progressively, reaching 16.9 m/s at $\alpha = 0.28°$ and peaking at 18.7 m/s at $\alpha = 0.51°$. At relatively small inclinations ($\alpha \leq 0.18°$), the increase was modest; however, once α exceeded this threshold, airflow acceleration became more pronounced. This behavior is attributed to the strengthening of a Venturi effect, Beyond the optimum slope, a slight reduction in velocity to 18.0 m/s at $\alpha = 0.56°$ was observed, indicating that excessive inclinations introduce flow separation and increased friction, which reduce aerodynamic efficiency. By contrast, the impact of α on maximum air temperature was less significant. For inclinations up to $\alpha = 0.37°$, the temperature remained nearly constant at approximately 322 K, suggesting negligible influence of mild slope variations on thermal performance. Beyond this point, a gradual increase was observed, with the temperature rising to 325 K. This increase can be attributed to the fact that as the slope angle α increases, the gap between the collector cover and the absorber plate becomes narrower, thereby reducing radiative and convective losses during the transfer of solar energy to the absorber.

Although this effect is relatively modest compared to the influence on airflow velocity, the findings indicate that steeper absorber slopes can slightly enhance the thermal conditions within the SCPP.

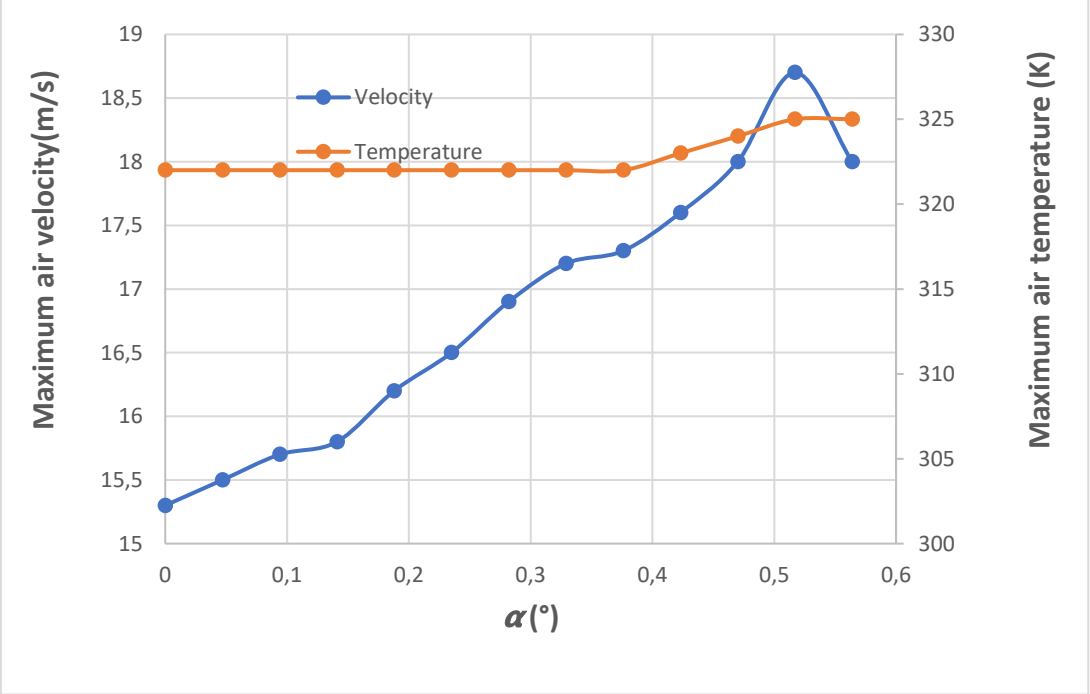

Figure IV. 6: Effect of absorber plate slope angle (α) on maximum air velocity and on maximum air temperature.

IV.3.1.2 Influence of absorber radius

This section analyzes the influence of the absorber radius on the overall performance of the solar chimney system, while keeping the inclination angle fixed at its previously identified optimal value of ($\alpha = 0.51°$). To isolate this effect, the absorber radius R is systematically varied from 5 m to 122 m, allowing for the evaluation of its impact on two key performance indicators: maximum air velocity and maximum air temperature. The corresponding numerical results are illustrated in Figure IV.7.

The findings show that absorber radius strongly affects airflow velocity. At small radii, velocity is relatively low, with a minimum value of 15.8 m/s recorded at R=5 m. As the radius increases, velocity rises progressively, reaching 16.7 m/s at (R=10 m), 17.5 m/s (at R=30 m), and 18.3 m/s at (R=50 m). Beyond this point, the increase continues but at a slower rate, ultimately attaining 18.9 m/s for radii between 110 m and 122 m. The improvement in velocity can be attributed to two primary mechanisms. First, a larger absorber radius enhances the transition of airflow from the collector to the chimney by reducing turbulence and flow

separation, thereby enabling smoother air entry into the chimney. Second, as the heated air moves from the wide collector to the narrower chimney inlet, it accelerates due to a Venturi-type effect.

In contrast, the absorber radius exerts only a marginal influence on maximum air temperature. Across the entire range, the temperature remains nearly constant, fluctuating between 324 K and 325 K. This stability indicates that increasing the radius affects only the aerodynamic behavior, with no noticeable impact on thermal performance.

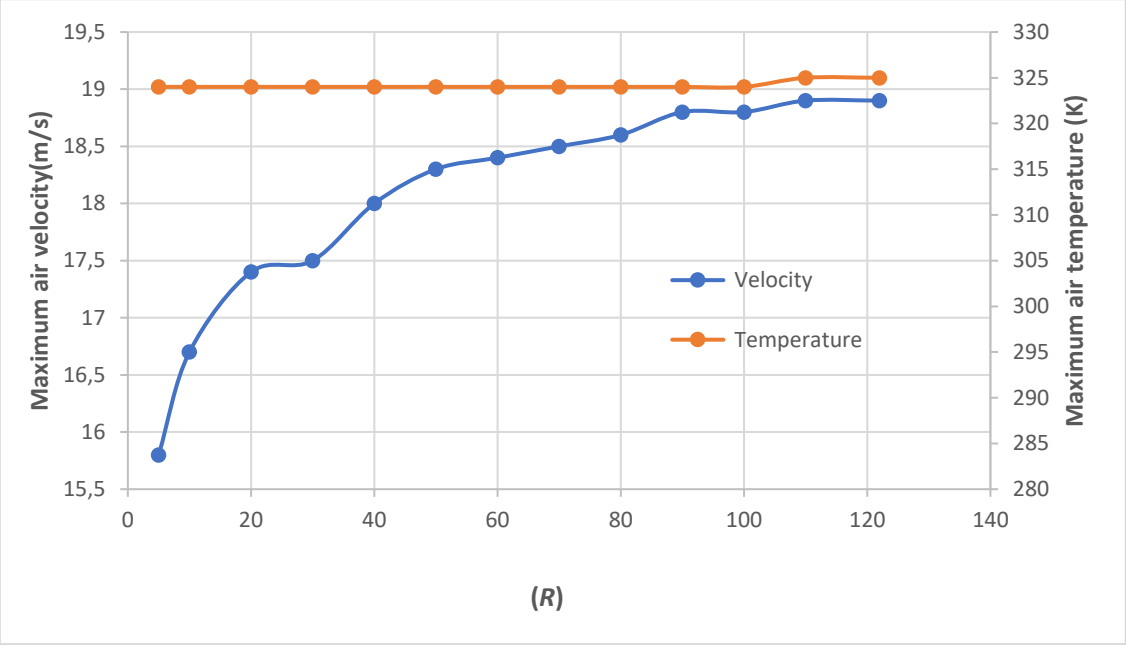

Figure IV. 7: Effect of absorber plate slope radius (R) on maximum air velocity and on maximum air temperature.

IV.3.2.3 Velocity and temperature distribution at the optimal absorber slope

Figures IV.8.a and IV.8.b illustrate the velocity and temperature distributions within the SCPP under the optimal absorber configuration, defined by a slope angle of ($\alpha = 0.51°$) and an absorber radius of ($R = 122$). As depicted in Figure IV.8.a, the airflow velocity is lowest at the collector inlet and progressively increases along the flow path, reaching a maximum of 18.7 m/s at the chimney base. Similarly, Figure IV.8.b shows that the air temperature begins at 302 K at the collector inlet and gradually rises toward the central region, attaining a peak of 325 K.

Overall, the results confirm that the sloped absorber surface constitutes a decisive design feature for SCPP performance.

At the optimal configuration, the system achieves an airflow velocity of 18.7 m/s and a net temperature rise of 23 K, underscoring the pivotal role of geometric optimization in enhancing system efficiency.

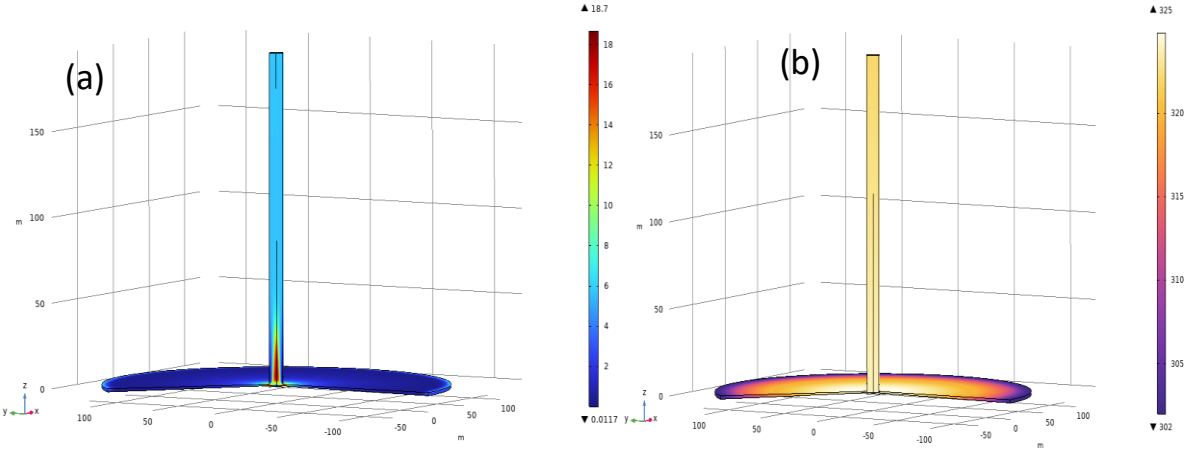

Figure IV. 8: Velocity and Temperature Distribution at the optimal absorber configuration in the SCPP (a) Velocity Distribution (b) Temperature Distribution

IV.3.2 Optimization of the collector configuration

After determining the optimal absorber plate surface, the study advances to the optimization of the collector configuration. This phase aims to refine the collector geometry to enhance solar energy absorption and improve system performance. The optimization process involves systematically varying the collector inclination angle β within the range of −1.5° to +1.5°, as illustrated in Figure IV.5. A positive inclination ($\beta > 0$) corresponds to an upward-sloping collector roof, which increases the distance between the collector cover and absorber as it extends outward.

In contrast, a negative inclination ($\beta < 0$) represents a downward-sloping collector roof, where the gap between the cover and absorber decreases toward the periphery. The case of ($\beta = 0$) denotes a horizontal collector roof. These configurations are evaluated to determine the optimal inclination that maximizes solar radiation absorption, enhances airflow acceleration, and improves the overall efficiency of the SCPP.

IV.3.2.1 Effect on air velocity in the SCCP

To assess the impact of collector inclinations on airflow behavior within the SCPP, the spatial distribution of velocity magnitude was examined throughout the whole system volume for each roof inclination (β = +1;5 to −1.5°), as illustrated in Figure IV.9.

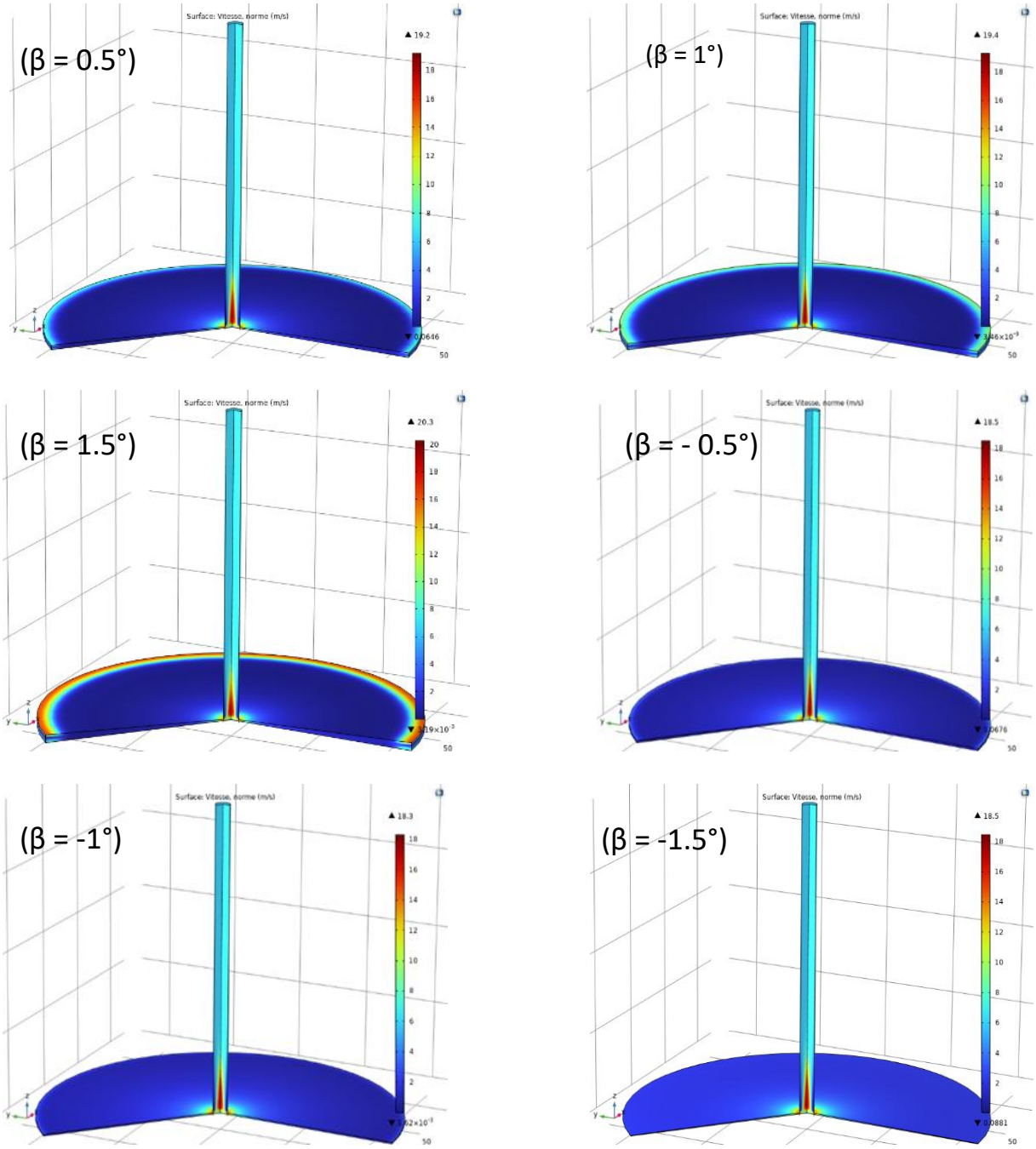

Figure IV. 9: Air velocity distribution in SCPP for different collectors Slopes (β).

Across all configurations, the velocity shows a gradual increase along the collector length, beginning with low values near the inlet and peaking at the chimney base. The

magnitude of this peak is not constant but varies with the collector inclination, a dependency clearly demonstrated in the numerical simulations results.

As shown in Figure IV.9, positive slopes (β = 0.5°to +1.5°) exhibit a clear upward trend in velocity. At (β = 0.5°), the maximum velocity reaches approximately 18.7 m/s, increasing to 19.8 m/s at (β = 1°), and further to 20.3 m/s at (β = 1.5°). The performance enhancement is primarily attributed to the superior capacity of inclined collectors to intercept incident solar radiation more effectively than flat configurations. In addition, a positive inclination amplifies the Venturi effect, thereby accelerating airflow and reducing turbulence-related dissipation within the system. In contrast, negative slopes (β = −0.5°, −1°, and −1.5°) do not yield any meaningful improvement in airflow velocity. The corresponding maximum velocities, 18.5 m/s, 18.3 m/s, and 18.5 m/s, remain nearly constant, indicating limited performance enhancement despite increasing negative inclination. This behavior indicates that negative slopes do not enhance the interception of incident solar radiation, which leads to reduced buoyancy forces and less effective airflow guidance. In addition, they disrupt the natural flow trajectory, thereby constraining the attainable airflow velocity.

IV.3.2.2 Effect on Air Temperature in the SCPP

To investigate the impact of collector inclination on the spatial distribution and evolution of air temperature within the system, the same methodology applied to the velocity field analysis was adopted, whereby the spatial distribution of temperature was examined across the entire system volume for each roof inclination (β = 1.5° to −1.5°). The corresponding results are presented in Figure IV.10, which illustrates the temperature distributions for the different roof configurations.

The outcomes of the numerical simulations demonstrate that both positive and negative collector inclinations yield a comparable overall distribution of air temperature within the SCPP. The thermal profile along the collector shows a progressive increase caused by the absorption of solar radiation, with the air entering near ambient conditions and attaining its maximum temperature at the collector center, followed by an almost steady state within the chimney. Nonetheless, the maximum temperature values vary noticeably with slope angle, underscoring that collector inclination plays a decisive role in shaping the thermal characteristics of the airflow inside the system.

For positive slopes (β = 0.5°to +1.5°), a gradual reduction in maximum temperature is observed with increasing inclination. Specifically, the peak temperature reaches 324 K at β = 0.5°,

decreases to 323 K at β = 1°, and further drops to 320 K at β = 1.5°. In contrast, for negative slopes (β = −0.5°, −1°, and −1.5°), the maximum temperature values are slightly higher, at 326 K, 325 K, and 326 K, respectively.

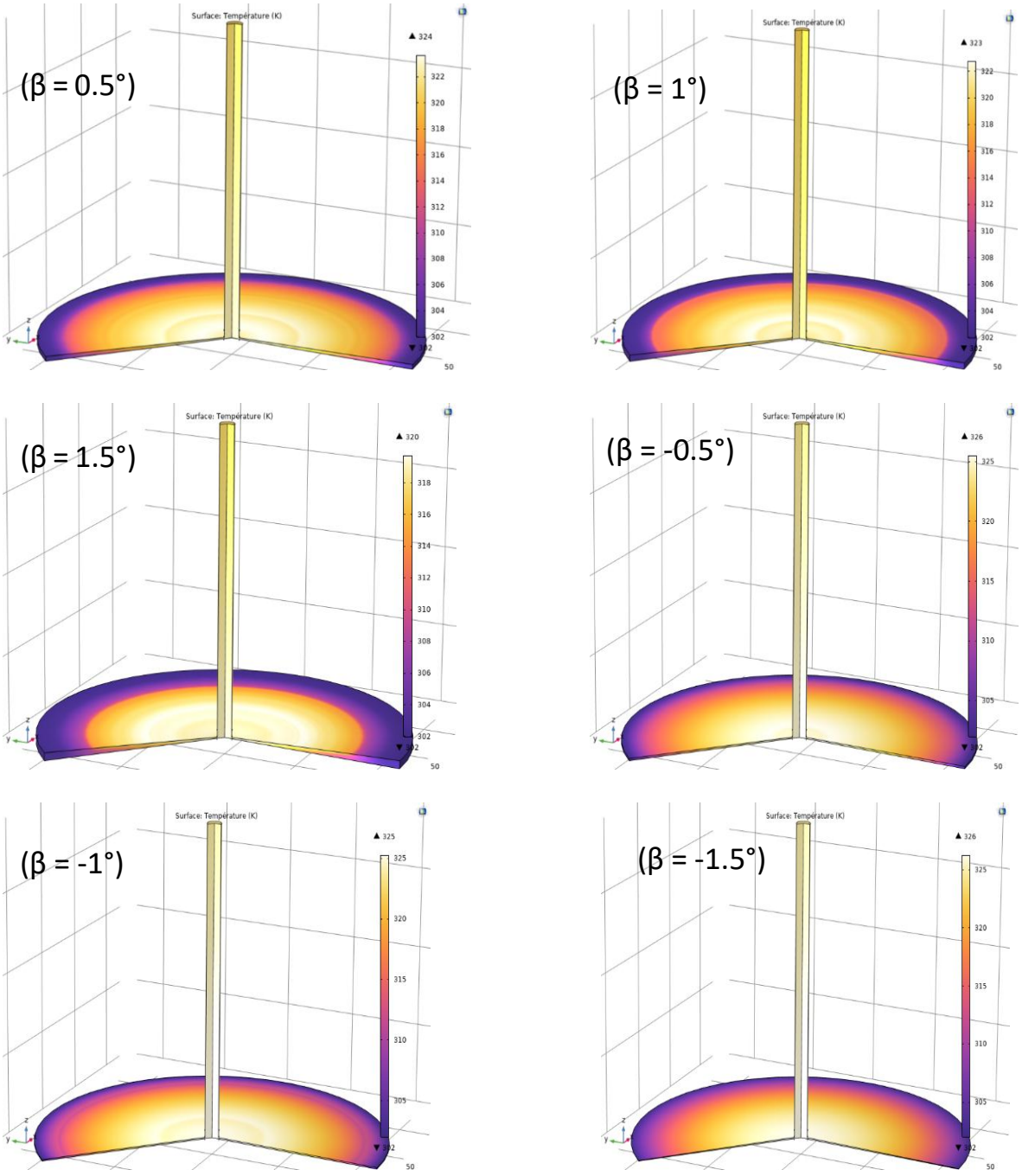

Figure IV. 10: Air temperature distribution in SCPP for different collectors Slopes (β).

These results are attributed to the fact that negative inclinations capture a larger fraction of incident solar radiation compared with positive slopes, as the narrower gap between the cover and absorber reduces radiative and convective losses while enhancing thermal energy retention within the collector. Consequently, configurations with negative inclinations exhibit higher

thermal performance relative to those with positive slopes. The comparison of these results confirms that collector roof angles exert a direct influence on the air temperature within the SCPP. Overall, the adoption of negative slopes promotes greater retention of internal heat, thereby extending the operational capability of the SCPP into nighttime hours while maintaining improved performance under peak conditions. These findings underscore the importance of carefully balancing thermal preservation with aerodynamic performance in order to achieve an optimal SCPP design. In this context, (β = 1.5) is identified as the optimal inclination angle for the collector, since it provides the maximum air velocity.

IV.3.3 Optimization of the Chimney Configuration

After determining the optimal values for the absorber slope α and the collector configuration β, these parameters are fixed to establish a stable basis for further analysis. The subsequent step investigates the effect of chimney inclination θ on the overall performance of the SCPP. The chimney inclination is varied within the range of −1.5° to +1.5°, as illustrated in Figure IV .5 A positive inclination ($\theta > 0$) corresponds to a conical chimney, in which the cross-sectional area gradually increases with height. Conversely, a negative inclination ($\theta < 0$) represents an inverted conical chimney, where the cross-sectional area decreases toward the outlet. These variations are examined to identify the most efficient configuration for enhancing airflow acceleration, strengthening the stack effect, and maximizing power output.

IV.3.3.1 Effect on maximum air velocity

The variation of maximum air velocity as a function of chimney inclination θ is shown in Figure IV.11 for both positive and negative configurations. The results demonstrate that the aerodynamic response of the system is strongly dependent on the direction and degree of inclination

For negative inclinations ($\theta < 0°$), the velocity decreases progressively, falling from 20.3 m/s at the vertical reference case ($\theta = 0°$) to 16.7 m/s at ($\theta = -1.5°$). This reduction arises from the inward contraction of the chimney cross-section, which restricts the flow passage and weakens the buoyancy-driven pressure difference. As a result, the airflow momentum diminishes, leading to lower velocity at the outlet. Conversely, positive inclinations ($\theta > 0°$) produce an initial enhancement in airflow velocity. A moderate divergence at (θ = 0.5°) yields the maximum value of 23.3 m/s, representing the most favorable configuration for accelerating the heated air stream. This improvement can be attributed to the gradual expansion of the chimney, which facilitates smoother flow guidance, reduces resistance, and promotes acceleration.

However, further increases in inclination beyond this optimum result in a gradual decline in velocity, with the value dropping to 22.6 m/s at (θ = 1.5°). At higher divergence, the excessive expansion induces turbulence and velocity dispersion, which disrupt the uniformity of the flow and reduce its effective acceleration.

Overall, the results establish that a conical chimney with (θ = 0.5°) represents the optimal configuration, as it yields the highest velocity and underscores the crucial role of chimney geometry in enhancing buoyancy-driven airflow and, consequently, the performance of the SCPP.

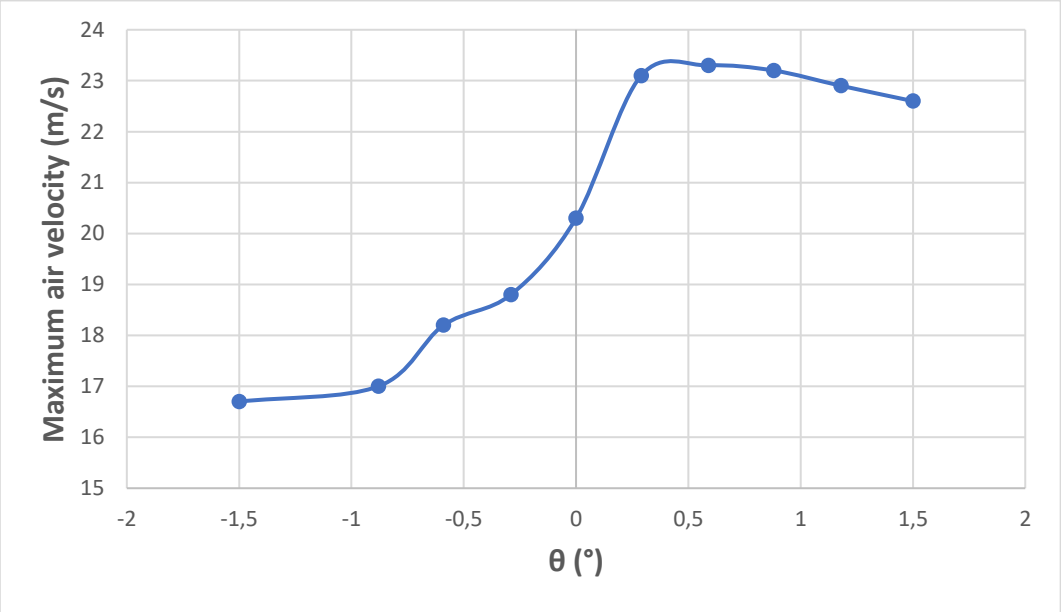

Figure IV. 11: variation of the maximum air Velocity in SCPP for different chimney inclination (θ).

IV.3.3.2 Effect on maximum air temperature

The variation of maximum air temperature with respect to chimney inclination θ is presented in Figure IV.12. As the figure shows, numerical simulations indicate that for negative inclination angles (θ < 0°), the maximum air temperature increases with the steepness of the slope. Specifically, the temperature rises from 320 K at the base case (θ = 0°) to 335 K at (θ = –1.5°), suggesting that a negatively inclined chimney promotes greater thermal accumulation. In contrast, for positive inclination angles (θ > 0°), the temperature remains nearly constant at approximately 321 K, regardless of slope, indicating only a negligible effect on thermal behavior. This asymmetry highlights that chimney inclination influences thermal performance differently depending on the tilt direction: negative inclinations enhance heat retention, whereas positive inclinations provide minimal additional gains.

Nevertheless, the thermal advantage of negative inclinations is offset by the simultaneous reduction in airflow velocity, which may constrain overall power generation. Therefore, both velocity and temperature must be considered in tandem to achieve a balanced and efficient SCPP design.

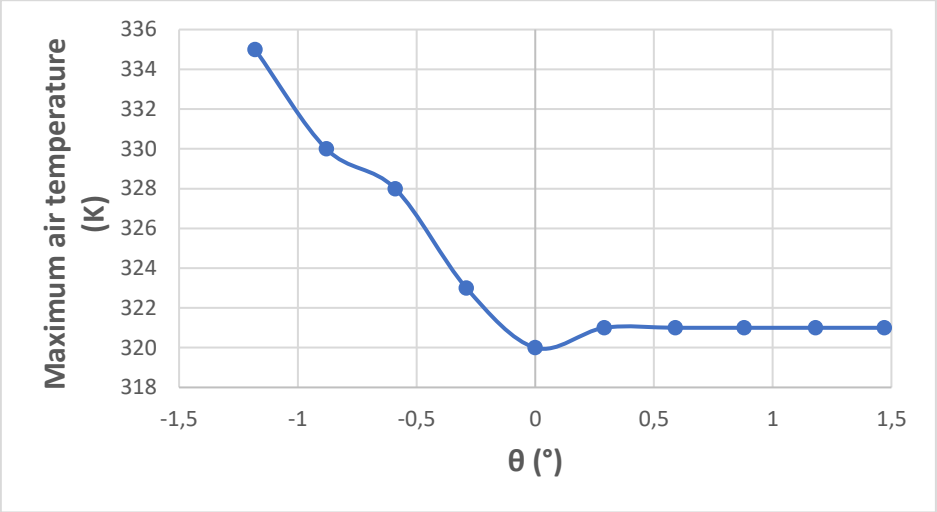

Figure IV. 12: variation of the maximum air temperature in SCPP for different chimney inclination (θ).

IV.3.3.3 Velocity and Temperature Distribution at the Optimal Chimney Inclination

Following the determination of the optimal chimney inclination angle θ, the final optimized configuration of the SCPP incorporates the most effective values of slope absorber central surface α and R, inclination collector slope β, and chimney inclination θ to achieve maximum system performance. Figure IV.13 illustrates the velocity and temperature distributions within the SCPP under these optimal conditions. As shown in Figure IV.13a, the airflow velocity exhibits a clear and progressive evolution along the flow path. At the collector inlet, the velocity begins at relatively low values and gradually accelerates as the air moves radially inward along the collector length, producing a continuous rise toward the chimney entrance. The highest velocity, reaching 23.3 m/s, is observed at the base of the chimney, clearly demonstrating the role of the conical chimney configuration with $\theta = 0.5°$ in enhancing flow acceleration. Importantly, despite the modification in chimney geometry, the velocity peak remains located at the chimney base. This ensures that the turbine can remain in its conventional position without requiring structural adjustments, while still benefiting from the aerodynamic improvements provided by the optimized configuration. Similarly, the temperature distribution presented in Figure IV.13b shows that the lowest air temperature occurs at the collector inlet, where the flow enters close to ambient conditions.

As the air progresses radially inward, its temperature increases gradually due to continuous solar heating, reaching a maximum value of 321 K near the center of the collector. Beyond this region, the thermal field within the chimney remains nearly steady, indicating a stabilized temperature profile. This gradient between the inlet and the central outlet of the collector plays a pivotal role in driving buoyancy-induced convection, thereby sustaining continuous airflow and enhancing the overall thermal performance of the system. These findings confirm that the optimal combination of θ, α, and β establishes a well-balanced system that maximizes both thermal and fluid dynamic performance. This final configuration results in higher airflow velocity, improved heat transfer, and enhanced overall efficiency of the SCPP, thereby optimizing its power generation potential.

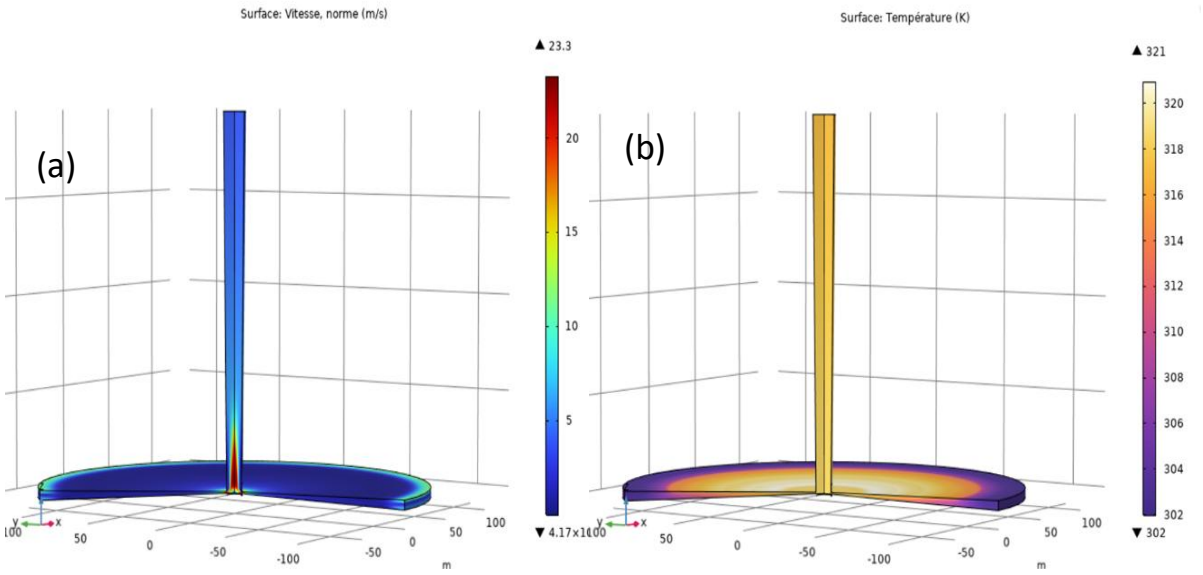

Figure IV. 13: Velocity and temperature distributions under the optimal configuration of the SCPP.

IV.4 Power Generation in SCCP: A comparative study

A comprehensive comparative assessment was conducted to evaluate the power output of the reference case of the Manzanares prototype and the optimized configuration proposed in this study. As shown in Figure IV .14, the reference case yields a power output of 50 kW. In contrast, the optimized configuration, which includes an optimal absorber slope, collector and chimney, results in a power output of 187.5kW. This represents a 275% increase over the reference case, indicating a significant enhancement in performance.

The results confirm the effectiveness of the proposed geometry optimization in substantially improving power generation in SCPPs, demonstrating that the optimizations presented in this study lead to superior performance compared to the Manzanares reference configuration.

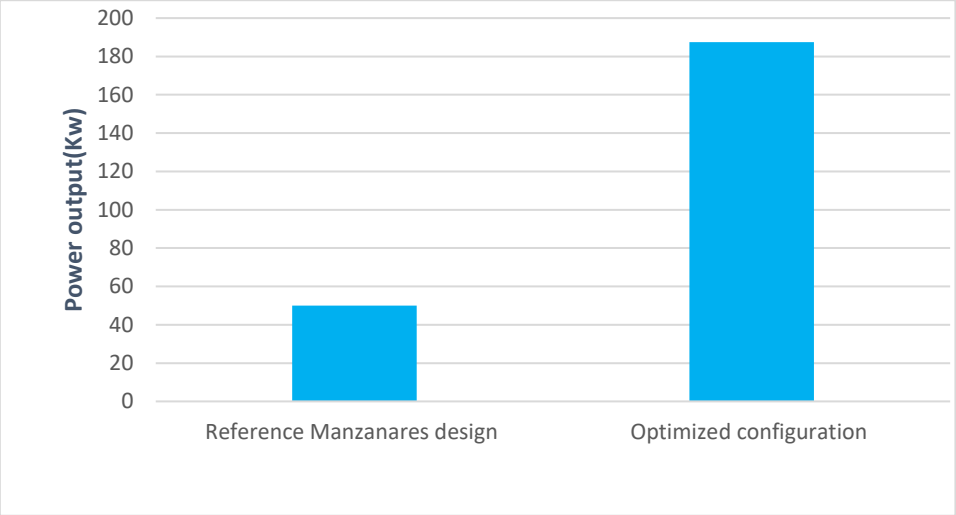

Figure IV. 14: Power Output for reference Manzanares design and optimized configuration.

IV.5 Conclusion

This chapter carried out a numerical investigation of SCPP using COMSOL Multiphysics, aimed at evaluating how geometric modifications influence system performance. The numerical model was first validated against experimental data and published numerical studies, confirming its robustness and predictive accuracy.

The optimization study systematically analyzed the three principal geometric components of the SCPP namely, the absorber plate, the collector, and the chimney with particular emphasis on their influence on airflow velocity and air temperature. For each component, numerical simulations were carried out to evaluate how geometric modifications affect the thermal and aerodynamic behavior of the system. This approach made it possible to establish clear correlations between design parameters and performance outcomes, highlighting the role of geometry in enhancing flow acceleration, improving thermal retention, and ultimately increasing power output. The key findings are summarized as follows:

- The optimization of the absorber plate, with a slope angle of $\alpha = 0.51°$ and an absorber radius of $R = 122$, enhanced flow acceleration and heat retention, resulting in a peak airflow velocity of 18.7 m/s and a maximum air temperature of 325 K.

- Adjusting the collector inclination to $\beta = 1.5°$ further improved performance, increasing the maximum airflow velocity to 20.3 m/s and yielding a temperature of 320 K.
- Incorporating a conical chimney with an inclination angle of $\theta = 0.5°$ produced the highest velocity within the system, reaching 23.3 m/s, while maintaining the air temperature at approximately 321 K.

- Integrating these optimized parameters resulted in a substantial improvement in overall system performance, with the SCPP achieving a power output of 187.5 kW corresponding to a 275% increase compared with the reference case.

In summary, the findings confirm that systematic optimization of the key geometric components namely the absorber, collector, and chimney lead to substantial enhancements in the performance of the SCPP.

GENERAL CONCLUSION

General conclusion

Solar chimney power plants have emerged as a promising renewable energy technology capable of addressing multiple global challenges, notably the accelerating climate crisis, the depletion of conventional energy resources, and the growing global demand for clean and sustainable power. Based on the fundamental principles of natural convection and the greenhouse effect, SCPPs offer an environmentally responsible method for converting solar radiation into continuous airflow, which in turn drives turbine-based electricity generation. With a relatively simple configuration comprising a solar collector, an absorber plate, a vertical chimney and a turbine, these systems are particularly attractive due to their low construction and maintenance costs compared to other renewable technologies. This economic viability, combined with their minimal environmental impact, highlights the potential of SCPPs as scalable and sustainable energy solutions. Another key advantage of SCPPs is their suitability for deployment in desert and semi-arid regions, where solar irradiance reaches some of the world's highest levels and vast areas of barren land remain unexploited. Algeria exemplifies such favorable conditions, making it an ideal setting for both experimental development and large-scale application of this renewable energy technology.

In this context, the present study provides a meaningful contribution to the understanding and optimization of SCPPs by investigating the effects of geometric design and environmental parameters through a combination of experimental and numerical approaches, taking into account local conditions where applicable.

In the first phase of this work, an experimental study was carried out in which a prototype solar chimney was designed and installed at our university, Faculty of Technology in Chlef, Algeria. The primary objective of the experimental investigation was to evaluate the impact of specific geometric parameters namely, the air inlet diameter and the number of air inlets on airflow velocity and temperature distribution within the system. In addition to geometric factors, the study examined the influence of key environmental variables, particularly solar irradiance and ambient air temperature, on the performance of the SCPP. Seasonal variations were also considered to assess how changes in local climatic conditions throughout the year affect the thermal behavior and overall efficiency of the system.

In the second phase, a numerical study was conducted to complement the experimental findings. This simulation-based analysis focused on geometric configurations that could not be tested experimentally, such as the absorber plate and collector and chimney. The numerical

model was developed using the physical characteristics and boundary conditions of the Manzanares prototype, enabling a controlled assessment of various design modifications. This modeling effort provided deeper insights into the role of geometry in optimizing system performance and offered valuable guidance for future design improvements aimed at enhancing the efficiency and feasibility of SCPPs.

The integration of both experimental and numerical approaches in this study has enabled a comprehensive evaluation of Solar Chimney Power Plant performances under varying design and environmental conditions. The findings obtained from each phase are summarized below.

Based on the findings from the experimental investigation:

- The experimental findings underscore the pivotal role of both the air inlet diameter and the number of air inlets in shaping the airflow dynamics and internal temperature distribution within the solar chimney system.
- Among the configurations tested, a 20 cm air inlet diameter provided the most effective balance. This configuration facilitated enhanced airflow velocity and temperature differential, indicating its suitability for performance optimization.
- The four-air-inlets arrangement consistently outperformed the two and six-air-inlets designs, demonstrating superior aerodynamic stability and thermal behavior. This highlights the importance of carefully tuning inlet geometry to maximize system efficiency.
- Furthermore, the analysis confirmed that solar irradiance is the dominant driver of system performance, exhibiting a strong positive correlation with internal temperature rise and airflow velocity. In contrast, ambient air temperature had a negligible impact, suggesting that the system's thermal response is primarily governed by solar irradiance input rather than external climatic fluctuations.
- Seasonal observations confirmed the system's reliability under varying climatic conditions, demonstrating its potential for continuous, year-round operation. Moreover, the integration of thermal storage materials beneath the collector improved nighttime performance by retaining heat and sustaining airflow beyond sunset, thereby enhancing overall system efficiency.

Based on the findings from the numerical simulations:

- Key geometric elements such as the absorber plate, collector, and chimney exert a significant influence on the performance of the SCPP.
- Strategic adjustments to these parameters notably improved airflow velocity and temperature distribution, resulting in enhanced overall system efficiency.
- The integration of optimized geometric values produced a marked increase in power output, clearly demonstrating the critical role of design optimization in maximizing SCPP performance.
- COMSOL Multiphysics proved to be an effective and robust simulation tool, enabling a detailed and accurate representation of the complex thermodynamic phenomena and fluid dynamics occurring within the solar chimney. This facilitated a deeper understanding of the system's real behavior, allowing precise evaluation of performance and supporting targeted design improvements.
- Collectively, these results affirm the effectiveness of targeted geometric and thermal design strategies in enhancing the efficiency and practicality of solar chimney systems. Notably, the environmental context of the Chlef region in Algeria where this study was conducted proves highly conducive to SCPP deployment, reinforcing the potential of this technology as a scalable and sustainable solution for clean energy generation in solar-rich environments.

Future Work

In our future work, we plan to hybridize the SCPP with photovoltaic and wind systems to ensure continuous power generation during periods of low solar input. We also aim to design decentralized and adaptable SCPP units tailored for rural and agricultural applications to promote energy autonomy. Additionally, we intend to integrate the SCPP into agrivoltaics systems to optimize land use by combining energy production with farming. On a larger scale, we will explore the connection of SCPPs to the national electrical grid to support grid stability and enhance the renewable energy mix. Finally, we will focus on improving system resilience by developing smart control strategies that adapt to climatic variations and ensure reliable year-round operation.

BIBLIOGRAPHY

Bibliography

[1] McKinsey & Company, "Global Energy Perspective 2024," *McKinsey & Company*, Sep. 17, 2024. https://www.mckinsey.com/industries/energy-and-materials/our-insights/global-energy-perspective

[2] IEA, "Growth in global energy demand surged in 2024 to almost twice its recent average - News - IEA," *IEA*, Mar. 24, 2025. https://www.iea.org/news/growth-in-global-energy-demand-surged-in-2024-to-almost-twice-its-recent-average

[3] Energy Institute, "Statistical Review of World Energy," *Statistical review of world energy*, 2024. https://www.energyinst.org/statistical-review

[4] Nsaif, Osama Sabbar. Numerical study of the effects of geometric parameters on performance of solar chimney power plants. MS thesis. 2019.,

[5] E. Cuce *et al.*, "Solar Chimney Power Plants: A Review of the Concepts, Designs and Performances," *Sustainability*, vol. 14, no. 3, p. 1450, Jan. 2022, doi: https://doi.org/10.3390/su14031450.

[6] Dhahri, Amel, and Ahmed Omri. 'A review of solar chimney power generation technology.' International Journal of Engineering and Advanced Technology 2.3 (2013): 1-17.

[7] J. Schlaich, R. Bergermann, W. Schiel, and G. Weinrebe, "Design of Commercial Solar Updraft Tower Systems—Utilization of Solar Induced Convective Flows for Power Generation," *Journal of Solar Energy Engineering*, vol. 127, no. 1, pp. 117–124, Feb. 2005, doi: https://doi.org/10.1115/1.1823493.

[8] P. Das and V. P. Chandramohan, "A review on solar updraft tower plant technology: Thermodynamic analysis, worldwide status, recent advances, major challenges and opportunities," *Sustainable Energy Technologies and Assessments*, vol. 52, p. 102091, Aug. 2022, doi: https://doi.org/10.1016/j.seta.2022.102091.

[9] W. HAAF, K. FRIEDRICH, G. MAYR, and J. SCHLAICH, "Solar Chimneys Part I: Principle and Construction of the Pilot Plant in Manzanares," *International Journal of Solar Energy*, vol. 2, no. 1, pp. 3–20, Jan. 1983, doi: https://doi.org/10.1080/01425918308909911.

[10] Pedram Karimi-Pour-Fard, H. Beheshti, and Ehsan Baniasadi, "Energy and exergy analyses of a solar chimney power plant with thermal energy storage," *International Journal of Exergy*, Jun. 2016.

[11] T. P. Fluri and T. W. Von Backström, "Performance analysis of the power conversion unit of a solar chimney power plant," *Solar Energy*, vol. 82, no. 11, pp. 999–1008, Nov. 2008, doi: https://doi.org/10.1016/j.solener.2008.05.001.

[12] H. Pastohr, "Thermodynamische Modellierung Eines Aufwindkraftwerkes," Ph.D. Thesis, Civil Engineering, Bauhaus-Universität Weimar, Weimar, Germany, 2004.

[13] H. H. Al-Kayiem and O. C. Aja, "Historic and recent progress in solar chimney power plant enhancing technologies," *Renewable and Sustainable Energy Reviews*, vol. 58, pp. 1269–1292, May 2016, doi: https://doi.org/10.1016/j.rser.2015.12.331.

[14] X. Zhou, F. Wang, and R. M. Ochieng, "A review of solar chimney power technology," *Renewable and Sustainable Energy Reviews*, vol. 14, no. 8, pp. 2315–2338, Oct. 2010, doi: https://doi.org/10.1016/j.rser.2010.04.018.

[15] W. HAAF, "Solar Chimneys," *International Journal of Solar Energy*, vol. 2, no. 2, pp. 141–161, Jan. 1984, doi: https://doi.org/10.1080/01425918408909921.

[16] A. El Hadj., " Contribution à l'étude expérimentale d'une cheminée solaire en Algérie," Thesis, UNIVERSITE KASDI MERBAH OUARGLA, 2021.

[17] Karimi-Pour-Fard, P.; Beheshti, H. Performance enhancement and environmental impact analysis of a solar chimney power plant: Twenty-four-hour simulation in climate condition of isfahan province, iran. Int. J. Eng. 2017, 30, 1260–1269. ,.

[18] M.T. Esfidani, S. Raveshi, M. Shahsavari, and A. Sedaghat, "Computational study on design parameters of a solar chimney," *2015 International Conference on Sustainable Mobility Applications, Renewables and Technology (SMART)*, Nov. 2015, doi: https://doi.org/10.1109/smart.2015.7399268.

[19] Hadda Nouar, Toufik Tahri, and Y. Chiba, "Study on the Performance of a solar chimney power plant Chlef, Algeria region," *2018 International Conference on Applied Smart Systems (ICASS)*, pp. 1–5, Nov. 2018, doi: https://doi.org/10.1109/icass.2018.8652067.

[20] A. Koonsrisuk, S. Lorente, and A. Bejan, "Constructal solar chimney configuration," *International Journal of Heat and Mass Transfer*, vol. 53, no. 1–3, pp. 327–333, Oct. 2009, doi: https://doi.org/10.1016/j.ijheatmasstransfer.2009.09.026.

[21] khlef, K.; Larbi, S. Energy Performance Analysis of a Solar Chimney Power Plant with and without Thermal Storage System. In Proceedings of the 6th International Conference on Automation, Control, Engineering and Computer Science, Istanbul, Turkey, 21–23 October 2019; Volume 11, pp. 1–7.,

[22] Rajput, S.R.; Nigam, S.R.; Sen, M. Integrated solar heat and wind power plant: Design and performance. Int. J. Eng. Sci. Manag. 2017, 7, 407–423.,.

[23] J. Li, P. Guo, and Y. Wang, "Effects of collector radius and chimney height on power output of a solar chimney power plant with turbines," *Renewable Energy*, vol. 47, pp. 21–28, Nov. 2012, doi: https://doi.org/10.1016/j.renene.2012.03.018.

[24] M. Tingzhen, L. Wei, and X. Guoliang, "Analytical and numerical investigation of the solar chimney power plant systems," *International Journal of Energy Research*, vol. 30, no. 11, pp. 861–873, 2006, doi: https://doi.org/10.1002/er.1191.

[25] R. Bhoraniya, M. Jiren, and A. Harichandan, "CFD analysis of solar chimney power plant: Effect of chimney height, shape and collector size," *Journal of Solar Energy Research*, vol. 4, no. 1, pp. 61–71, Jan. 2019, doi: https://doi.org/10.22059/jser.2019.70911.

[26] Dhahri, A.; Omri, A.; Orfi, J. Study of the influence of geometric parameters on a solar chimney power system. In Proceedings of the 7th International Congress on Renewable Energy and the Environment, Sousse, Tunisia, 19–21 March 2013.,.

[27] A. A. Gitan, S. H. Abdulmalek, and S. S. Dihrab, "Tracking collector consideration of tilted collector solar updraft tower power plant under Malaysia climate conditions," *Energy*, vol. 93, pp. 1467–1477, Dec. 2015, doi: https://doi.org/10.1016/j.energy.2015.09.009.

[28] H. Semai, A. Bouhdjar, and S. Larbi, "Canopy slope effect on the performance of the solar chimney power plant," *International Journal of Green Energy*, vol. 14, no. 3, pp. 229–238, Nov. 2016, doi: https://doi.org/10.1080/15435075.2016.1253580.

[29] E. Gholamalizadeh and M.-H. Kim, "CFD (computational fluid dynamics) analysis of a solar-chimney power plant with inclined collector roof," *Energy*, vol. 107, pp. 661–667, Jul. 2016, doi: https://doi.org/10.1016/j.energy.2016.04.077.

[30] A. Hassan, M. Ali, and A. Waqas, "Numerical investigation on performance of solar chimney power plant by varying collector slope and chimney diverging angle," *Energy*, vol. 142, pp. 411–425, Jan. 2018, doi: https://doi.org/10.1016/j.energy.2017.10.047.

[31] Jitendra Ahirwar and P. Sharma, "Analyzing the effect of solar chimney power plant by varying chimney height, collector slope and chimney diverging angle," *International Journal of Innovative Research in Technology*, vol. 6, no. 7, pp. 213–219, Dec. 2019.

[32] E. Gholamalizadeh and M.-H. Kim, "Multi-Objective Optimization of a Solar Chimney Power Plant with Inclined Collector Roof Using Genetic Algorithm," *Energies*, vol. 9, no. 11, p. 971, Nov. 2016, doi: https://doi.org/10.3390/en9110971.

[33] Y. J. Choi, D. H. Kam, Y. W. Park, and Y. H. Jeong, "Development of analytical model for solar chimney power plant with and without water storage system," *Energy*, vol. 112, pp. 200–207, Oct. 2016, doi: https://doi.org/10.1016/j.energy.2016.06.023.

[34] M. Ghalamchi, A. Kasaeian, and M. Ghalamchi, "Experimental study of geometrical and climate effects on the performance of a small solar chimney," *Renewable and Sustainable Energy Reviews*, vol. 43, pp. 425–431, Mar. 2015, doi: https://doi.org/10.1016/j.rser.2014.11.068.

[35] P. J. Cottam, P. Duffour, P. Lindstrand, and P. Fromme, "Effect of canopy profile on solar thermal chimney performance," *Solar Energy*, vol. 129, pp. 286–296, May 2016, doi: https://doi.org/10.1016/j.solener.2016.01.052.

[36] D. Toghraie, A. Karami, M. Afrand, and A. Karimipour, "Effects of geometric parameters on the performance of solar chimney power plants," *Energy*, vol. 162, pp. 1052–1061, Nov. 2018, doi: https://doi.org/10.1016/j.energy.2018.08.086.

[37] X. Zhou, J. Yang, B. Xiao, and G. Hou, "Simulation of a pilot solar chimney thermal power generating equipment," *Renewable Energy*, vol. 32, no. 10, pp. 1637–1644, Aug. 2007, doi: https://doi.org/10.1016/j.renene.2006.07.008.

[38] S. S. Al-Azawiey, H. H. Al-Kayiem, and S. B. Hassan, "On the Influence of Collector Size on the Solar Chimneys Performance," *MATEC Web of Conferences*, vol. 131, p. 02011, 2017, doi: https://doi.org/10.1051/matecconf/201713102011.

[39] S. Larbi, A. Bouhdjar, and T. Chergui, "Performance analysis of a solar chimney power plant in the southwestern region of Algeria," *Renewable and Sustainable Energy Reviews*, vol. 14, no. 1, pp. 470–477, Jan. 2010, doi: https://doi.org/10.1016/j.rser.2009.07.031.

[40] X. Zhou, F. Wang, J. Fan, and R. M. Ochieng, "Performance of solar chimney power plant in Qinghai-Tibet Plateau," *Renewable and Sustainable Energy Reviews*, vol. 14, no. 8, pp. 2249–2255, Oct. 2010, doi: https://doi.org/10.1016/j.rser.2010.04.017.

[41] M. O. Hamdan, "Analysis of solar chimney power plant utilizing chimney discrete model," *Renewable Energy*, vol. 56, pp. 50–54, Aug. 2013, doi: https://doi.org/10.1016/j.renene.2012.09.047.

[42] E. Gholamalizadeh and S. H. Mansouri, "A comprehensive approach to design and improve a solar chimney power plant: A special case – Kerman project," *Applied Energy*, vol. 102, pp. 975–982, Feb. 2013, doi: https://doi.org/10.1016/j.apenergy.2012.06.012.

[43] P. Guo, J. Li, and Y. Wang, "Annual performance analysis of the solar chimney power plant in Sinkiang, China," *Energy Conversion and Management*, vol. 87, pp. 392–399, Nov. 2014, doi: https://doi.org/10.1016/j.enconman.2014.07.046.

[44] G. M. Ngala, M. B. Oumarou, A. B. Mohammad, and M. Shuwa, "Evaluation of Solar Chimney Power Plant in Semi-Arid Region of Nigeria," *Arid zone journal of engineering technology and environment/Arid Zone Journal of Engineering Technology and Environment*, vol. 11, pp. 1–12, Jul. 2017.

[45] Cherif Khelifi, Fateh Ferroudji, and M. Ouali, "Analytical Modeling and Optimization of a Solar Chimney Power Plant," *International Journal of Engineering Research in Africa*, vol. 25, pp. 78–88, Aug. 2016, doi: https://doi.org/10.4028/www.scientific.net/jera.25.78.

[46] Kalantar, V.; Zare, M. Simulation of flow and heat transfer in 3D solar chimney power plants-numerical analysis. In Proceedings of the Jordan International Energy Conference, Amman, Jordan, 20–22 September 2011.,

[47] M. Najmi, A. Nazari, H. Mansouri, and G. Zahedi, "Feasibility study on optimization of a typical solar chimney power plant," *Heat and Mass Transfer*, vol. 48, no. 3, pp. 475–485, Sep. 2011, doi: https://doi.org/10.1007/s00231-011-0894-5.

[48] A. Ayadi, A. Bouabidi, Z. Driss, and M. S. Abid, "Experimental and numerical analysis of the collector roof height effect on the solar chimney performance," *Renewable Energy*, vol. 115, pp. 649–662, Jan. 2018, doi: https://doi.org/10.1016/j.renene.2017.08.099.

[49] Alibakhsh Kasaeian, E. Heidari, and Sh. Nasiri Vatan, "Experimental investigation of climatic effects on the efficiency of a solar chimney pilot power plant," *Renewable & Sustainable Energy Reviews*, vol. 15, no. 9, pp. 5202–5206, Dec. 2011, doi: https://doi.org/10.1016/j.rser.2011.04.019.

[50] A. Ayadi, Z. Driss, A. Bouabidi, and M. S. Abid, "Experimental and numerical study of the impact of the collector roof inclination on the performance of a solar chimney power plant," *Energy and Buildings*, vol. 139, pp. 263–276, Mar. 2017, doi: https://doi.org/10.1016/j.enbuild.2017.01.047.

[51] Al-Kayiem, H.H.; Al-Nakeeb, Q.A. Geometry alteration effect on the performance of a solar–wind power system. In Proceedings of the International Conference on Energy and Environment, Selangor, Malaysia, 28–30 August 2006; pp. 50–55.,.

[52] Shahi, D.V.V.; Gupta, M.A.; Nayak, M.V.S. CFD Analysis of solar chimney wind power plant by Ansys Fluent. Int. J. Technol. Res. Eng. 2018, 5, 3746–3751.,.

[53] E. Cuce, H. Sen, and P. M. Cuce, "Numerical performance modelling of solar chimney power plants: Influence of chimney height for a pilot plant in Manzanares, Spain," *Sustainable Energy Technologies and Assessments*, vol. 39, p. 100704, Jun. 2020, doi: https://doi.org/10.1016/j.seta.2020.100704.

[54] X. Zhou, J. Yang, B. Xiao, G. Hou, and F. Xing, "Analysis of chimney height for solar chimney power plant," *Applied Thermal Engineering*, vol. 29, no. 1, pp. 178–185, Jan. 2009, doi: https://doi.org/10.1016/j.applthermaleng.2008.02.014.

[55] Y. Xu and X. Zhou, "Performance of divergent-chimney solar power plants," *Solar Energy*, vol. 170, pp. 379–387, Aug. 2018, doi: https://doi.org/10.1016/j.solener.2018.05.068.

[56] S. Hu, D. Y. C. Leung, and M. Z. Q. Chen, "Effect of Divergent Chimneys on the Performance of a Solar Chimney Power Plant," *Energy Procedia*, vol. 105, pp. 7–13, May 2017, doi: https://doi.org/10.1016/j.egypro.2017.03.273.

[57] A. Kasaeian, M. Ghalamchi, and M. Ghalamchi, "Simulation and optimization of geometric parameters of a solar chimney in Tehran," *Energy Conversion and Management*, vol. 83, pp. 28–34, Jul. 2014, doi: https://doi.org/10.1016/j.enconman.2014.03.042.

[58] M. A. dos S. Bernardes, A. Voß, and G. Weinrebe, "Thermal and technical analyses of solar chimneys," *Solar Energy*, vol. 75, no. 6, pp. 511–524, Dec. 2003, doi: https://doi.org/10.1016/j.solener.2003.09.012.

[59] S. Nizetic, N. Ninic, and B. Klarin, "Analysis and feasibility of implementing solar chimney power plants in the Mediterranean region," *Energy*, vol. 33, no. 11, pp. 1680–1690, Nov. 2008, doi: https://doi.org/10.1016/j.energy.2008.05.012.

[60] R. Sangi, "Performance evaluation of solar chimney power plants in Iran," *Renewable and Sustainable Energy Reviews*, vol. 16, no. 1, pp. 704–710, Jan. 2012, doi: https://doi.org/10.1016/j.rser.2011.08.035.

[61] A. Al Alawin, O. Badran, A. Awad, Y. Abdelhadi, and A. Al-Mofleh, "Feasibility study of a solar chimney power plant in Jordan," *Applied Solar Energy*, vol. 48, no. 4, pp. 260–265, Oct. 2012, doi: https://doi.org/10.3103/s0003701x12040020.

[62] M. Motoyama, K. Sugitani, Y. Ohya, T. Karasudani, T. Nagai, and S. Okada, "Improving the Power Generation Performance of a Solar Tower Using Thermal Updraft Wind," *Energy and Power Engineering*, vol. 06, no. 11, pp. 362–370, 2014, doi: https://doi.org/10.4236/epe.2014.611031.

[63] Y. Ohya, M. Wataka, K. Watanabe, and T. Uchida, "Laboratory Experiment and Numerical Analysis of a New Type of Solar Tower Efficiently Generating a Thermal Updraft," *Energies*, vol. 9, no. 12, p. 1077, Dec. 2016, doi: https://doi.org/10.3390/en9121077.

[64] H. Nasraoui, Z. Driss, A. Ayedi, and H. Kchaou, "Numerical and Experimental Study of the Aerothermal Characteristics in Solar Chimney Power Plant with Hyperbolic Chimney Shape," *Arabian Journal for Science and Engineering*, vol. 44, no. 9, pp. 7491–7504, Mar. 2019, doi: https://doi.org/10.1007/s13369-019-03821-x.

[65] Pattanashetti, J.S.; Madhukeshwara, N. Numerical Investigation and Optimization of Solar Tower Power Plant. Int. J. Res. Aeronaut. Mech. Eng. 2014, 2, 92–94.,.

[66] B. Ghorbani, M. Ghashami, Mehdi Ashjaee, and Hamid Hosseinzadegan, "Electricity production with low grade heat in thermal power plants by design improvement of a hybrid dry cooling tower and a solar chimney concept," vol. 94, pp. 1–11, Apr. 2015, doi: https://doi.org/10.1016/j.enconman.2015.01.044.

[67] P. Das and C. V.P., "Performance characteristics of divergent chimney solar updraft tower plant," *International Journal of Energy Research*, Mar. 2020, doi: https://doi.org/10.1002/er.5304.

[68] Koonsrisuk, A.; Chitsomboon, T. Effect of tower area on the potential of solar tower. In Proceedings of the 2nd Joint International Conference on Sustainable Energy and Environment, Bangkok, Thailand, 21–23 November 2006; pp. 1–6.,.

[69] D. K. Mandal, N. Biswas, A. Barman, R. Chakraborty, and N. K. Manna, "A novel design of absorber surface of solar chimney power plant (SCPP): Thermal assessment, exergy and regression analysis," *Sustainable Energy Technologies and Assessments*, vol. 56, p. 103039, Mar. 2023, doi: https://doi.org/10.1016/j.seta.2023.103039.

[70] N. Biswas, Dipak Kumar Mandal, N. K. Manna, and Ali Cemal Benim, "Novel stair-shaped ground absorber for performance enhancement of solar chimney power plant," *Applied thermal engineering*, vol. 227, pp. 120466–120466, Jun. 2023, doi: https://doi.org/10.1016/j.applthermaleng.2023.120466.

[71] E. Cuce, P. M. Cuce, H. Sen, K. Sudhakar, U. Berardi, and U. Serencam, "Impacts of Ground Slope on Main Performance Figures of Solar Chimney Power Plants: A Comprehensive CFD Research with Experimental Validation," *International Journal of Photoenergy*, vol. 2021, pp. 1–11, May 2021, doi: https://doi.org/10.1155/2021/6612222.

[72] A. Atia, Said Bouabdallah, Badia Ghernaout, M. Teggar, and Toufik Benchatti, "Investigation of various absorber surface shapes for performance improvement of solar chimney power plant," *Applied thermal engineering*, vol. 235, pp. 121395–121395, Nov. 2023, doi: https://doi.org/10.1016/j.applthermaleng.2023.121395.

[73] Pinar Mert Cuce, Erdem Cuce, and Harun Sen, "Improving Electricity Production in Solar Chimney Power Plants with Sloping Ground Design: An Extensive CFD Research," *Journal of Solar Energy Research Updates*, vol. 7, pp. 122–131, Jan. 2020, doi: https://doi.org/10.31875/2410-2199.2020.07.10.

[74] Dipak Kumar Mandal, N. Biswas, N. K. Manna, and Ali Cemal Benim, "Impact of chimney divergence and sloped absorber on energy efficacy of a solar chimney power plant (SCPP)," *Ain Shams Engineering Journal/Ain Shams Engineering Journal* , vol. 15, no. 2, pp. 102390–102390, Feb. 2024, doi: https://doi.org/10.1016/j.asej.2023.102390.

[75] T. P. Fluri and T. W. Von Backström, "Performance analysis of the power conversion unit of a solar chimney power plant," *Solar Energy*, vol. 82, no. 11, pp. 999–1008, Nov. 2008, doi: https://doi.org/10.1016/j.solener.2008.05.001.

[76] M. Tingzhen, L. Wei, X. Guoling, X. Yanbin, G. Xuhu, and P. Yuan, "Numerical simulation of the solar chimney power plant systems coupled with turbine," *Renewable Energy*, vol. 33, no. 5, pp. 897–905, May 2008, doi: https://doi.org/10.1016/j.renene.2007.06.021.

[77] L. Zuo, P. Dai, Z. Yan, C. Li, Y. Zheng, and Y. Ge, "Design and optimization of turbine for solar chimney power plant based on lifting design method of axial-flow hydraulic turbine impeller," *Renewable Energy*, vol. 171, pp. 799–811, Jun. 2021, doi: https://doi.org/10.1016/j.renene.2021.02.121.

[78] P. Caicedo, D. Wood, and C. Johansen, "Radial Turbine Design for Solar Chimney Power Plants," *Energies*, vol. 14, no. 3, p. 674, Jan. 2021, doi: https://doi.org/10.3390/en14030674.

[79] Alibakhsh Kasaeian, Amir Houshang Mahmoudi, Fatemeh Razi Astaraei, and Afshin Hejab, "3D simulation of solar chimney power plant considering turbine blades," vol. 147, pp. 55–65, Sep. 2017, doi: https://doi.org/10.1016/j.enconman.2017.05.029.

[80] P. Das and V. P. Chandramohan, "Computational study on the effect of collector cover inclination angle, absorber plate diameter and chimney height on flow and performance parameters of solar updraft tower (SUT) plant," *Energy*, vol. 172, pp. 366–379, Apr. 2019, doi: https://doi.org/10.1016/j.energy.2019.01.128.

[81] F. Cao, Q. Liu, T. Yang, T. Zhu, J. Bai, and L. Zhao, "Full-year simulation of solar chimney power plants in Northwest China," *Renewable Energy*, vol. 119, pp. 421–428, Apr. 2018, doi: https://doi.org/10.1016/j.renene.2017.12.022.

[82] Shahin Nasirivatan, Alibakhsh Kasaeian, Mehrdad Ghalamchi, and Mehran Ghalamchi, "Performance optimization of solar chimney power plant using electric/corona wind," *Journal of Electrostatics*, vol. 78, pp. 22–30, Oct. 2015, doi: https://doi.org/10.1016/j.elstat.2015.09.007.

[83] R. Rabehi, A. Chaker, Z. Aouachria, and M. Tingzhen, "CFD analysis on the performance of a solar chimney power plant system: Case study in Algeria," *International Journal of Green Energy*, vol. 14, no. 12, pp. 971–982, Jul. 2017, doi: https://doi.org/10.1080/15435075.2017.1339043.

[84] M. Ghalamchi, A. Kasaeian, M. Ghalamchi, and A. H. Mirzahosseini, "An experimental study on the thermal performance of a solar chimney with different dimensional parameters," *Renewable Energy*, vol. 91, pp. 477–483, Jun. 2016, doi: https://doi.org/10.1016/j.renene.2016.01.091.

[85] P. Das and V.P. Chandramohan, "Experimental studies of a laboratory scale inclined collector solar updraft tower plant with thermal energy storage system," *Journal of Building Engineering*, vol. 41, pp. 102394–102394, Mar. 2021, doi: https://doi.org/10.1016/j.jobe.2021.102394.

[86] H. H. Al-Kayiem, M. A. Aurybi, S. I. U. Gilani, A. A. Ismaeel, and S. T. Mohammad, "Performance evaluation of hybrid solar chimney for uninterrupted power generation," *Energy*, vol. 166, pp. 490–505, Jan. 2019, doi: https://doi.org/10.1016/j.energy.2018.10.115.

[87] S. Lal, S. C. Kaushik, and R. Hans, "Experimental investigation and CFD simulation studies of a laboratory scale solar chimney for power generation," *Sustainable Energy Technologies and Assessments*, vol. 13, pp. 13–22, Feb. 2016, doi: https://doi.org/10.1016/j.seta.2015.11.005.

[88] P. N. Belkhode *et al.*, "Performance analysis of roof collector used in the solar updraft tower," *Sustainable Energy Technologies and Assessments*, vol. 48, pp. 101619–101619, Sep. 2021, doi: https://doi.org/10.1016/j.seta.2021.101619.

[89] Khadersab Adamsab, Eugene Vega, and Abdulhamid Hamdan Al-Hinai, "An Experimental Investigation of a Small-scale Solar Updraft Tower in the Sultanate of Oman," *Journal of Advanced Research in Fluid Mechanics and Thermal Sciences*, vol. 93, no. 1, pp. 212–221, Mar. 2022, doi: https://doi.org/10.37934/arfmts.93.1.212221.

[90] R. Balijepalli, V. P. Chandramohan, and K. Kirankumar, "Development of a small scale plant for a solar chimney power plant (SCPP): A detailed fabrication procedure, experiments and performance parameters evaluation," *Renewable Energy*, vol. 148, pp. 247–260, Apr. 2020, doi: https://doi.org/10.1016/j.renene.2019.12.001.

[91] "R. Naceur, M. A. Bezzerrouk, M. Bousmaha, A. Akriche, I. Hattabi, D. Sahel, Experimental and CFD analysis of performance of solar chimney power plant prototype. Journal of Applied Energies. 2, 11–26 (2023)."

[92] T. Mekhail, A. Rekaby, M. Fathy, M. Bassily, and R. Harte, "Experimental and Theoretical Performance of Mini Solar Chimney Power Plant," *Journal of Clean Energy Technologies*, vol. 5, no. 4, pp. 294–298, Jul. 2017, doi: https://doi.org/10.18178/jocet.2017.5.4.386.

[93] D. Kumar Mandal, S. Pradhan, R. Chakraborty, A. Barman, and N. Biswas, "Experimental investigation of a solar chimney power plant and its numerical verification of thermo-physical flow parameters for performance enhancement," *Sustainable Energy Technologies and Assessments*, vol. 50, p. 101786, Mar. 2022, doi: https://doi.org/10.1016/j.seta.2021.101786.

[94] X. Zhou, J. Yang, B. Xiao, and G. Hou, "Experimental study of temperature field in a solar chimney power setup," *Applied Thermal Engineering*, vol. 27, no. 11–12, pp. 2044–2050, Aug. 2007, doi: https://doi.org/10.1016/j.applthermaleng.2006.12.007.

[95] A. Azizi, T. Tahri, M. H. Sellami, L. Segni, R. Belakroum, and K. Loudiyi, "Experimental and CFD investigation of small-scale solar chimney for power generation. Case study: southeast of Algeria," *DESALINATION AND WATER TREATMENT*, vol. 160, pp. 1–8, 2019, doi: https://doi.org/10.5004/dwt.2019.24167.

[96] K. Ikhlef, S. Larbi, and İ. Üçgül, "Experimental study of different thermal storage system effects on the performance of a small prototype solar chimney power plant," *Renewable Energy*, vol. 200, pp. 516–526, Nov. 2022, doi: https://doi.org/10.1016/j.renene.2022.09.087.

[97] E. Shabahang Nia and M. Ghazikhani, "Dimensional investigation of solar chimney power plant based on numerical and experimental results," *Thermal Science and Engineering Progress*, vol. 37, p. 101548, Jan. 2023, doi: https://doi.org/10.1016/j.tsep.2022.101548.

[98] M. F. C. Esmail, A. Khodary, T. Mekhail, and E. Hares, "Effect of wind speed over the chimney on the updraft velocity of a solar chimney power plant: An experimental study," *Case Studies in Thermal Engineering*, vol. 37, p. 102265, Sep. 2022, doi: https://doi.org/10.1016/j.csite.2022.102265.

[99] D. Eryener and H. Kuscu, "Hybrid transpired solar collector updraft tower," *Solar Energy*, vol. 159, pp. 561–571, Jan. 2018, doi: https://doi.org/10.1016/j.solener.2017.11.035.

[100] M.-H. Huang *et al.*, "Experimental and numerical studies for applying hybrid solar chimney and photovoltaic system to the solar-assisted air cleaning system," *Applied Energy*, vol. 269, p. 115150, Jul. 2020, doi: https://doi.org/10.1016/j.apenergy.2020.115150.

[101] O. Ben, Med Ridha Ouahrani, Med Hassen Sellami, and Ladjel Segni, "Experimental investigations of hybrid: geothermal water/solar chimney power plant," *Energy Sources Part A Recovery Utilization and Environmental Effects*, vol. 46, no. 1, pp. 15474–15491, Aug. 2020, doi: https://doi.org/10.1080/15567036.2020.1810830.

[102] D. M. Aliaga *et al.*, "Modified solar chimney configuration with a heat exchanger: Experiment and CFD simulation," *Thermal science and engineering progress*, vol. 22, pp. 100850–100850, May 2021, doi: https://doi.org/10.1016/j.tsep.2021.100850.

[103] Bagher Mokhtari Shahdost, Fatemeh Razi Astaraei, Amir Ebrahimi-Moghadam, and Mohammad Hossein Ahmadi, "Experimental and numerical investigations of a novel chimney system for power generation using the combination of fossil fuel power plant exhaust gases and ambient air," *Energy Science & Engineering*, vol. 7, no. 3, pp. 764–776, Apr. 2019, doi: https://doi.org/10.1002/ese3.306.

[104] L. Zuo *et al.*, "Experimental research on the operation characteristics of solar chimney power plant combined with distillation (SCPPCD)," *Applied Energy*, vol. 326, p. 120029, Nov. 2022, doi: https://doi.org/10.1016/j.apenergy.2022.120029.

[105] A. Akbarzadeh, P. Johnson, and R. Singh, "Examining potential benefits of combining a chimney with a salinity gradient solar pond for production of power in salt affected areas," *Solar Energy*, vol. 83, no. 8, pp. 1345–1359, Aug. 2009, doi: https://doi.org/10.1016/j.solener.2009.02.010.

[106] T. Ming, R. K. de Richter, F. Meng, Y. Pan, and W. Liu, "Chimney shape numerical study for solar chimney power generating systems," *International Journal of Energy Research*, vol. 37, no. 4, pp. 310–322, Sep. 2011, doi: https://doi.org/10.1002/er.1910.

[107] N. Pasumarthi and S. A. Sherif, "98/03934 Experimental and theoretical performance of a demonstration solar chimney model—part II: experimental and theoretical results and economic analysis," *Fuel and Energy Abstracts*, vol. 39, no. 5, p. 368, Sep. 1998, doi: https://doi.org/10.1016/s0140-6701(98)93929-7.

[108] L. B. Hooi and S. K. Thangavelu, "A parametric simulation of solar chimney power plant," *IOP Conference Series: Materials Science and Engineering*, vol. 297, p. 012057, Jan. 2018, doi: https://doi.org/10.1088/1757-899x/297/1/012057.

[109] N. Pasumarthi and S. A. Sherif, "Experimental and theoretical performance of a demonstration solar chimney model—Part I: mathematical model development," *International Journal of Energy Research*, vol. 22, no. 3, pp. 277–288, Mar. 1998, doi: https://doi.org/10.1002/(sici)1099-114x(19980310)22:3%3C277::aid-er380%3E3.0.co;2-r.

[110] https://www.alldatasheet.com/, "sdvdfvddfv," Jan. 21, 5AD.

[111] https://www.holdpeak.com/product/247.html, "Anemometer HP-866A_Digital Measuring Instruments-Digital Multimeter-Infrared Thermometer-Zhuhai JiDa Huapu instrument Co.,Ltd.," *Holdpeak.com*, 2021. https://www.holdpeak.com/product/247.html (accessed Feb. 25, 2025).

[112] S. R. Keshari, C. V.P., and P. Das, "A 3D numerical study to evaluate optimum collector inclination angle of Manzanares solar updraft tower power plant," *Solar Energy*, vol. 226, pp. 455–467, Sep. 2021, doi: https://doi.org/10.1016/j.solener.2021.08.062.

[113] A. S. Avcı, H. Karakaya, and A. Durmuş, "Numerical and experimental investigation of solar chimney power plant system performance," *Energy Sources, Part A: Recovery, Utilization, and Environmental Effects*, pp. 1–19, Apr. 2020, doi: https://doi.org/10.1080/15567036.2020.1744772.

[114] B. Djaouida, Z. Aouachria, A. H. Benmachiche, and S. Ali, "Controlling power output of solar chimney power plant according to demand," *International Journal of Ambient Energy*, pp. 1–15, Sep. 2018, doi: https://doi.org/10.1080/01430750.2018.1517677.

[115] D. K. Mandal, P. Goswami, S. Pradhan, R. Chakraborty, N. A. Khan, and P. Bose, "A Numerical experimentation on fluid flow and heat transfer in a SCPP," *IOP conference series. Materials science and engineering*, vol. 1080, no. 1, pp. 012027–012027, Feb. 2021, doi: https://doi.org/10.1088/1757-899x/1080/1/012027.

[116] Haythem Nasraoui, Zied Driss, A. Ayadi, Abdallah Bouabidi, and Hedi Kchaou, "Numerical and experimental study of the impact of conical chimney angle on the thermodynamic characteristics of a solar chimney power plant," *Proceedings of the Institution of Mechanical Engineers, Part E: Journal of Process Mechanical Engineering*, vol. 233, no. 5, pp. 1185–1199, Jun. 2019, doi: https://doi.org/10.1177/0954408919859160.

[117] M. Saad, N. Ahmed, M. Mahmood, and M. B. Sajid, "Performance enhancement of solar updraft tower plant using parabolic chimney profile configurations: A numerical analysis," *Energy Reports*, vol. 8, pp. 4661–4671, Nov. 2022, doi: https://doi.org/10.1016/j.egyr.2022.03.134.

[118] S. H. Fallah and M. S. Valipour, "Evaluation of solar chimney power plant performance: The effect of artificial roughness of collector," *Solar Energy*, vol. 188, pp. 175–184, Aug. 2019, doi: https://doi.org/10.1016/j.solener.2019.05.065.

[119] H. Nasraoui, Z. Driss, and H. Kchaou, "Novel collector design for enhancing the performance of solar chimney power plant," *Renewable Energy*, vol. 145, pp. 1658–1671, Jan. 2020, doi: https://doi.org/10.1016/j.renene.2019.07.062.

[120] E. Ö. Yapıcı, E. Ayli, and O. Nsaif, "Numerical investigation on the performance of a small scale solar chimney power plant for different geometrical parameters," *Journal of Cleaner Production*, vol. 276, p. 122908, Dec. 2020, doi: https://doi.org/10.1016/j.jclepro.2020.122908.

[121] H. NOUAR, "Investigation of Climate Effects on the Performance of Solar Chimney Power Plants Using Numerical and Analytical Models: A Case Study for Chlef, Algeria," *PRZEGLĄD ELEKTROTECHNICZNY*, vol. 1, no. 3, pp. 115–120, Mar. 2021, doi: https://doi.org/10.15199/48.2021.03.22.

[122] C. Méndez and Yusuf Bicer, "Comparison of the influence of solid and phase change materials as a thermal storage medium on the performance of a solar chimney," *Energy science & engineering*, vol. 9, no. 8, pp. 1274–1288, Mar. 2021, doi: https://doi.org/10.1002/ese3.892.

[123] A. A. Sedighi, Z. Deldoost, and B. M. Karambasti, "Effect of thermal energy storage layer porosity on performance of solar chimney power plant considering turbine pressure drop," *Energy*, vol. 194, p. 116859, Mar. 2020, doi: https://doi.org/10.1016/j.energy.2019.116859.

ANNEXES

1. Manufacturer Datasheet of The HP86A anemometers

HP86A Anemometer: A handheld digital instrument that measures wind speed and air temperature in multiple units (m/s, km/h, ft/min, knots, mph). It displays current, average, maximum, and minimum readings, includes an LCD with backlight and low-battery indication, and can log data for 24 hours.

Technical Specifications:

Air velocity	**Range**	**Resolution**	**Accuracy**
m/s	1.10 - 25.00m/s	0.01m/s	± (3% + 0.30 m/s)
km/h	4.0 - 90.0km/h	0.1km/h	± (3% + 1.0km/h)
ft/min	220 – 4920ft/min	1ft/min	± (3% + 40ft/m)
MPH	2.5 – 56.0MPH	0.1MPH	± (3% + 0.4MPH)
knots	2.2 – 48.0knots	0.1knots	± (3% + 0.4knots)
Air Temperature	-10~60℃(14~140℉)	0.1℃/℉	2.0℃(4.0℉)

Display	Dual line, 4-digit LCD
Display Update	2 times/sec
Sensors	Air velocity sensor: NTC-type precision thermistor
Automatic Power off	Auto shut off in 10 minutes without operation to preserve battery Life
Operating Temperature	0 to 50°C (32 to 122°F)
Storage Temperature	-10 to 60°C (14 to 140°F)
Operating Humidity	<80% RH
Storage Humidity	<80% RH
Operating Altitude	2000 meters (7000ft) maximum
Battery	One 9 volt battery
Weight; **Dimensions**	172g ; 213*54*36mm

Button Functions

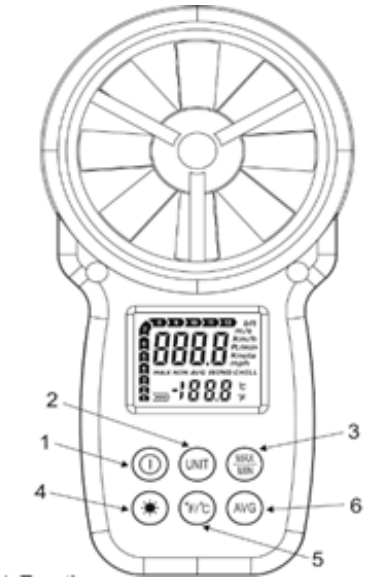

① **Power:** Turn the unit on/off

② **Unit:** Cycle through wind speed units (m/s, km/h, ft/min, knots, mph)

③ **Max/Min:** Display maximum or minimum wind speed

④ **Backlight:** Turn LCD backlight on/off (active 15 s)

⑤ **°C/°F:** Switch temperature display unit

⑥ **Average:** Display average wind speed over 15 seconds

2. Manufacturer Datasheet of the Vantage Pro 2

A high-accuracy weather station that measures and displays temperature, humidity, barometric pressure, wind speed and direction, rainfall, windchill, dew point, and solar/UV data (Plus models). It transmits weather information up to 1000 ft (305 m) to a console display, with optional repeaters to extend range, and includes sensors, anemometer, rain collector, cables, and mounting hardware.

Vantage Pro2 Console Display Features

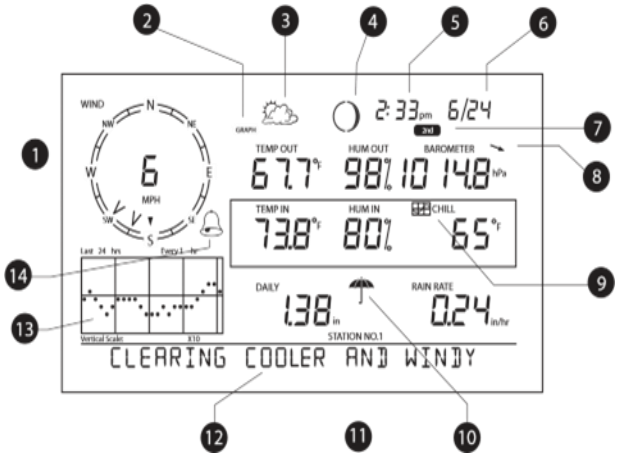

1. Compass Rose
2. Graph & Hi/Low Mode Settings
3. Forecast Icons
4. Moon Phase Indicator
5. Time/Sunrise Time
6. Date/Sunset Date
7. 2ND Button Indicator
8. Barometric Trend Arrow
9. Graph Icon
10. Current Rain Icon
11. Station Number Indicator
12. Weather Ticker
13. Graph Field
14. Alarm Icon

Technical Specifications:

Parameter	Specification
Size / Weight	445 × 264 × 406 mm / 5.4 kg
Wireless / Range	868.0–868.6 MHz / 300 m sight, 60–120 m obstacles
Wind	Units mph, km/h, m/s, kts; Range 3–290 km/h; Accuracy ±3 km/h; Sensor Buckets + Hall effect
Wind Direction	0–360°; Accuracy ±3°; Sensor Vane + potentiometer
Temperature Outdoor	-40–65°C; Accuracy ±0.3°C; Sensor Silicon diode
Temperature Indoor	0–60°C; Accuracy ±0.5°C
Windchill	Calculated; Accuracy ±1
Humidity Outdoor	1–100% RH; Accuracy ±2%; Sensor Film capacitor
Humidity Indoor	1–100% RH; Accuracy ±2%
Rainfall / Rate	0–762 mm; Accuracy ±3–5%; Sensor Tilting trough
Dew Point	-76–54°C; Accuracy ±1.5°C
Atmospheric Pressure	540–1100 hPa; Accuracy ±1 hPa
Receiving Console	Measures Temp, Humidity, Pressure; Power 5 VDC; Display IPS LED
ISS (Outdoor Sensors)	Measures Temp, Humidity, Wind, Rain, Windchill, Gusts; Power Solar + battery; Temp -40–65°C

3. Manufacturer Datasheet of the DHT11

The DHT11 is a digital temperature and relative humidity sensor integrating a resistive humidity element and an NTC temperature sensor with an internal 8-bit microcontroller

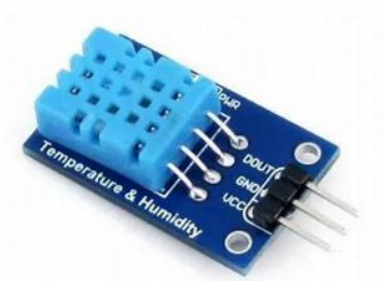

Technical Specifications:

Parameter	Specification
Humidity range	20–90 %RH
Humidity accuracy	±5 %RH
Temperature range	0–50 °C
Temperature accuracy	±2 °C
Resolution	1 %RH / 1 °C
Operating voltage	3–5.5 V
Current consumption	≤ 2.5 mA (measuring)
Sampling period	≥ 1 s
Output signal	Single-wire digital
Package	4-pin single-row

Typical Application

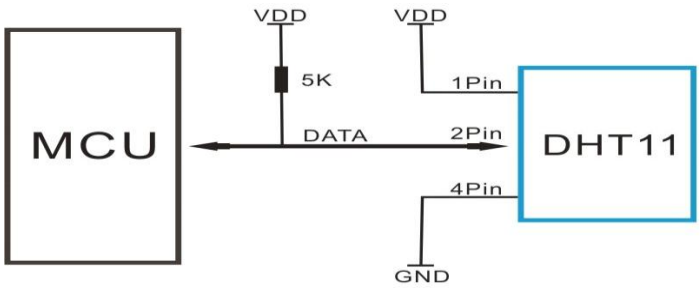

Fig: Pin configuration figure